On the blast resistance of laminated glass

P. A. Hooper[a], R. A. M. Sukhram[b], B. R. K. Blackman[a], J. P. Dear[a,*]

[a] *Imperial College London, Department of Mechanical Engineering, Exhibition Road, London, SW7 2AZ*
[b] *Arup, 13 Fitzroy Street, London, W1T 4BQ*

Abstract

Blast resistant glazing systems typically use laminated glass to reduce the risk of flying glass debris in the event of an explosion. Laminated glass has one or more bonded polymer interlayers to retain glass fragments upon fracture. With good design, the flexibility of the interlayer and the adhesion between layers enable laminated glass to continue to resist blast after the glass layers fracture. This gives protection from significantly higher blast loads when compared to a monolithic pane. Full-scale open-air blast tests were performed on laminated glass containing a polyvinyl butyral (PVB) interlayer. Test windows of size 1.5 m × 1.2 m were secured to robust frames using structural silicone sealant. Blast loads were produced using charge masses of 15 kg and 30 kg (TNT equivalent) at distances of 10 m to 16 m. Deflection and shape measurements of deforming laminated glass were obtained using high-speed digital image correlation. Measurements of loading at the joint, between the laminated glass and the frame, were obtained using strain gauges. The main failure mechanisms observed were the cohesive failure of the bonded silicone joint and delamination between the glass and interlayer at the pane edge. A new finite element model of laminated glass is developed and calibrated using laboratory based tests. Predictions from this model are compared against the experimental results.

Keywords: Laminated, glass, blast, digital image correlation, polyvinyl butyral

1. Introduction

Annealed float glass is often used in windows but is a brittle material that offers little resistance to the blast waves produced by explosions. When it fails it breaks into very sharp fragments that can travel at high velocity. Historically, the majority of injuries from bomb blasts have been from flying glass fragments Smith (2001). Laminated glass has been found to be effective at mitigating these risks and is now often used

*Corresponding author
Email address: j.dear@imperial.ac.uk (J. P. Dear)

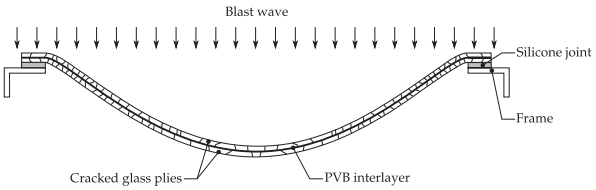

Figure 1: Example of postcrack deformation in laminated glass due to blast loading.

to protect building occupants by retaining glass fragments on a polyvinyl butyral (PVB) interlayer upon fracture (Figure 1). Significant resistance to blast loading is seen in laminated glass even after the glass layers have fractured. It is important to understand the conditions for and types of failure mechanism in laminated glass in order to optimise the design of facade structures.

Whilst there are some analytical and finite-element (FE) based approaches to predicting the response of laminated glass to blast loading, there is little experimental data available for validation of these models. Furthermore current FE models deal only with the uncracked phase of the laminated glass response. This phase only makes up a small portion of the total resistance offered to a blast wave. There is a therefore a need to develop models that predict the laminated glass response after the glass fractures. This paper aims to address these gaps by describing experimental results from four well instrumented full-scale open-air blast tests on lamented glass. The paper also details a FE based approach to modelling the post-fracture laminated glass response and compares it with the experimental data acquired.

2. Background

The behaviour of uncracked laminated glass has been studied by several researchers including Norville et al. (1998), Behr et al. (1993) and Hooper (1973). The flexural stiffness of laminated glass is dependent on the fraction of horizontal shear force transferred between the glass layers by the PVB interlayer. At one extreme the PVB transfers no horizontal shear stress and its only function is to maintain the separation distance between the glass layers. In this case, each glass layer bends independently and the total laminate flexural stiffness is the sum of the flexural stiffness of the individual glass layers. At the other extreme, significant flexural stresses exist within the interlayer in addition to the transfer of all the horizontal shear stress between the glass layers. The limiting case occurs when the stress distribution varies linearly through the thickness and would only be obtained when the elastic modulus of the PVB interlayer equals that of the glass layers.

The analysis by Norville et al. showed that for most laminates the PVB interlayer only needs to transfer

a fraction of horizontal shear stress between the glass layers to give a section modulus exceeding that of the equivalent monolithic pane. The equivalent monolithic pane was defined as a monolithic pane of the same thickness as the total thickness of the glass layers in a laminate. For example, a 6 mm monolithic pane would be equivalent to a 7.52 mm laminated pane consisting of two 3 mm glass layers and 1.52 mm PVB interlayer. Since PVB is a viscoelastic material, the amount of horizontal shear stress transferred between the glass layers is dependent on the rate of applied loading and temperature. It was found that under short duration loads that laminated glass has a higher section modulus than the equivalent monolithic pane. The increase in section modulus also reduces the peak tensile stress on the outer surface of the glass layers for a given load and accounts for an apparent increase in fracture strength for a given load when compared to an equivalent monolithic pane.

Bennison et al. (1999) and van Duser et al. (1999) used a Generalized Maxwell Series model to account for the time dependent modulus of PVB interlayers. Terms in the Maxwell model were determined experimentally using dynamic mechanical analysis. The time dependent PVB material model was used in finite element models of a plate subjected to uniform pressure loading and biaxial flexure. It was found that for most laminates the peak tensile stress on the outer surface of the glass layers was lower than that for an equivalent monolithic pane. The advantage of this approach is that the PVB shear modulus is calculated during the analysis and therefore accounts for time dependent effects. Variation in shear modulus at different temperatures was also taken into account by using the Williams-Landel-Ferry (WLF) equation (Williams et al., 1955) to shift the time dependent shear modulus curve to a different temperature.

The strength of annealed glass has a wide statistical variation. Test data gathered in the development of the glazing standard prEN 13474-3 (CEN/TC129, 2008) includes tensile strength results from over 700 annealed glass samples from different manufacturers using the ring-on-ring test method. As expected, a wide variation in breaking strength was found, from 30 MPa to 120 MPa at a loading rate of 2 $^{\mathrm{MPa}}/_{\mathrm{s}}$. The data can be characterised statistically using a Weibull distribution. For normal design purposes a breaking strength of 45 MPa is given based on 95% of samples not failing below this stress. Smith (Cormie et al., 2009) extrapolated this strength data to the higher strain rates experienced in blast loading using a relationship proposed by Charles (1958) and arrived at a dynamic breaking strength for annealed glass in the region of 80 MPa.

The mechanical behaviour of laminated glass after cracking has been investigated by Muralidhar et al. (2000). In this study, laminated glass with an aligned crack in each glass layer was subjected to constant rate tensile loading (a displacement rate of 1 $^{\mathrm{mm}}/_{\mathrm{s}}$ was used). Under these conditions, PVB delaminates

from the glass at the crack edge and deforms to bridge the crack. It was found that under constantly increasing displacement, the tensile force rises to a steady state value. They also used different hyperelastic material models to calculate the fracture energy associated with the delamination process. However, no viscous energy dissipation was accounted for in the analysis. The calculated fracture energy values include this dissipation energy and therefore overestimate the actual energy involved in the fracture process. The loading rates investigated were also too slow relative to those experienced during blast loading.

Static loading of fractured laminated glass plates was studied theoretically and experimentally by Seshadri et al. (2002). Plates constructed from a single glass and a single PVB layer were loaded centrally by a spherical steel surface at a constant rate of displacement. The glass layer was indented before loading to create a known flaw and a simple regular fracture pattern. Post breakage behaviour of the laminate was modelled using the work on PVB delamination described previously. Good agreement between experimental results and predictions was found. However, only a single glass layer was studied so the restraining effects of a second glass layer were not taken into account. Their approach is also difficult to apply to practical situations where there may be many thousands of cracks and where the crack pattern is not known in advance.

2.1. Glazing materials for blast protection

For increased protection from blast, modern glazing systems use laminated glass bonded to robust framing with structural silicone adhesives. Laminated glass consists of one or more polymer layers sandwiched between layers of glass. Polyvinyl butyral (PVB) is the most common interlayer and is bonded between the glass layers by the application of pressure and heat. It is commercially manufactured in sheets 0.38 mm thick for the architectural glazing market. More than one PVB sheet can be used in an interlayer, increasing the overall interlayer thickness in multiples of 0.38. Current recommendations for blast resistance advise a minimum interlayer thickness of 1.52 mm (Home Office Scientific Development Branch, 2008). Annealed float glass is the most common material used for the glass layers due its low cost. However, tempered glass can also be used where increased initial strength is required, although slight undulations from the tempering process can make laminating difficult. For situations where impact and ballistic strength is a consideration, additional layers of polycarbonate are used in the laminate.

Under blast loading a laminated glass pane initially deflects in a manner similar to a monolithic pane, that is as an elastic plate. This is termed the precrack phase of the laminated glass response. Fracture of the glass layers again occurs when the tensile stress at a flaw anywhere on the glass surface is high enough to cause crack propagation. After the glass layers fracture, the laminate is said to be in the postcrack phase

of the response. In this phase the glass fragments are held bonded to the PVB interlayer, giving continued resistance to the blast wave. The cracked laminate behaves similarly to a membrane and is able to undergo large deflections without further damage (Figure 1). Failure of the laminate occurs by PVB tearing and the conditions for this are not well understood. To be effective the laminated glass needs to be strongly fixed to a supporting structure. If the joint or framing structure is not strong enough, the pane could detach and enter a building at high velocity, injuring occupants.

Structural silicone sealant is commonly used to bond the laminate to a framing structure. In commercial buildings the framing is often constructed from extruded aluminium alloy sections. The laminate is restrained at two or four edges of the pane with a silicone bonded joint on one or both faces of the laminate. Securing all four edges on both sides is the recommended practice for blast resistance. However, single-sided joints are increasingly preferred by architects for aesthetic reasons. Minimum joint dimensions are calculated with reference to the dead-weight of the pane, the wind loading and thermal expansion. Current recommendations for blast resistance advise a double-sided silicone joint of at least 35 mm in depth (Home Office Scientific Development Branch, 2008). Other methods of restraining laminated glass exist such as rubber gaskets, glazing tape and mechanical point fixings. These systems are generally considered to give inferior blast protection to silicone bonded edges.

3. Air blast experimental method

In this paper, laminated glass panes have been tested with different blast loads in four open-air blast experiments. For each test an explosive charge was detonated in front of a test cubicle housing a matching pair of windows. The aim of the experiments was to measure the deflections, strains and edge reaction forces produced in a full-scale blast test for validation of analytical and finite element models. All eight laminated glass panes were of size 1.5 m × 1.2 m and were constructed from two 3 mm thick layers of annealed float glass and a 1.52 mm thick PVB interlayer. Two windows were tested at a time and were secured to the front of a steel cubicle approximately 3 m × 3 m × 3 m as detailed in Figure 2a. Window 1 was fully instrumented and provides the results described in this paper. Window 2 was not fully instrumented and was there to provide a symmetrical setup. The basic cubicle was designed and constructed by the Centre for the Protection of National Infrastructure (CPNI). The laminated glass was bonded on all four edges to a steel subframe with a 6 mm thick single-sided joint and nominal bonded depth of 20 mm. A two-part structural silicone sealant was used for the joint (Dow Corning 993 structural glazing sealant). The subframe was attached to the front of the steel cubicle using bolts.

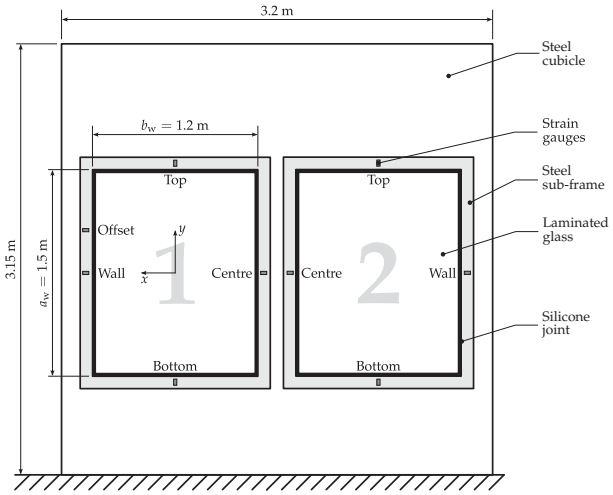

(a) Test cubicle front

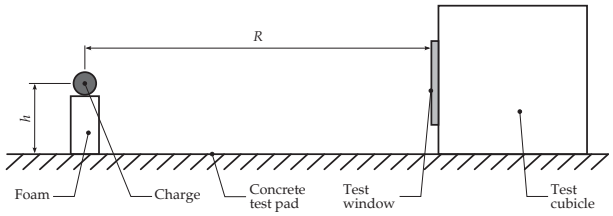

(b) Side elevation

Figure 2: Test view plan and side on with DIC view

In each test the charge was positioned symmetrically in front of the cubicle, raised on foam blocks to height of 1.5 m (corresponding to the window centre height) as shown in Figure 2b. Testing took place on a 100 m × 100 m concrete test pad to minimise energy loss in ground shock and crater formation. Tests 1 and 2 were conducted with 12.8 kg C4 charges (15 kg TNT equivalent) at stand off distances of 10 m and 13 m respectively. Tests 3 and 4 were conducted with 25.6 kg C4 charges (30 kg TNT equivalent) at stand off distances of 16 m and 14 m respectively. The blast pressure-time history for each test was recorded using stand-alone free-field and reflected pressure gauges (type 102-A06 from PCB Piezotronics) at the same stand-off distances as the cubicle. The reflected pressure gauges were mounted in a concrete block of the same dimensions as the test cubicle. Three gauges were located around the centre position of where the window would be located and an average was taken. The test parameters are summarised in Table 1 and were chosen to take the laminated glass up to the point of PVB tearing.

3.1. High-speed digital image correlation

High-speed 3D digital image correlation was used to measure the full-field rear-surface position of a single window during each blast test. Two high-speed cameras were positioned inside the test cubicle at a working

Table 1: Blast test configurations.

Test	Charge weight* W (kg)	Stand-off R (m)	Window size $a_w \times b_w$ (m)	Number of panels	Laminate layup $[d_g, d_{PVB}, d_g]$ (mm)
1	15	10	1.5 × 1.2	2	[3, 1.52, 3]
2	15	13	1.5 × 1.2	2	[3, 1.52, 3]
3	30	16	1.5 × 1.2	2	[3, 1.52, 3]
4	30	14	1.5 × 1.2	2	[3, 1.52, 3]

* TNT equivalent

distance s_w from the test window and centred on the window centre point. The camera setup used is shown in Figure 3a. Only Window 1 in Figure 2a was imaged due to limited availability of matching pairs of high speed cameras.

The included angle between the cameras was set to 25° to provide good sensitivity to out-of-plane motion without sacrificing in-plane sensitivity (Sutton et al., 2009). Two models of high-speed camera were used in this testing; the Phantom V4 and Phantom V5 manufactured by Vision Research. Table 2 details the configuration of each camera type and which camera type was used in each test.

The aperture of each lens was set to the widest opening (smallest f-number) that would allow the object to remain in focus over the anticipated movement range. This ensured that the maximum amount of light reached the camera sensor, enabling smaller exposure times. Exposure time, t_{ex}, for each camera was set to the smallest possible time whilst still obtaining a high-contrast speckle pattern. This approach minimises any motion blur during the exposure. The cameras were synchronised using a TTL pulse, generated when a frame exposure starts, from the first camera into the second camera. If the cameras were not synchronised, movement in between the starting times for the frame exposures for each camera would cause errors in the positions calculated by the DIC algorithm. The cameras were remotely triggered simultaneously, 150 ms before the charge was detonated.

A heavy duty studio-type camera stand was used to hold the cameras in position during the blast. Rubber isolating feet were used on the stand base to isolate it from ground shock. Ballast was also added to the stand base to increase mass and minimise any motion of the stand. The cameras were mounted on a single beam which was then attached to the camera stand. This arrangement minimises any movement of cameras relative to each other.

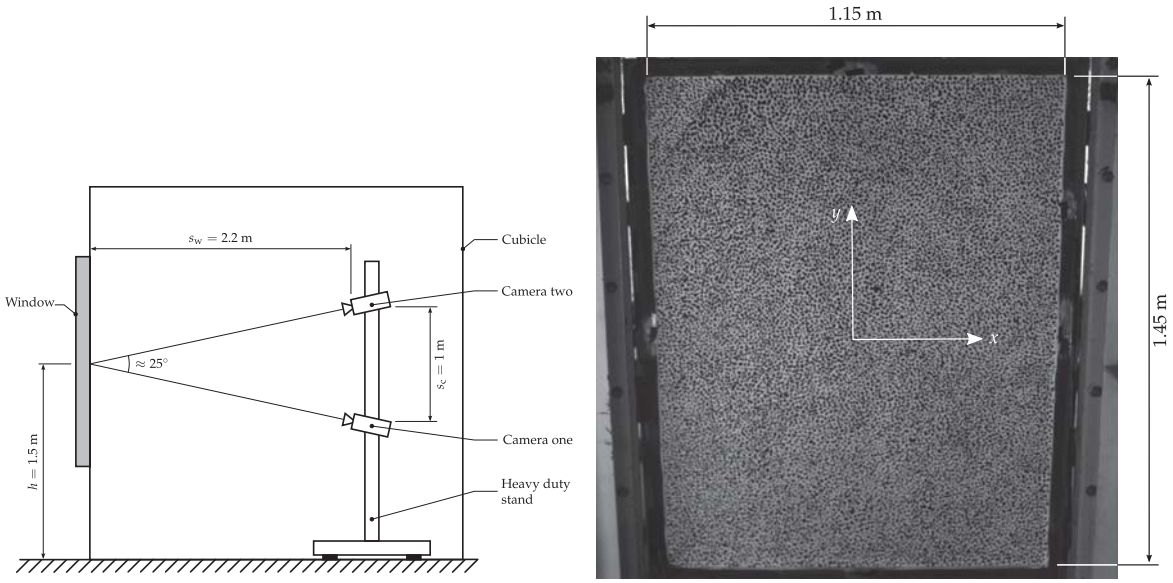

(a) High-speed camera setup.

(b) Speckle pattern viewed from the top camera.

Figure 3: High-speed camera setup.

Table 2: Digital image correlation setup.

Test	Camera Type	Resolution (pixels)	Frame rate (Hz)	Focal length (mm)	Pixel size (μm)	t_{ex} (μs)	s_w (m)	s_c (m)	d_s (mm)	d_p (mm)	n_p
1	Phantom V4	512 × 512	1000	8	16	40	2.2	1	9	28	2100
2	Phantom V4	512 × 512	1000	8	16	40	2.2	1	9	31	1600
3	Phantom V5	1024 × 1024	1000	24	16	76	2.2	1	5	21	3300
4	Phantom V5	1024 × 1024	1000	24	16	76	2.2	1	5	19	4400

3.1.1. Speckle pattern and lighting

To enable the image correlation algorithm to track the window surface a stochastic speckle pattern was applied to the rear surface of the window as shown in Figure 3b. Acrylic paint was used as it provides good flexibility and good adhesion to the glass surface. The image correlation technique is more robust with high-contrast speckle patterns. A high-contrast pattern was achieved by applying a white base coat and allowing it to dry before painting black speckles over the top. The black speckles were either painted by hand using an artists brush or with a foam block (containing multiple speckles carved into the base), with care taken to ensure a random pattern was achieved

The minimum speckle diameter, d_s, was determined from the size of the test panel and the camera resolution. For accurate pattern matching, each speckle should be sampled by at least a 3 by 3 pixel array (Sutton et al., 2009). Each speckle should therefore be over 3 pixels in diameter. Dividing the panel size by the camera resolution and multiplying by 3 then gives the minimum speckle diameter. The approximate speckle size used for each panel is given in Table 2.

Light from the explosion can cause over-exposure of the cameras inside the cubicle. To mitigate this problem black acrylic paint was applied to the front of the window (facing the charge) to reduce the light transmitted through the window. Two 1.25 kW halogen flood lights were used to illuminate the window from inside the cubicle, providing even and constant lighting conditions during the test.

3.1.2. Computation of 3D position and strain

In each window the position and strain of the entire rear surface was calculated using the ARAMIS image correlation software produced by GOM mbH. For full details of the image correlation method refer to Sutton et al. (2009). Each camera setup was calibrated before the blast by taking between 14-25 image pairs of a known calibration grid. These image pairs were imported into the software to determine the calibration parameters for each of the eight particular test setups. Accuracy of the calibration was verified by placing a speckled object 300 mm away from the window surface and capturing an image. This image was then analysed in ARAMIS to check the calculated distance between the object and window surface, as well as the overall window dimensions. Central displacement calculated by this system during a blast test has been verified using a linear displacement laser gauge (Arora et al., 2011). The sequences of image pairs captured during the blast were then imported for analysis. The flash from the detonation was used synchronise the image sequences with the pressure and strain data. An image of the undeformed window was set as the reference image and all correlation calculations were made relative to this image. After calculation the coordinates and corresponding strain values of each point were then exported for further analysis. The

calculated data for each image pair will be referred to as stage data. The number of points computed, n_{p}, and the approximate point spacing, d_{p}, are given in Table 2 for each test.

An estimate of the uncertainty introduced by noise in the images was made by comparing images of the laminated pane before detonation of the charge. The maximum error in the computed out-of-plane displacement was of the order of ± 0.1 mm. The maximum error in the computed in-plane strain components was of the order of $\pm 0.05\%$.

The coordinate system origin was defined as the centre point of each window as viewed in Figure 3b. The x-axis was defined as positive in the horizontal direction towards the right-hand edge of the cubicle and the y-axis was defined as positive in the vertical direction towards the top of the cubicle. In an undeformed state the rear surface of a window lies on the xy-plane. The z-axis, normal to the xy-plane, was defined as positive for inward deflection (towards the cameras).

3.1.3. Post-processing of image correlation data

Analysis of the image correlation data was conducted using the numerical computation software MATLAB. The computed displacements and strains at each stage were imported into the software and interpolated onto to a regular spaced grid to enable easy analysis. Central displacement time histories were generated by compiling values at the regular grid centre. Cross-sections were generated by taking values across the centre of the regular grid in the horizontal and vertical direction for each stage.

Out-of-plane velocity fields were found by computing the numerical derivative of the displacement field with respect to time, using the central differencing method. The acceleration fields were then found by computing the numerical derivative of the velocity field with respect to time. Central velocity and acceleration time-histories were then compiled from the values at the grid centre. The strain rate fields were found using the same method, computing the numerical derivative of the strain field with respect to time. The slope at each point on the deformed window surface was found by computing the numerical gradient of the displacement field in the x and y directions. The numerical gradient was again calculated using the central differencing method. The slope at the centre of each edge was then used to calculate the angle formed between the displaced window and the frame.

3.2. Edge reaction force measurement

Strain gauges were used to measure the edge reaction forces for all eight test windows. Pairs of foil strain gauges were bonded to the steel subframe at the midpoint of each edge. Strain gauges of type CAE-06-062UW-120 were used with AE-10 adhesive, both from Vishay Measurements Group. The position of the gauges on the subframe cross-section is shown in Figure 4a. Four strain gauge pairs were bonded to the

midpoint on each frame edge. An additional pair was attached to the frame of window one in tests three and four offset by 350 mm above the midpoint on the wall edge to record variation in reaction force along the edge. Each gauge was connected in quarter bridge configuration to a Vishay 2120A strain gauge amplifier housed in a smaller cubicle behind the main test cubicle. The output from each strain gauge amplifier was recorded at 500 kHz.

3.2.1. Postfracture edge reaction analysis

The strain readings from each gauge were used to calculate the tension in the cracked laminate, F, by considering the subframe as a built-in cantilever beam. The geometry of the joint used in this analysis is shown in Figure 4b where θ is the angle of pull, l_g is the distance between the centre of the strain gauges and the end of the steel angle, d_e is the distance between the middle of the steel angle thickness and the middle of the laminate thickness, and d_a is the thickness of the steel angle.

The strain variation across the beam at point P is a combination of the direct axial strain, ε_A, and the bending strain, ε_B, as shown in Figure 4c. The strain, ε, varies across the thickness as a function of the distance from the centre, y_a,

$$\varepsilon = \varepsilon_\mathrm{B}\frac{2y_\mathrm{a}}{d_\mathrm{a}} + \varepsilon_\mathrm{A} \tag{1}$$

and ε is positive in tension. At the outer surface of the beam (facing the blast wave) $y_\mathrm{a} = {}^{d_\mathrm{a}}/_2$ and the strain $\varepsilon_\mathrm{o} = \varepsilon_\mathrm{B} + \varepsilon_\mathrm{A}$. At the inner surface $y_\mathrm{a} = -{}^{d_\mathrm{a}}/_2$ and the strain $\varepsilon_\mathrm{i} = \varepsilon_\mathrm{A} - \varepsilon_\mathrm{B}$. The axial and bending strain can be calculated directly from the gauge readings ε_o and ε_i ,

$$\varepsilon_\mathrm{A} = \frac{\varepsilon_\mathrm{o} + \varepsilon_\mathrm{i}}{2} \tag{2}$$

$$\varepsilon_\mathrm{B} = \frac{\varepsilon_\mathrm{o} - \varepsilon_\mathrm{i}}{2} \tag{3}$$

The axial strain is produced by the horizontal component of F and can be found by assuming the beam is linear elastic and that F and θ are constant along the edge length,

$$\varepsilon_\mathrm{A} = \frac{F\cos\theta}{bEd_\mathrm{a}} \tag{4}$$

where ${}^F/_b$ is the force per unit edge length (perpendicular to the page in Figure 4b) and E is the Young's modulus of the beam. Rearranging in terms of force per unit length of edge bond gives,

$$\frac{F}{b} = \frac{E d_{\mathrm{a}}}{\cos\theta}\varepsilon_{\mathrm{A}} \tag{5}$$

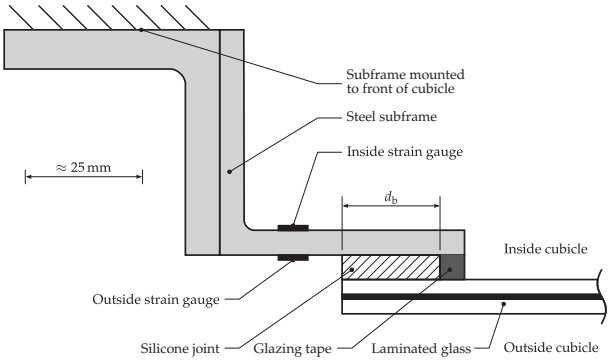

(a) Subframe cross section.

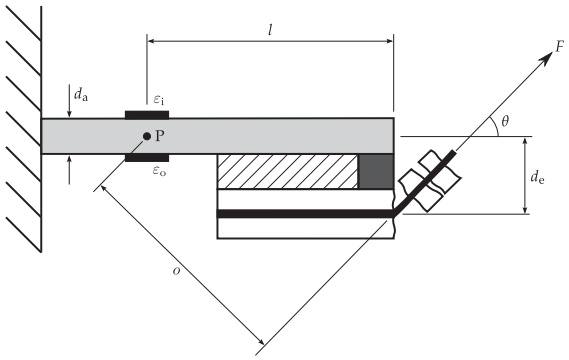

(b) Simplified geometry.

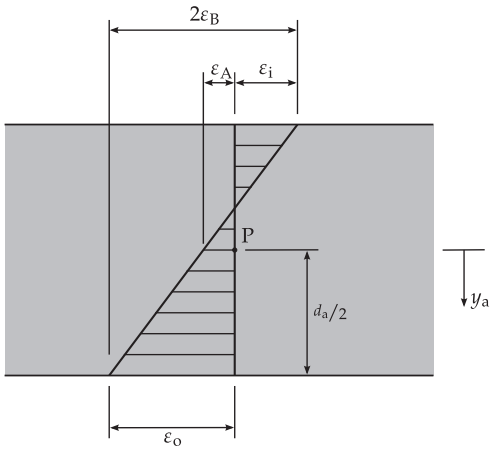

(c) Strain variation across the steel angle at the strain gauge location.

Figure 4: Cross section of edge fixing and strain gauge arrangement.

The bending strain is produced by a moment about point P created by a couple Fd_{o},

$$M_{\mathrm{P}} = Fd_{\mathrm{o}} \tag{6}$$

where distance d_{o} can be calculated from,

$$d_{\mathrm{o}} = l_{\mathrm{g}} \sin\theta + d_{\mathrm{e}} \cos\theta \tag{7}$$

assuming the steel angle only experiences small deflections. This moment causes the internal strains at P. The incremental force due to the strain at a point on the beam cross-section is $\mathrm{d}F_{\varepsilon} = E\varepsilon b\,\mathrm{d}y_{\mathrm{a}}$. The moment of $\mathrm{d}F_{\varepsilon}$ about P is $\mathrm{d}M_{\mathrm{P}} = y_{\mathrm{a}}\,\mathrm{d}F_{\varepsilon}$. The total moment over the entire cross section is therefore,

$$M_{\mathrm{P}} = Eb \int_{-d_{\mathrm{a}}/2}^{d_{\mathrm{a}}/2} y_{\mathrm{a}}\varepsilon\,\mathrm{d}y_{\mathrm{a}} \tag{8}$$

Substituting Equation 1 into 8 and integrating across the thickness gives,

$$M_{\mathrm{P}} = Ebd_{\mathrm{a}}^2 \frac{\varepsilon_{\mathrm{B}}}{6} \tag{9}$$

Equation 9 is simply the bending equation for a rectangular beam. The axial strain present in the beam does not contribute to M_{P} since its net moment is zero.

Setting Equation 6 equal to 9 and rearranging gives the force per unit of edge length in terms of bending strain,

$$\frac{F}{b} = \frac{Ed_{\mathrm{a}}^2}{6(l_{\mathrm{g}} \sin\theta + d_{\mathrm{e}} \cos\theta)} \varepsilon_{\mathrm{B}} \tag{10}$$

Equations 5 and 10 can be solved simultaneously to give,

$$\tan\theta = \frac{d_{\mathrm{a}}}{6l_{\mathrm{g}}} \frac{\varepsilon_{\mathrm{B}}}{\varepsilon_{\mathrm{A}}} - \frac{d_{\mathrm{e}}}{l_{\mathrm{g}}} \tag{11}$$

$$\frac{F}{b} = Ed_{\mathrm{a}} \sqrt{\varepsilon_{\mathrm{A}+}^2 \left(\varepsilon_{\mathrm{B}} \frac{d_{\mathrm{a}}}{6l_{\mathrm{g}}} - \varepsilon_{\mathrm{A}} \frac{d_{\mathrm{e}}}{l_{\mathrm{g}}} \right)^2} \tag{12}$$

These equations can be used to find both the force and angle of pull at the frame edge after the glass layers have fractured. However, both equations rely on the ability to separate out the axial strain from the bending strain using the gauge readings ε_{o} and ε_{i}. The axial strain is particularly difficult to extract reliably and is sensitive to a number of variables. It was found that the measured axial strain, ε_{A}, was not accurate

enough to reliably calculate the angle and force using Equations 11 and 12. Therefore, measurements for the angle of pull were made directly from analysis of the DIC displacement results. This was done using the two deflection points closest to the specimen edge at each strain gauge location. Then, using the measured angle in Equation 10 removes the need to find the axial strain component. For these reasons Equation 10, combined with the angle measured by DIC, was used to calculate all the edge forces after fracture of the glass plies.

4. Laminated glass finite element model

A finite element (FE) model of a 1.5 m × 1.2 m laminated glass pane with layup [3, 1.52, 3] mm was constructed in the Abaqus finite element software package. To simplify the modelling procedure the response of the laminated glass was split into two separate models, one to describe the precrack response and one to describe the postcrack response. A maximum stress criterion was used to determine the time of fracture of the glass layers. When a maximum principal stress greater than 80 MPa was observed (Cormie et al., 2009), the glass was assumed to have fractured and precrack model was stopped, with the current strain, position, and velocity of each element in the model then written to an output file. These were then imported into the postcrack model as initial conditions, along with any remaining load if the precrack model failed before the blast pressure pulse was over. The time-varying blast pressure was applied as a uniform pressure field across the window surface. This simplification allows symmetry conditions to be used, reducing computation time.

4.1. Precrack model

Two models were developed to describe the initial precrack response of the laminated glass, one simplified model using shell elements and one using solid continuum elements to capture the viscoelastic response of the PVB interlayer. The more complex solid continuum element model was developed to show that the simplified shell element model adequately captures the precrack response.

4.1.1. Shell element model

Shell elements describe the bending and in-plane (membrane) deformation of structures in which one dimension is significantly smaller than the others (plate-like structures). The S4R shell element in Abaqus is a 3D quadrilateral finite-membrane-strain shell element and was chosen to capture the laminated glass behaviour in this model.

A typical mesh generated by discretising the laminated glass pane into shell elements is shown in Figure 5. The coordinate system origin was defined at the centre of the laminated pane (shown by **O** in Figure 5) with the x-axis in the horizontal direction, the y-axis in the vertical direction and the z-axis positive in the

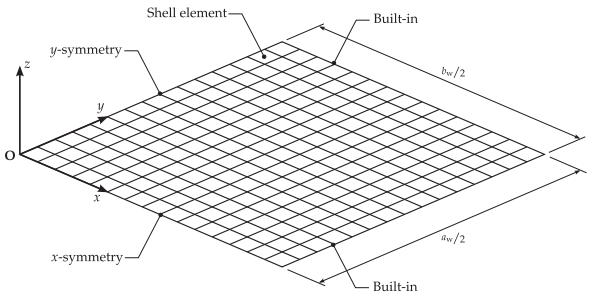

Figure 5: Simplified one-quarter model of laminate glass pane with shell elements.

direction of the applied pressure. This is the same coordinate system used in the DIC measurements. Only one quarter of the laminated glass pane was modelled as the assumption of a uniform pressure field across the window surface allows symmetry conditions to be imposed along the x-axis and y-axis. Displacements and rotations at the remaining two edges were assumed to be zero, giving a built-in type boundary condition similar to that provided by a deep joint. This is a simplification as the elasticity of a silicone joint will allow for some movement at the laminated glass edges. However, results of the simulation will be conservative since preventing this movement will increase stress levels in the pane, causing failure to occur earlier than in reality.

The cross-sectional behaviour of the shell elements was calculated from the material properties and thickness of each layer in the laminated glass. The glass layers were modelled with a linear elastic material model and their material properties are given in Table 3. Two material models for the PVB interlayer were analysed, a simple linear elastic material model and a viscoelastic material model to capture stress relaxation in the interlayer.

The solution of the model was found using the explicit solver in Abaqus (version 6.9). The time step used in the analysis was automatically controlled by the program to ensure numerical stability throughout the analysis. The number of elements in the finite element mesh was increased until the deflection profile at time of fracture converged on a solution. The converged shell element model had 1008 elements, each 20 mm × 20.4 mm. Typical computation time using a 2 GHz dual-core desktop processor was between 20 and 60 seconds for a refined mesh.

4.1.2. Small strain viscoelastic properties of PVB

The viscoelastic properties of PVB at small strains was measured using a TA Instruments Q800 dynamic mechanical analysis (DMA) machine. In DMA a sinusoidal strain is applied to a sample and the resulting stress is measured in order to calculate the storage modulus (the ratio between in-phase stress component

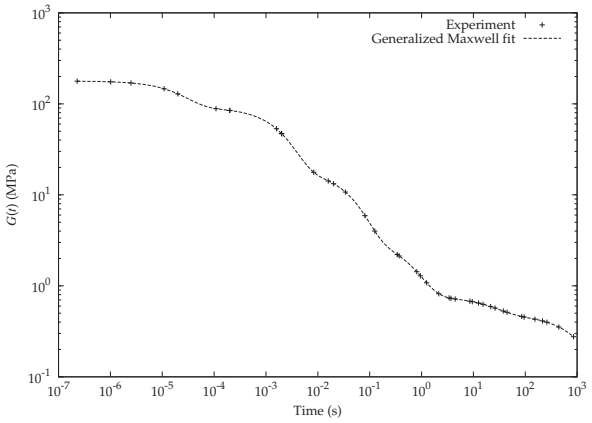

Figure 6: Shear relaxation curve for PVB measured using DMA.

Table 3: Section properties for laminated glass.

Layer	Material	Thickness (mm)	Density (kg/m^3)	Young's modulus (GPa)	Poisson's ratio
1	Glass	3	2530	72	0.22
2	PVB	1.52	1100	0.53*	0.485
3	Glass	3	2530	72	0.22

* Instantaneous elastic modulus for linear-elastic behaviour.

and strain) and loss modulus (the ratio between out-of-phase stress component and strain). This method was performed over a range of frequencies and temperatures to characterise the material at different time scales. The results of the DMA testing were used to construct a shear relaxtion curve using the procedure outlined in Bennison et al. (1999).

The experimentally determined shear relaxation curve is shown in Figure 6 along with a Generalized Maxwell model fit. In the linear elastic model a Young's modulus value of 530 MPa was used. This value corresponds to the instantaneous shear modulus value measured using dynamic mechanical analysis (DMA) and describes the behaviour at short time scales. The viscoelastic material model was defined in Abaqus using the Generalized Maxwell model fitted to DMA results. The terms used in the Generalized Maxwell model are given in Table 4.

4.1.3. Limitations of shell elements

The S4R shell element formulation in Abaqus accounts for nonlinear material behaviour and changes in layer thickness due to in-plane stress by recalculating section properties during the analysis (Simulia, 2010). However, shell elements assume that there is a linear variation of in-plane strain across the thickness of the

Table 4: Terms for viscoelastic material model of PVB.

i	G_i/G_0	τ_i (s)
1	0.49016	2.45×10^{-5}
2	0.40844	2.21×10^{-3}
3	0.08522	4.98×10^{-2}
4	0.01389	6.24×10^{-1}
5	0.00159	2.49×10^{1}

* Instantaneous shear modulus $G_0 = 178\,\text{MPa}$, long-term shear modulus $G_\infty = 0.125\,\text{MPa}$

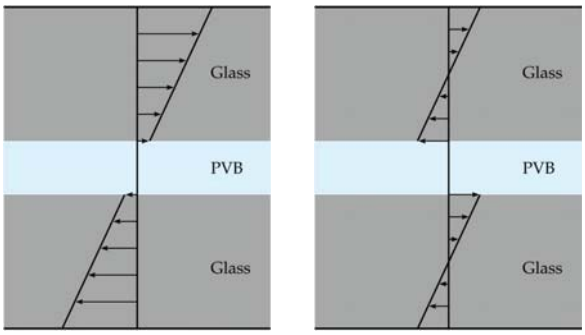

(a) Linear (b) Nonlinear

Figure 7: In-plane stress distribution through laminated glass thickness.

shell section when placed under bending. This is similar to the assumption in classical beam theory that plane sections in the undeformed beam remain plane when the beam is loaded.

In laminated glass this assumption may not be valid if there is a significant difference in the modulus values between the glass and PVB layers. Figure 7a shows the flexural stress distribution in the laminated glass if the in-plane strain varies linearly. The flexural stress distribution in each glass layer is collinear, that is they lie on a single straight line. The stress in the PVB layer is not visible because it is orders of magnitude less than that in the glass due to the difference in moduli. If the modulus in the PVB is drastically lower than that of the glass, the in-plane strain across the thickness of the shell section may depart significantly from the assumed linear variation. The extreme case is when the PVB's only function is to maintain the separation distance between the glass layers. The stress distribution in this case is shown in Figure 7b.

Norville et al. (1998) developed an analytical model of laminated glass beams where the in-plane strain across the thickness was allowed to depart from the linear assumption. The effective section moduli that they

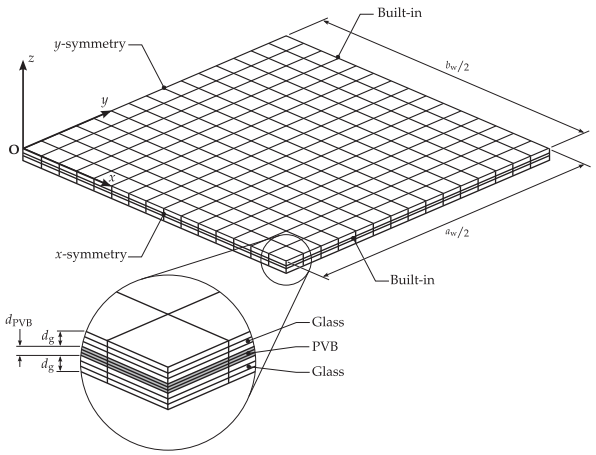

Figure 8: Solid element one-quarter model of laminate glass pane.

calculated for laminated glass beams approached those of monolithic beams of the same overall thickness when the loading duration was short or the temperature was low. This indicates that the assumption of a linear variation of in-plane strain across the thickness of the shell section is likely to be valid. To validate this further a full 3D solid element model of the laminated glass pane was also developed.

4.1.4. Solid element model

To fully capture cross-sectional behaviour of the laminated glass and the effects of viscoelasticity in the PVB interlayer a model using 3D solid continuum elements was constructed. By using a number of solid continuum elements over the thickness of the laminated glass the nonlinear variation of in-plane strain across the laminate thickness can be accounted for. The C3D8I solid continuum element in Abaqus was chosen for this model as it provides a good description of bending behaviour whilst remaining relatively computationally efficient (Simulia, 2010).

A typical structured regular mesh generated by discretising the laminated glass pane into solid elements is shown in Figure 8. The model is very similar to the shell element model except that each layer has three elements across its thickness, giving a total of nine elements across the thickness of the laminated pane. The material properties used were the same as those for the shell element model, as given in Tables 3 and 4. Simulation were conducted with both a linear elastic and viscoelastic material model of the PVB interlayer. This was to verify the results of the shell element model and to investigate the effect of the viscoelasticity on the laminated pane response. In both cases geometric nonlinearity was accounted for in the simulation.

The explicit solver in Abaqus was used again to find the solution and the number of elements in the finite element mesh was increased until the deflection profile at time of fracture converged on a solution.

The converged solid element model had 3 elements through each ply, giving a total of 9 through the thickness of the laminate. The laminated pane was divided into 5 mm × 5 mm blocks, giving a total of 162,000 elements. Typical computation time for the solid element model using a 2 GHz dual-core desktop processor was between 10 and 20 hours for a refined mesh, a significant increase over the shell element model.

4.1.5. Effect of viscoelasticity in the PVB

To determine the effect of viscoelasticity in the PVB interlayer on the blast response of the laminate glass, the two precrack models were solved with and without viscoelasticity in the interlayer. A blast load with a peak reflected pressure of 130 kPa and a positive phase duration of 6.5 ms, giving a total reflected impulse of 423 kPa · ms, was applied to the laminated glass pane. This blast loading would be equivalent to that generated by a 30 kg TNT charge at a stand off distance of 14 m, the same loading as in test 4. The analysis was run until the maximum principal tensile stress in the glass layers exceeded 80 MPa (Cormie et al., 2009).

Figure 9 shows a comparison of the profiles predicted by the two models with and without viscoelasticity in the interlayer at a time of 1.2 ms, the approximate time of fracture in the glass. The solid element model without viscoelasticity and both shell element models give near identical deflection profiles. Viscoelasticity in the shell element model has little effect because a nonlinear variation of in-plane strain across the pane thickness is not possible with these elements. The flexural stresses in the interlayer are too small compared to those in the glass layers to make a significant difference to the response. The agreement between the elastic solid element and elastic shell element models suggests that the difference in modulus between the glass and PVB layers is not large enough to cause a significant departure from the assumption of a linear variation of in-plane strain across the pane thickness.

The deflection profile predicted by the viscoelastic solid element model departs slightly from those generated by the other three simulations. This is because a small amount of relaxation occurs in the interlayer, increasing the difference in modulus between the glass and PVB layers and reducing the flexural stiffness of the laminated glass section. Figure 10 shows the in-pane stress distribution across the thickness, y_l, of the laminate at $x = 360$ mm and $y = 0$ mm, the location of maximum stress on the horizontal cross-section, for the different models. As expected the shell elements show a collinear stress distribution in each glass layer and small stresses in the PVB interlayer. The stress distribution does not intersect through zero since there is also a tensile membrane stress; the shell is not in pure bending.

In the solid element model, the in-plane stress distributions in each glass layer remain parallel but are now offset. The linear in-plane strain distribution across the laminate thickness is no longer enforced and

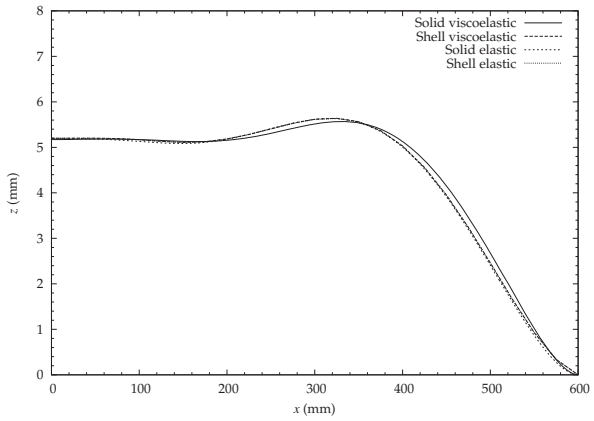

Figure 9: Comparison of deflection profiles at the pane centre ($y = 0\,\text{mm}$) and a time of 1.2 ms produced by different models.

each glass layer is allowed to bend somewhat independently. The offset in the stress distributions in each glass layer is determined by how much horizontal shear force the PVB interlayer transfers from one glass layer to the other. In the extreme case shown in Figure 7b no horizontal shear force was transferred between the glass layers. In Figure 10 only a small reduction in the horizontal shear force transfer is seen. The reduction in the horizontal shear force transfer is dependent on the PVB modulus. The solid viscoelastic model shows a greater offset in the stress distributions in each glass layer than the solid elastic model due to stress relaxation in the interlayer.

The effect of this stress relaxation in the interlayer on the overall deflection profile is small (Figure 9). The maximum principal stress in the glass layers is also reduced by stress relaxation in the interlayer,

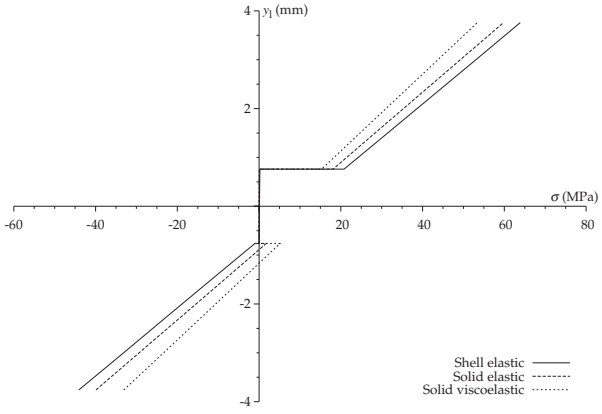

Figure 10: Comparison of maximum principal in-plane stress predicted at $x = 360\,\text{mm}$ and $y = 0\,\text{mm}$ by different models.

meaning the glass is likely to fracture at a later time. The effects of stress relaxation may become more pronounced in long duration loading cases, in which the peak pressure to cause failure is lower and in which the glass takes tens of milliseconds to fracture. In these cases the flexural stiffness of the laminate would decrease over time, reducing the stress in the glass layers and delaying fracture.

4.2. Postcrack model

A shell element model was constructed to model the postcrack phase of the laminated glass response. The postcrack model was identical to the precrack shell element model except for modified material properties to describe the stress-strain response of cracked laminated glass. Cracks in the glass layers were assumed to have developed instantaneously and densely across the whole window pane at the end of the precrack model. The elastic modulus of the glass layers was therefore reduced to approximately zero to account for this[1]. The glass layers were not removed completely from the model since their mass still contributed to the response of the laminate.

The material properties of the interlayer were changed to describe the overall tensile stress-strain response of the cracked laminated glass, investigated experimentally using a high-speed servo-hydraulic test machine. Figure 11 shows the experimental setup for measuring the stress-strain response of cracked laminated glass at different strain rates. A Johnson-Cook (JC) plasticity model was chosen to describe the rate dependent stress-strain response of cracked laminated glass. The JC model is empirically based and was originally developed to describe the effects of strain rate and temperature on the plastic deformation of metals (Johnson and Cook, 1985). When the effects of temperature are ignored, the stress required for plastic flow is defined as

$$\sigma = \left(A + B\varepsilon_{\mathrm{p}}^{n}\right)\left(1 + C\ln\frac{\dot{\varepsilon}}{\dot{\varepsilon}_0}\right) \tag{13}$$

where ε_{p} is the plastic strain, $\dot{\varepsilon}$ is the strain rate, $\dot{\varepsilon}_0$ is a reference strain rate and A, B, C and n are material constants. The terms in the first bracket describe the yield stress of the material as the plastic strain increases at the reference strain rate. The second bracket accounts for the increase in yield stress with increasing strain rates.

The JC plasticity model does not completely capture the behaviour of cracked laminated glass. Use of the JC plasticity model in Abaqus requires that the initial elastic modulus is independent of strain rate. The modulus of cracked laminated glass was observed to show a dependence on strain rate. For randomly cracked

[1] A value of 1 Pa was used as Abaqus will not accept zero stiffness.

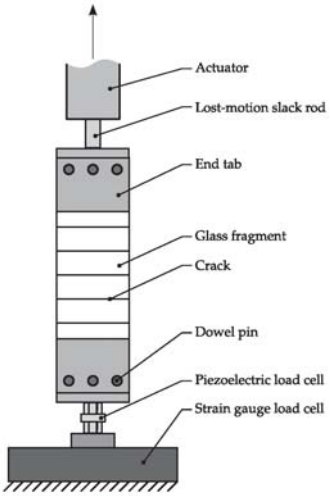

(a) Test setup

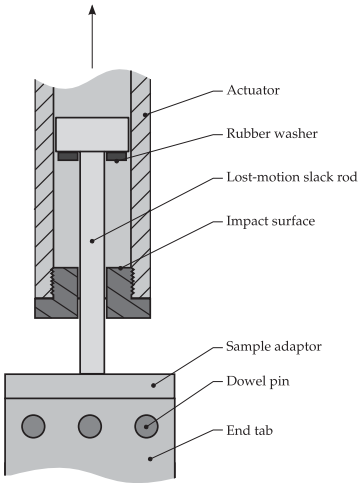

(b) Lost motion device

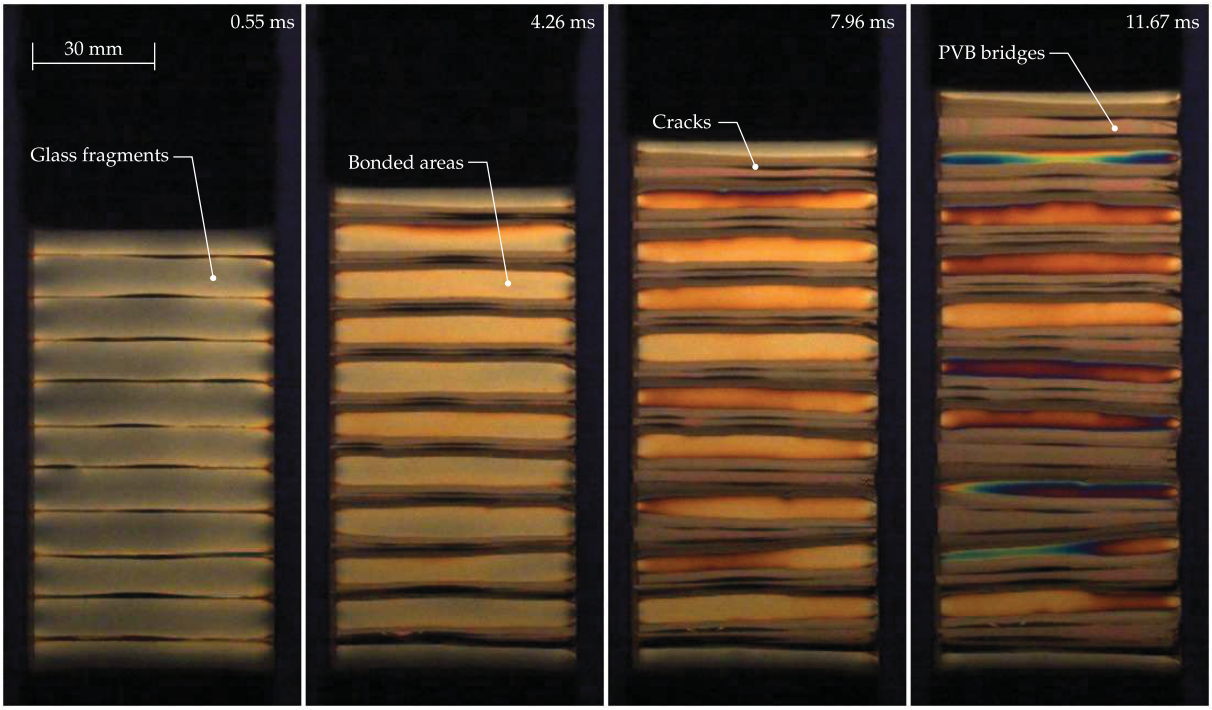

(c) Cracked laminated glass test viewed through polarizing filters

Figure 11: Cracked laminated setup with images of delamination process.

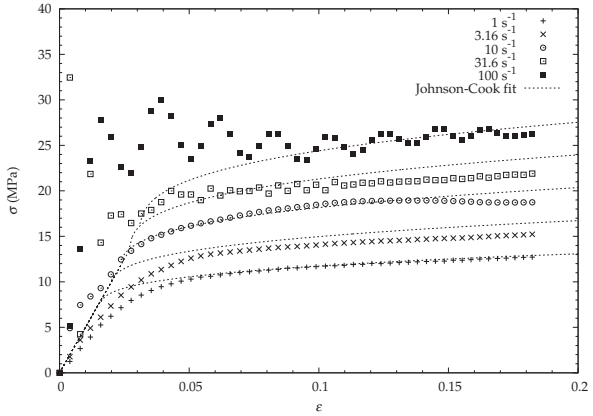

Figure 12: Johnson-Cook model of 7.52 mm cracked laminated glass.

laminated glass with an interlayer thickness of 1.52 mm the observed modulus varied between 0.3 GPa and 14 GPa for strain rates between $1\,s^{-1}$ and $100\,s^{-1}$. However, strain rates observed in blast testing were in the order of $1\,s^{-1}$ to $10\,s^{-1}$. These equate to moduli values of 0.3 GPa to 0.8 GPa. An assumed initial modulus of 0.55 GPa was therefore chosen to represent the modulus at the expected strain rates.

The JC model was designed for plasticity. Any deformation above the yield stress is permanent and only the elastic deformation is recovered on the removal of the applied stress. The cracked laminated glass is not fully plastic and if given enough time will exhibit some recovery to almost its initial length. If it is assumed that the time scale for complete recovery is orders of magnitude greater than the duration of the blast response, then the deformation of cracked laminated glass is essentially plastic over the time scales of interest. If the postcrack model is only used up to the point of maximum deflection, it is assumed that recovery effects can be ignored.

Equation 13 was fitted to the experimental data obtained for randomly cracked laminated glass with an interlayer thickness of 1.52 mm using nonlinear regression. Material constants A, B and n were determined first by fitting the model to the data obtained at a reference strain rate $\dot{\varepsilon}_0$ of $1\,s^{-1}$. The constant C was then determined by fitting the model to the data obtained at increased strain rates. Figure 12 shows a comparison between the stress-strain curves calculated by the JC model and the experimental results. The determined material constants are given in Table 5. The oscillation of stress at the high strain rates ($100\,s^{-1}$) are dynamic inertial effects due to the test method and are not part of the material response.

4.3. Blast load prediction

The blast load applied to the window in the laminated glass finite element model was predicted using the Air3D software packages (Rose, 2001). The Air3D simulations were conducted using the ftt_air3d

Table 5: Constants for Johnson-Cook model of cracked 7.52 mm laminated glass.

A (MPa)	B (MPa)	C	n
6.72	10.6	0.248	0.303

(version 1) variant of the Air3D code with adaptive mesh refinement and detonation modelling using the Jones-Wilkins-Lee (JWL) equation-of-state (Dobratz and Crawford, 1985). Each simulation was conducted with an initial 1D solution of the detonation and blast wave between the charge centre and the ground (the charge was assumed to be spherical). Once the wavefront reached the ground the 1D solution was remapped to a 2D analysis of the blast wave. This was so that ground reflections were included in addition to the wave directly from the charge (the ground was assumed to be a perfect reflector). This analysis was carried out until the wavefront reached the test cubicle. After this a full 3D analysis of the interaction between the blast wave and the cubicle was performed. This was to account for the reduced impulse on the window due to clearing effects. The cubicle was modelled as a rigid target and a plane of symmetry was defined in the vertical direction between the charge centre and the centre of the test cubicle. A pressure monitoring point was defined at the centre of the window to record reflected pressure. The cell size used in the simulations was refined until the calculated reflected impulse converged on a solution.

5. Results and discussion

The experimental results from the full scale blast tests are presented and compared with the predictions of the laminated glass finite element model to give a clear account of the behaviour of laminated glass under blast loading and to demonstrate the applicability of the model to different blast loads. The FE predictions were made using the pressure output from the Air3d simulations. Figure 13 shows measured central displacement-time histories for each test and these data are compared with predictions from the FE model. Measured reflected pressure time histories are also shown along with those predicted by Air3d as detailed in Section 4.3. These data are synchronised so that $t = 0$ ms corresponds to the arrival of the blast wave.

The measured central displacement data shows good agreement with predictions in the early phase of the laminated glass response. The effect of restraint at the edges on the central displacement is minimal at this stage and the central displacement is largely determined by the applied pressure and the area mass density of the laminate. A summary of the blast pressures and the response of the laminated glass pane in each test is given in Table 6 and Table 7.

Table 6: Summary of DIC measurements for each test.

Test	W (kg)	R (m)	$z_{\max}$ (mm)	$v_{\max}$ (m/s)	$a_{\max}$ (km/s^2)	$\varepsilon_{\max}$	$\dot{\varepsilon}_{\max}$ (s^{-1})	$\theta_{a,\max}$ (deg)	$\theta_{b,\max}$ (deg)	Failure description
1*	15	10	179	27.3	6.1	0.15	20	34	37	Joint failed at all edges. Pane came to rest soon after joint failed and fell outside the cubicle.
2	15	13	173	17.4	3.4	0.04	10	24	23	Pane rebounded. Joint failed at inner edge on rebound.
3*	30	16	205	20.5	3.6	0.06	10	26	27	Joint failed at inner edge leading to top edge.
4*	30	14	140	29.0	6.0	0.06	15	30	34	Joint failed at all edges. Significant inward velocity after failure and pane impacted screen protecting cameras.

* Values taken up to the point of failure.

In Test 1 (15 kg at 10 m) the single sided joint failed around the perimeter. The joint failure was first observed at 9 ms (180 mm displacement). The pane reaches a maximum velocity of 26 m/s and came to rest at a displacement of approximately 350 mm.

In Test 2 (15 kg at 13 m) the pane reached a maximum deflection of approximately 170 mm at 14 ms before rebounding. The single sided joint began to fail on the rebound phase. No tearing of the PVB interlayer was observed. The peak velocity was approximately 18 m/s.

In Test 3 (30 kg at 16 m) a displacement of approximately 200 mm was reached before the joint began to fail down the left hand edge at a time of 12 ms. The DIC technique was unable to compute results beyond this time due saturation of the images from light entering around the failed joint. No tearing of the PVB interlayer was observed. The peak velocity was approximately 21 m/s.

In Test 4 (30 kg at 14 m) the joint had completely failed around the perimeter by 8 ms at a displacement of approximately 265 mm. The pane was still accelerating at this point and continued travelling into the cubicle until it impacted a screen protecting the cameras. The peak velocity was approximately 34 m/s. No tearing of the PVB interlayer was observed.

The following figures (Figures 14 to 17) show the images captured by the high speed camera alongside the displacement and strain measured using DIC and are compared with the predictions from the laminated glass FE model. In all cases, the magnitude and contour shape of the out-of-plane displacement plots for DIC measurements and FE predictions agree very well. The maximum in-plane principal strain plots show regions of high strain along the edges for both DIC and laminated glass FE model but there are some differences in strain magnitude.

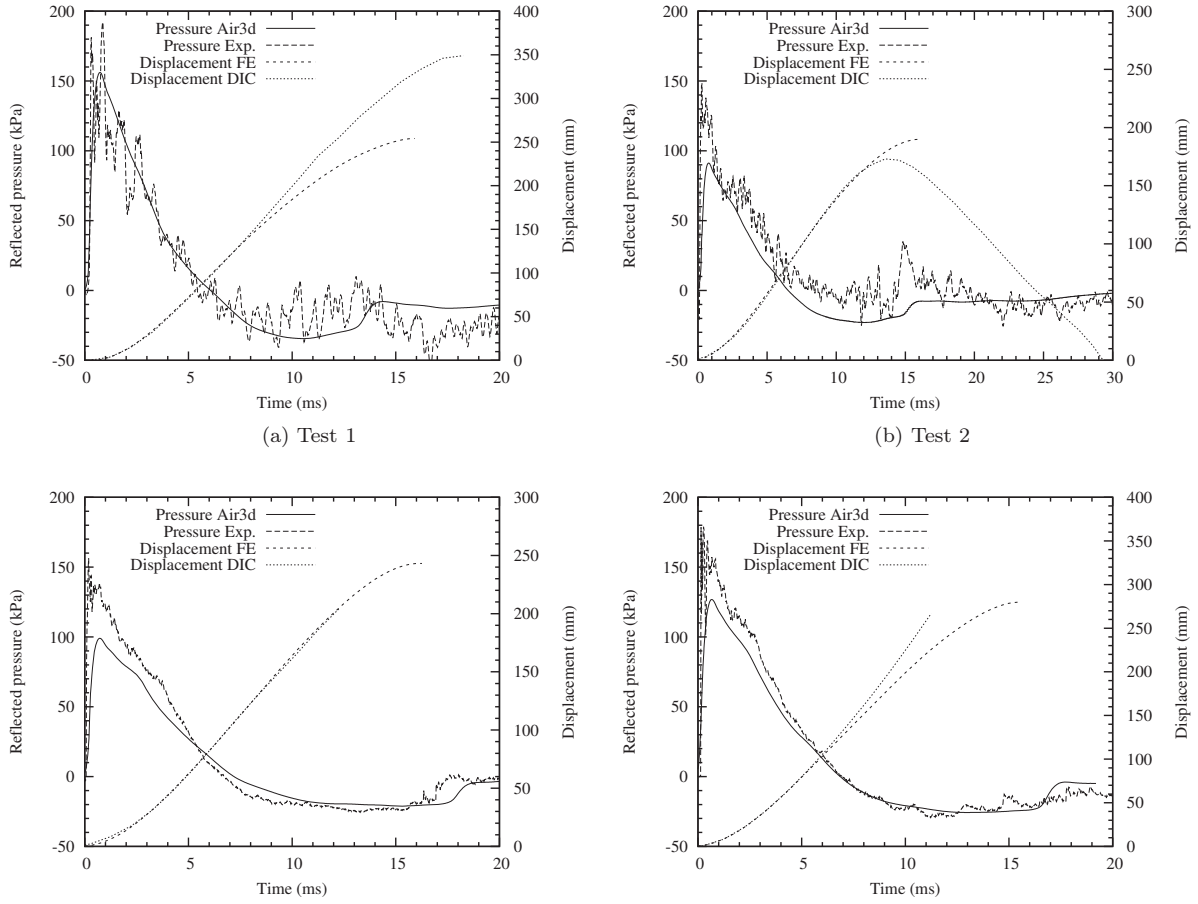

(a) Test 1 (b) Test 2

(c) Test 3 (d) Test 4

Figure 13: Comparison of measured and predicted reflected pressure and central displacement for each test.

5.1. Deflected shape and strain

The contour lines in Figures 14 to 17 are approximately rectangular in shape and are spaced more tightly close to the window edges. This indicates that the deformed areas are concentrated around the window edges and that the central region of the window is largely flat and undeformed. In some of the DIC displacement plots the contour lines are not rectangular and surround an area towards the bottom left of the plots, indicating that the window has deflected more in this region. This is because the pressure and impulse on the window are higher near to the bottom of the window due to the blast wave reflecting from the ground. The blast wave arrival time was also sooner here.

Under blast loading the window pane has a peak initial acceleration and quickly acquires an approximately uniform velocity field across its surface. If the blast wave duration is short compared to the natural

Table 7: Peak pressure and positive impulse at pane centre.

			Experiment		Air3d	
Test	W (kg)	R (m)	p_r (kPa)	i_r (kPa · ms)	p_r (kPa)	i_r (kPa · ms)
1	15	10	180	391	155	391
2	15	13	140	284	91.2	284
3	30	16	132	413	99.0	344
4	30	14	152	461	127	413

period of the pane response the subsequent deflection occurs entirely due to the momentum of the pane. At the edges of the window the pane is at rest due to the frame. This restraint causes a transverse deceleration wave to propagate inwards from each edge towards the centre. In the early stages of the response, the centre region of the window is ahead of the deceleration wavefront and continues to travel inwards, unaffected by the restraint at the edge. Behind the deceleration wavefront the pane loses the momentum it initially acquired and effectively comes to rest. The result is a deflected shape that consists of a relatively flat central region with deformed curved regions close to the edges. The maximum deflection occurs when the transverse waves reach the window centre and the whole profile is curved (when taken across the shortest dimension).

Figures 14 to 17 also show how the strain is not uniform and concentrates close to the window edge, leaving the central region relatively unstrained. Lines of strain can be seen passing through the central region in the later frames of the DIC measurements and are indicators for the fracture paths in the glass plies. The white areas in the last frames of Test 1 are where the image correlation has been unable to calculate strain data due to missing facets.

Figure 18 shows displacement cross-sections taken horizontally through the window at $y = 0$ mm for each test. The axes have both been scaled equally so that the profile is not exaggerated. Each line is plotted at 2 ms intervals and clearly show the relatively flat central region deflecting into the cubicle and deformed curved regions close to the edges. As the pane deflects further the flat central region becomes smaller until the whole profile is curved. This is due to the restraint at the edges causing transverse waves to propagate inwards towards the centre from each edge.

The ends of the profiles measured using DIC deflect approximately into the cubicle despite the window being restrained at this point. There are two reasons for this behaviour. The frame to which the window was attached exhibited a small degree of compliance and deflected in response to the blast load. Also, the DIC method can not track right into the window edges. As a result there will always be an offset between

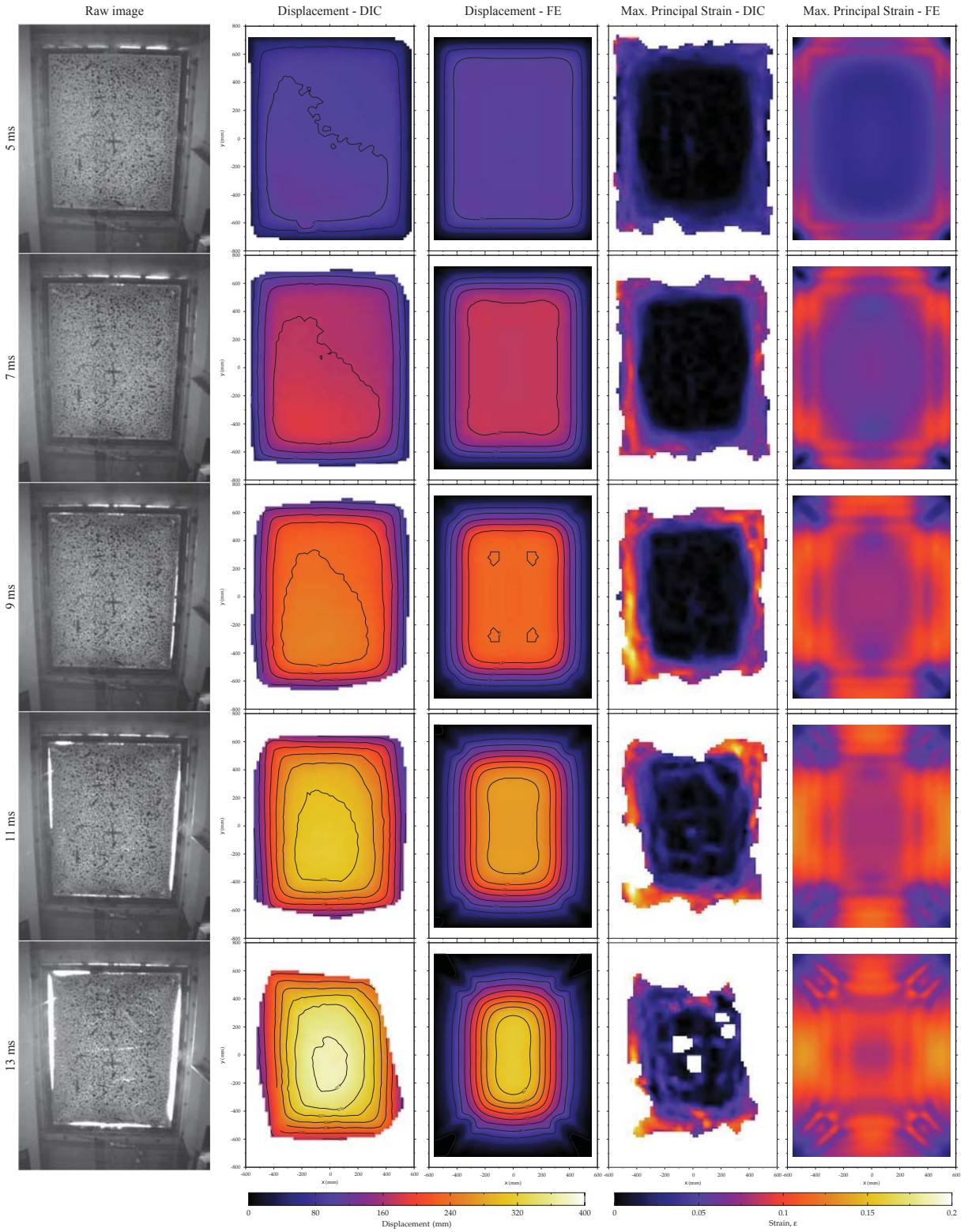

Figure 14: Sequence of images from high speed camera alongside out-of-plane displacement and maximum in-plane principal strain measured using DIC and predictions from the laminated glass FE model for Test 1 (15 kg at 10 m).

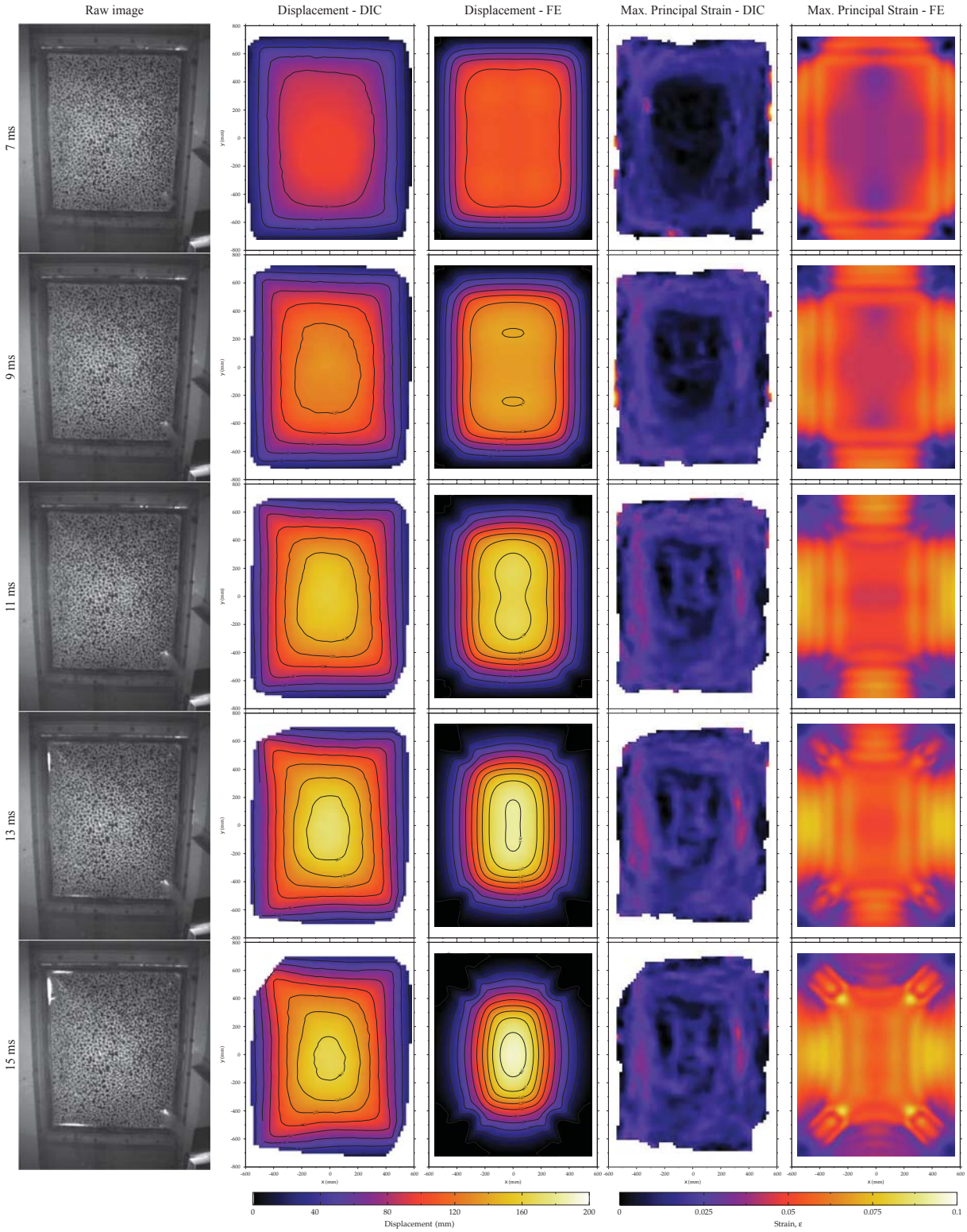

Figure 15: Sequence of images from high speed camera alongside out-of-plane displacement and maximum in-plane principal strain measured using DIC and predictions from the laminated glass FE model for Test 2 (15 kg at 13 m).

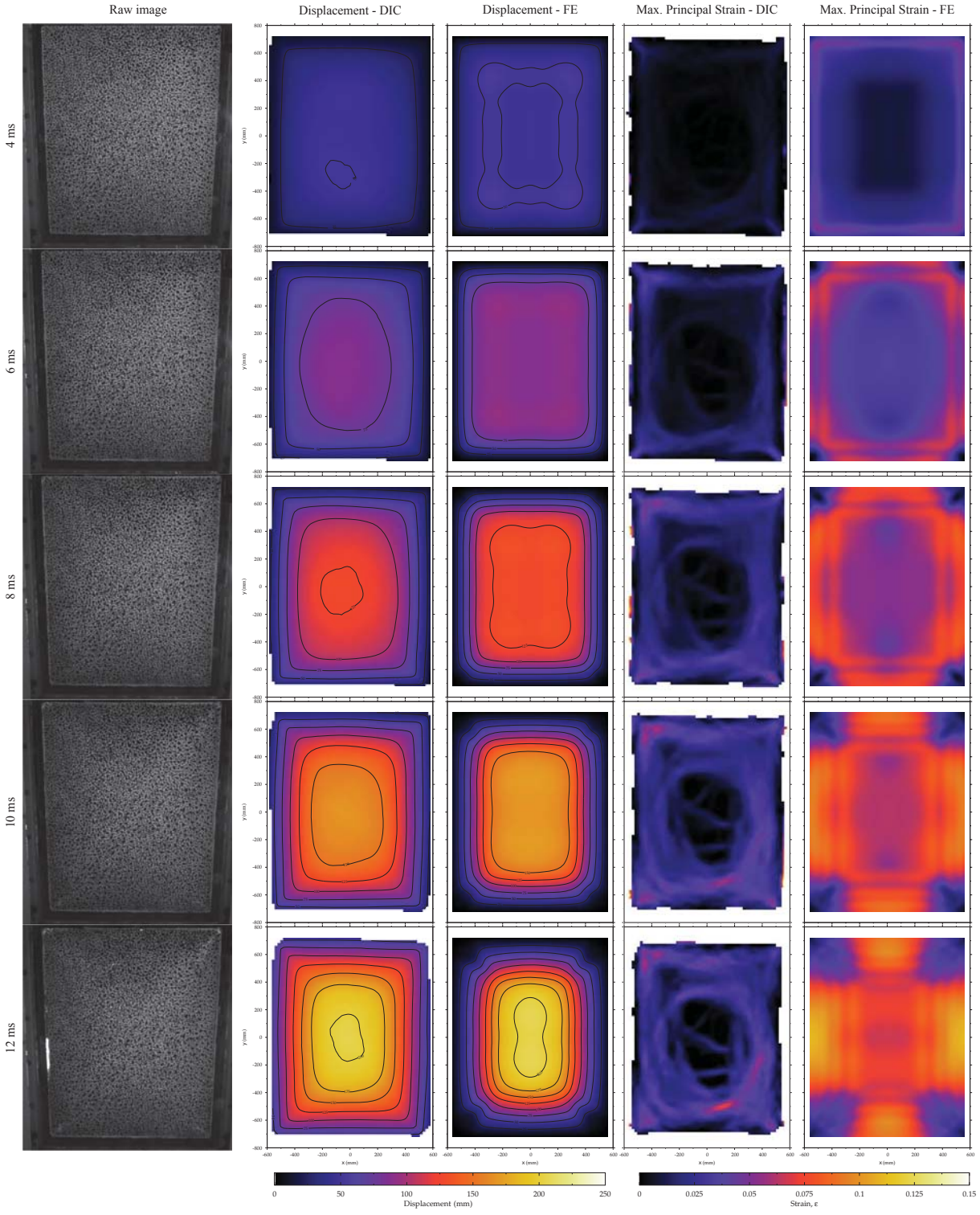

Figure 16: Sequence of images from high speed camera alongside out-of-plane displacement and maximum in-plane principal strain measured using DIC and predictions from the laminated glass FE model for Test 3 (30 kg at 16 m).

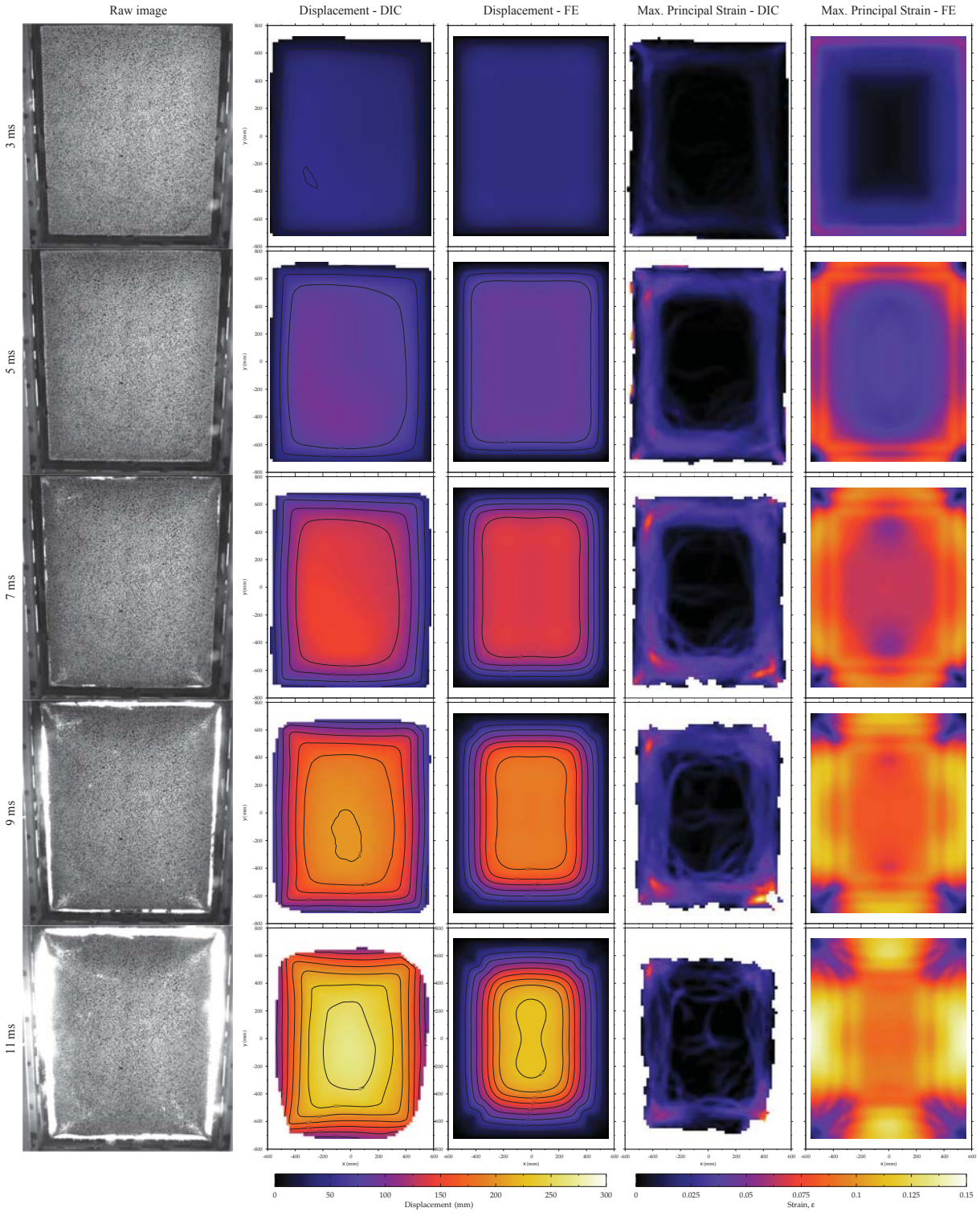

Figure 17: Sequence of images from high speed camera alongside out-of-plane displacement and maximum in-plane principal strain measured using DIC and predictions from the laminated glass FE model for Test 4 (30 kg at 14 m).

the window edge and the last point tracked.

Figure 18 also shows a comparison of the experimentally obtained deflection profiles against the laminated glass finite element model. In early phases the profiles show good agreement with the experimental profile, except for a small deviations close to the edge. These differences result from the assumption that the window edges are fixed to a rigid structure in the finite element model when in the experiments this boundary condition is impossible to obtain. In the later stages of Tests 1 and 4, the predicted profiles begin to depart more significantly from the measured profiles. In these tests the joint fails completely, allowing large displacements at the edges. In later stages of Tests 2 and 3, the measured and predicted profiles also depart but less significantly. At the edge of the profile, the laminated pane begins to rebound, giving the pane a negative velocity in this region. The region that has rebounded increases in size until it reaches the centre of the pane, at which point the maximum central deflection is reached. This behaviour was not observed in the experimental profiles. Possible reasons for this deviation are discussed in more detail in Section 5.4.

5.2. Reaction force and edge angles

Figure 19 compares the predicted and measured edge reactions forces and angle of pull at the midpoint of the vertical edge ($x = 570\,\text{mm}$, $y = 0\,\text{mm}$) for each test. A definition of the angle of pull and reaction force can be found in Section 3.2.1. The reaction forces measured in blast testing have a shape that is similar to the FE predictions if the high frequency oscillations in the experimental data are ignored. These high frequency oscillations are due to vibrations in the supporting window frame and cubicle which were not included in the finite element simulation. The magnitude of the force predicted by the FE model is consistently larger than that measured in blast testing. This is possibly due to the flexibility of the test cubicle. Also shown in Figure 19 is the time-history of the angle of pull (θ in Figure 4b) formed at the same location for each test. The angle at each edge increases steadily after the blast wave arrives reaching values of the order of 30° to 40°. The angles measured in the experiments increase slower than those predicted by the FE model. This is due to the movement of cubicle at the window edge reducing the effective angle formed. Peak measured edge reaction forces and angles of pull are summarised in Table 8.

5.3. Pressure impulse analysis

A pressure-impulse analysis was conducted using the finite element model to determine the level of predicted damage over a wide range of charge sizes and stand-off distances. The model was run with peak reflected pressures in the range of 1 kPa to 1 MPa and positive impulses in the range of $10\,\text{kPa}\cdot\text{ms}$ to $10\,\text{MPa}\cdot\text{ms}$. For simplicity the blast load applied to the pane was idealised as a triangular pressure pulse with zero rise-time and no negative phase. A bracketing procedure was used to find the pressures and

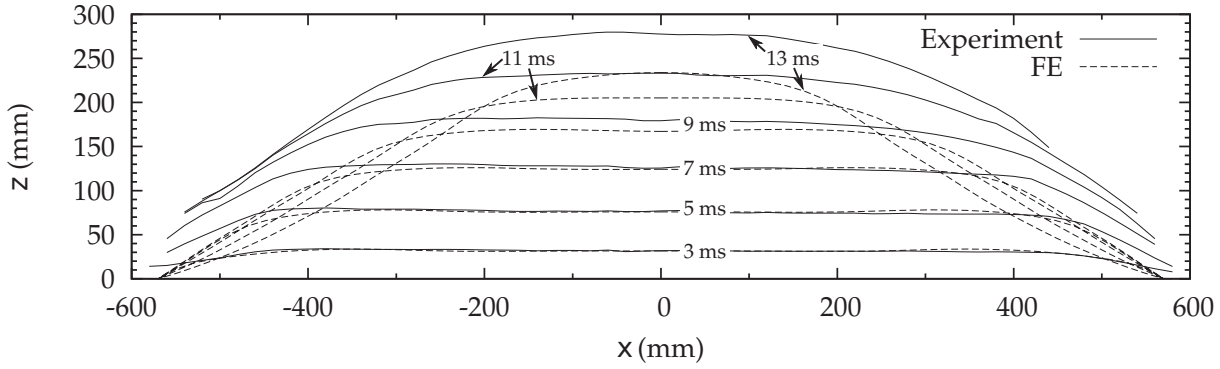

(a) Test 1

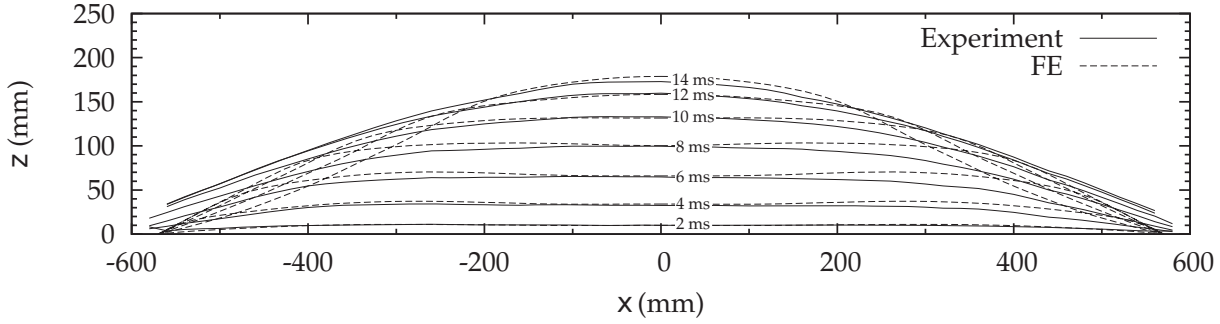

(b) Test 2

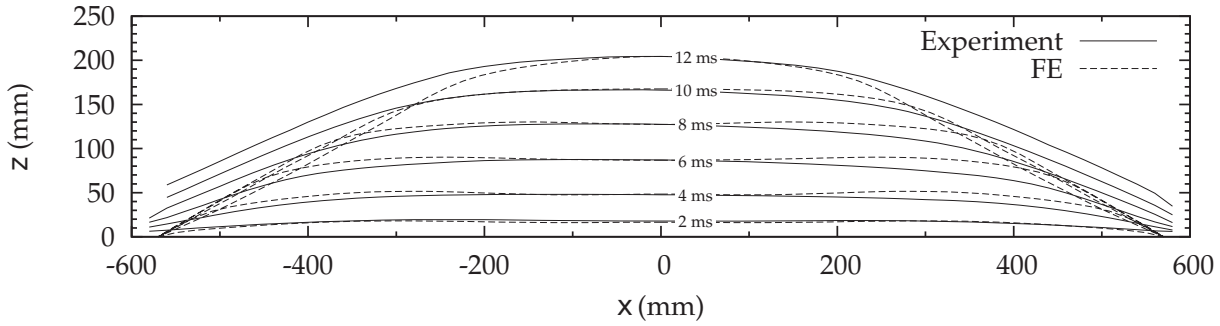

(c) Test 3

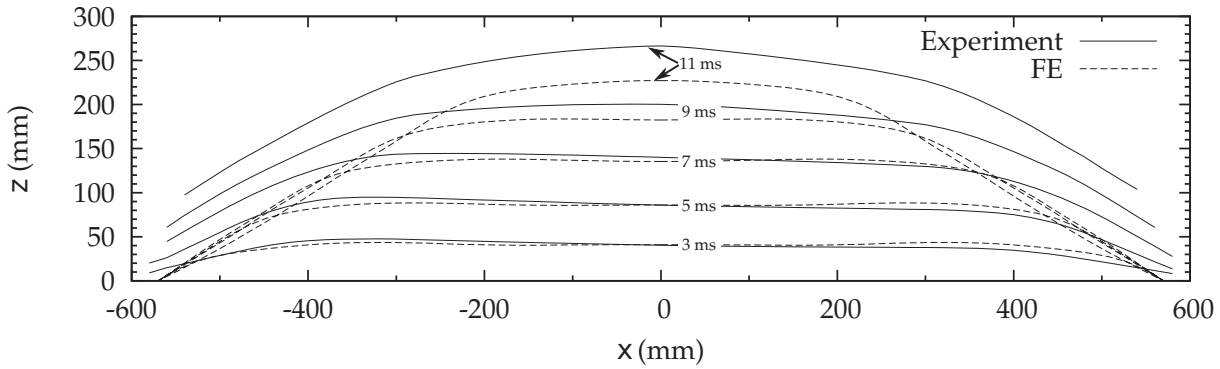

(d) Test 4

Figure 18: Comparison of the measured DIC and predicted laminated glass FE model profiles taken horizontally at the window centre for each test.

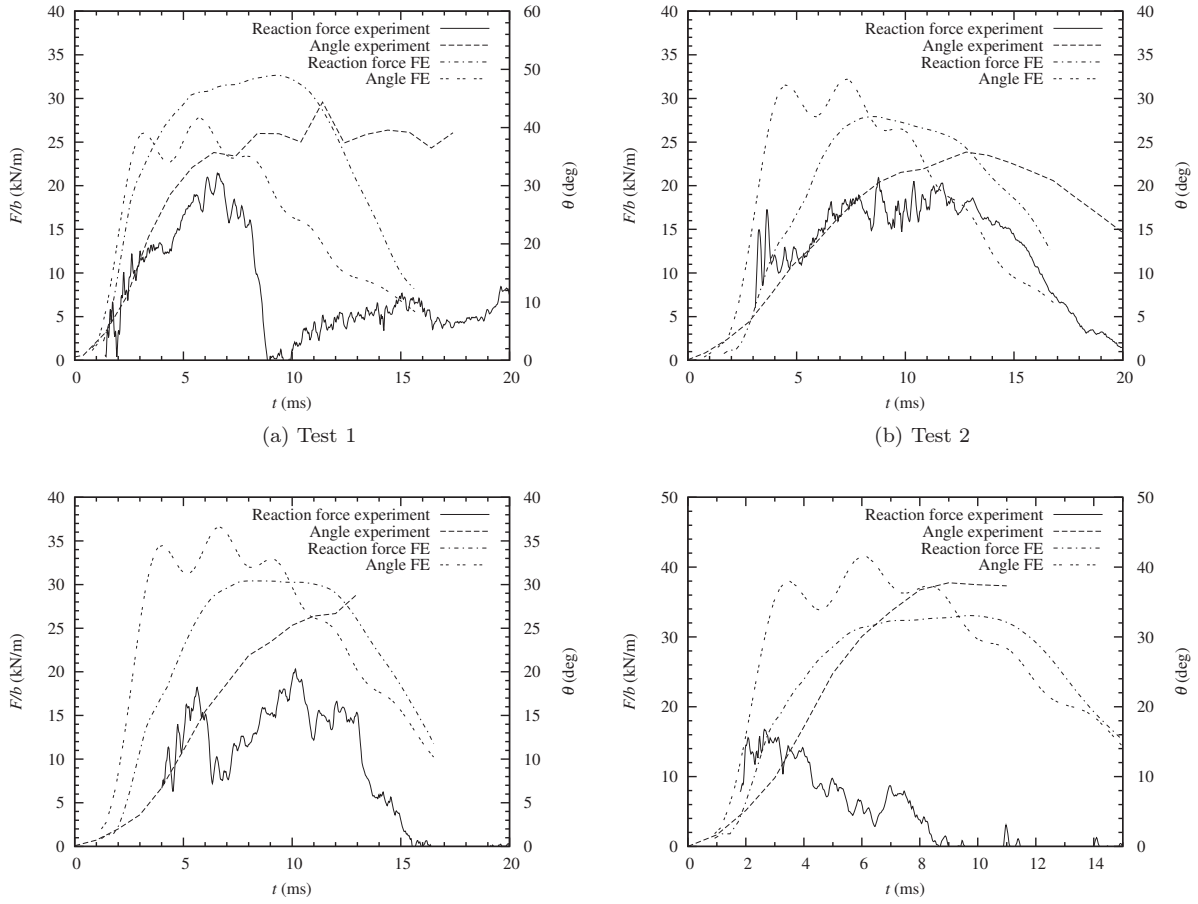

(a) Test 1 (b) Test 2

(c) Test 3 (d) Test 4

Figure 19: Comparison of reaction forces and angle formed at window edge.

Table 8: Edge reaction failure forces (see Figure 2a for strain gauge locations).

			F_f/b (kN/m)					θ_f (deg)				
Test	W (kg)	R (m)	Top	Bottom	Centre	Wall	Offset	Top	Bottom	Centre	Wall	Offset
1	15	10	22	-	-	21	-	34	26	27	35	-
2*	15	13	-	16	24	30	-	20	24	23	23	-
3	30	16	15	10	20	19	11	26	26	27	26	23
4	30	14	19	23	18	15	14	30	30	34	18	31

* Maximum values on inward stroke.

impulses required to produce constant levels of damage. The levels of constant damage investigated were defined by the point of first cracking in the glass plies and when the peak in-plane principal strain in the

cracked laminated glass reached levels of 5%, 10%, 15% and 20% before maximum deflection.

Figure 20 shows the iso-damage curves produced by the model at these damage levels. Lines of constant charge weight and stand-off distance have been overlaid on the figure to allow easy determination of the reflected pressure and impulse for a particular threat (assuming infinite facade dimensions). If the applied pressure and impulse for a particular blast load lies toward the lower left of an iso-damage line then the laminate will not reach that level of damage. If the applied pressure and impulse lie toward the upper right of an iso-damage line then the laminate will have exceeded that level of damage.

The curves show asymptotic behaviour in both pressure and impulse. The pressure asymptote (horizontal) is formed at the minimum pressure required to cause a certain level of damage. At this pressure the level of damage experienced will not increase with an increasing impulse. This asymptote is also known as the quasi-static asymptote as it represents loads which vary slowly with respect to the response of the pane. Similarly the impulsive asymptote (vertical) is formed at the minimum impulse required to cause a certain level of damage. At this asymptote, any increase in the applied pressure has no effect on the damage level obtained. A maximum strain of 20% is suggested as being the maximum strain that the laminate can safely experience. This iso-damage level can be used to assess whether the laminate is safe for a particular blast load.

Smith (Smith, 2001; Cormie et al., 2009) has developed a single-degree-of-freedom (SDOF) model, consisting of an equivalent load, mass and nonlinear resistance function, to describe the behaviour of laminated glass under blast loading. Figure 20 compares the predicted iso-damage curve of the SDOF model against the laminated glass FE model developed in this paper for a 7.52 mm thick 1.5 m $\times$ 1.2 m laminated pane.

The predicted iso-damage curves for fracture of the glass plies show good agreement on the pressure asymptote (long duration pulses) but differ on the impulsive asymptote (short duration pulses). In the impulsive case, the SDOF model predicts that a greater impulse is required for cracking at any given pressure. The pressures and impulses required to produce this behaviour are only reproducible from small charges at small stand-off distances. Under these conditions the pressure distribution across the window will not be uniform. Both models assume a uniform pressure distribution and as a result will overestimate the resistance at these loads. The laminated glass FE model could be extended to include the nonuniform pressure distribution to yield more accurate estimates of cracking in this regime.

The predictions of safe strain levels in the cracked laminate produced by the finite element and SDOF models are also shown in Figure 20. The safe limit used by the SDOF model for this pane size was determined from the pressures and impulses required to produce a peak central deflection of 200 mm. This equates to

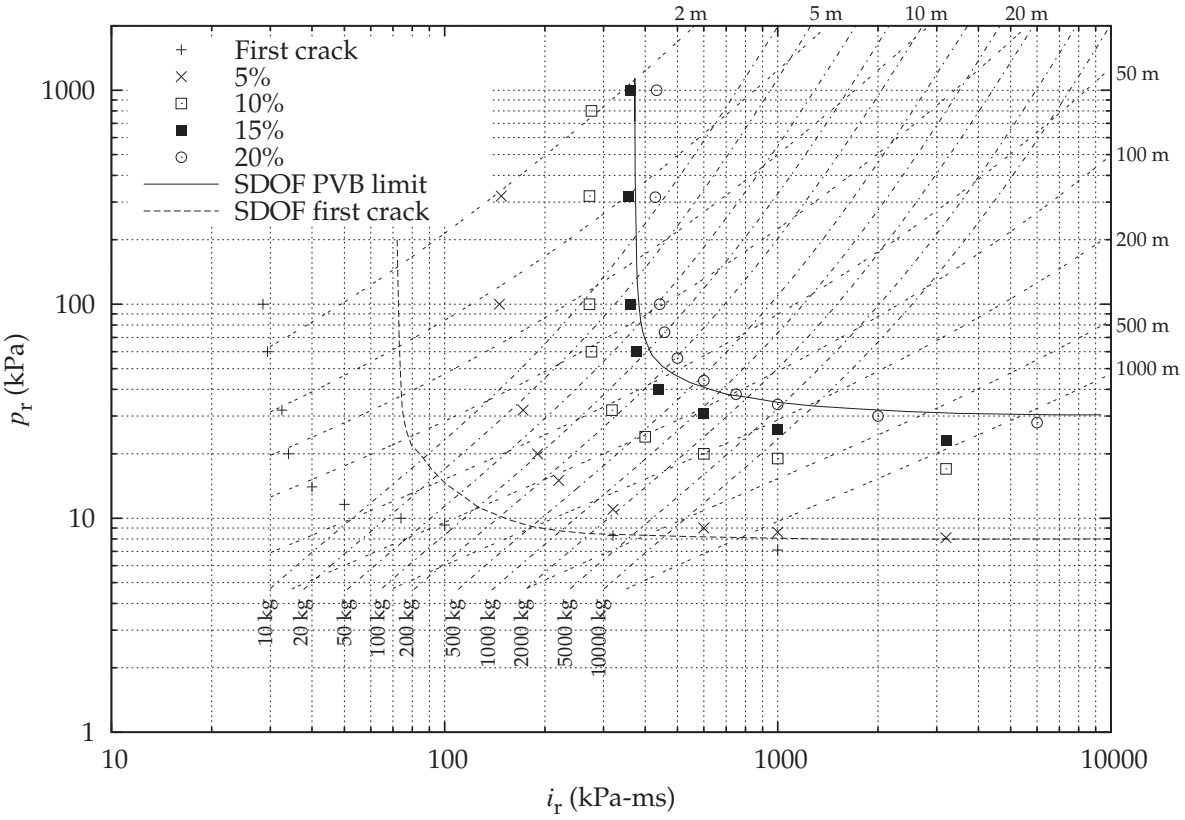

Figure 20: Iso-damage curve predictions compared with SDOF model (Cormie et al., 2009).

a maximum in-plane strain of approximately 9%. This limiting deflection was set from observations made in numerous blast tests. Good agreement is seen between the SDOF iso-damage curve and the 20% strain level iso-damage curve produced by the finite element model. A slight increase in the position of the impulsive asymptote is seen with the 20% strain finite element iso-damage curve when compared to the SDOF prediction. The finite element iso-damage curves are shown at different strain levels to show the sensitivity to the maximum acceptable strain criteria. The use of an iso-damage curve at a reduced strain may be more appropriate in certain applications, for example, where the window is expected to operate at low temperatures.

5.4. Limitations of the finite element model

5.4.1. Material model of cracked laminated glass

In the development of the finite element model it was assumed that the behaviour of cracked laminated glass could be adequately modelled by reducing the stiffness in the glass layers to zero and using a Johnson-Cook plasticity law to describe the overall response of the cracked laminate. The reduction in stiffness in

the glass layers gives the cracked laminate very little flexural stiffness. It was assumed that the cracked laminate only acts as a membrane. However, the cracked laminate will only act as a pure membrane if all the cracks in the glass plies are aligned and there is enough tensile strain in the membrane to ensure that adjacent fragments do not make contact as it curves. It is more likely that cracks in each ply do not line up exactly, resulting in some residual flexural stiffness after the glass fractures. Omitting this residual flexural stiffness from the model is likely to be a contributing factor to the differing deflection profiles in Figure 18.

An initial rate-independent modulus was combined with a rate-dependent plasticity law to describe the behaviour of the cracked laminate. The initial modulus was based on results from tensile tests on cracked laminated glass at the strain rates observed in blast testing. Strain rates of the same order were predicted by the finite element model for the blast test discussed and give confidence in this assumption.

The model assumes that fracture of the glass plies occurs instantaneously and with an even density across the laminate. The fracture pattern is known to vary across the laminate (Hooper et al., 2011), with the crack density largely being a function of the stress distribution at the time of fracture. In the cracked laminated glass tests it was observed that the initial modulus increased and nominal failure strain decreased with increased crack spacing, whereas the plateau stress was unaffected. The finite element model used here ignores these effects and could as a result overestimate the safety limit of the pane.

5.4.2. Boundary conditions

The boundary conditions used in the finite element model correspond to an infinitely stiff supporting structure. Comparisons with the experimental deflection profiles show that there is flexibility at the boundary. If the period of oscillation of the boundary coincides with that of the laminated pane then it will act to reduce the stresses in the laminate and joint. If the boundary rebounds before the laminate pane reaches maximum deflection then the stress in the laminate and joint could increase. This effect has been neglected in this analysis and could be a factor in determining the safe limit of a laminated pane under blast loading.

5.4.3. Fluid structure interaction

In this analysis the pressure distribution across the window face was assumed to be uniform. Furthermore, the blast pressure in the model acts as a time varying static pressure, always resulting in a force normal to the face of each shell element. This is not an accurate representation of the way in which the blast wave interacts with the structure and is likely to be another contributing factor to the differing deflection profiles in Figure 18. The load acting on the pane arises from both the static and dynamic pressure in the blast wave. The pressures calculated here assume that the blast wave is reflecting normal to an infinitely rigid surface. However, the pane quickly accelerates when hit by the blast wave, reducing the effective dynamic

pressure of the wave and the total impulse acting on the pane. Air behind the pane has also been neglected and is likely to offer some damping effect. It is therefore possible that the calculated pressures overestimate the load on the pane, giving conservative estimates for the pressures and impulses required to cause failure. More accurate modelling of the interaction between the blast wave and moving pane is possible with coupled fluid dynamics simulations, but at the expense of a significant increase in computational time.

6. Conclusions

In this paper, a series of four open-air blast experiments on laminated glass windows to measure deflection and edge reaction forces are described. Four laminated glass samples of layup [3, 1.52, 3] mm were loaded with peak reflected pressures and positive reflected impulses ranging from 91.2 kPa to 155 kPa and 284 kPa · ms to 413 kPa · ms respectively.

The high-speed image correlation results have allowed a detailed analysis of the response of laminated glass under blast loading. The deflected shape of the windows showed a flat central region deflecting into the cubicle with curved and strained regions concentrated close to the edges. The fracture pattern in the glass plies was largely determined by the stress created by the curvature at the time of fracture. As the panes deflected further the flat central region became smaller until the whole profile was curved. The restraint at the edges caused transverse deceleration waves to propagate inwards towards the centre from each edge. Displacements before failure of over 200 mm were observed. Peak observed velocities and accelerations at the centre of the pane ranged from 17 $^{m}/_{s}$ to 31 $^{m}/_{s}$ and 3 $^{km}/_{s^2}$ to 6 $^{km}/_{s^2}$ respectively. Strain in the cracked laminated glass was observed to reach values of 15% without tearing for a 1.52 mm interlayer. Strain rates between 10 s^{-1} and 40 s^{-1} were also observed.

For three of the tests, the samples failed at the silicone joint but for one test the joint did not fail and the window rebounded, coming to rest without significant joint damage. The image correlation results showed that the angle of pull was approximately constant along the edges. The mean tension in the cracked laminate and angle of pull at failure were found to be 20 ± 5 $^{kN}/_{m}$ and $30° \pm 5°$ respectively. Failure in the joint region is the most undesirable mode of failure because the majority of the laminated pane becomes detached from the frame and can contain sufficient kinetic energy to cause serious injury to building occupants. This highlights the need for proper specification of joint sizes and framing relative to the tearing strength of the cracked laminated glass.

A finite element model has been developed to predict the response of the laminated glass to blast loading in the precrack and postcrack phases. The model was constructed using shell elements and was split into two

distinct phases to describe the precrack and postcrack response. In the precrack phase it was determined that the effects of viscoelasticity in the PVB interlayer were negligible at short time scales by comparing the results of the shell element model against a full solid continuum element model.

The postcrack phase of the laminate response was modelled by reducing the stiffness of the glass layers to zero and using a rate-dependent plasticity law to describe the membrane response of the cracked laminate. A pressure-impulse analysis was conducted using the model to determine iso-damage levels for varying charge weights and stand off distances. The iso-damage curves agreed well with those generated using a single-degree-of-freedom analysis, with a 20% maximum strain damage curve being approximately equivalent to a maximum 200 mm deflection damage curve produced using the single-degree-of-freedom model.

Comparisons between the predictions generated using the model and experimental data from blast testing showed that the finite element model agrees very well initially. Differences in the predicted response could be due to the omission of any residual flexural stiffness in the cracked laminate after the glass plies fracture and flexibility in the supporting structure. Overall, the response of the laminated glass FE model captures the deformation behaviour up to maximum deflection for full-scale blast evaluation of laminated glass panes subject to different charge and stand-off conditions. As such it is a useful design tool for optimising blast mitigation of glass facade structures. The model is also applicable to laminated glass under impact and blast conditions such as those experienced in transport applications.

Acknowledgements

The authors acknowledge the Engineering and Physical Sciences Research Council (EPSRC) and Arup for financially supporting Dr Paul Hooper during his PhD. We acknowledge the many constructive discussions with David C. Smith and David Hadden of Arup. The authors also thank the Centre for the Protection of National Infrastructure (CPNI) for providing access to the GL group test facilities at RAF Spadeadam and Amit Puri and Hari Arora for their assistance during the full scale blast tests.

References

References

Arora, H., Hooper, P. A., Dear, J. P., 2011. Dynamic response of full-scale sandwich composite structures subject to air-blast loading. Composites Part A: Applied Science and Manufacturing 42 (11), 1651 – 1662.

Behr, R. A., Minor, J. E., Norville, H. S., 1993. Structural behavior of architectural laminated glass. Journal of Structural Engineering 119 (1), 202–222.

Bennison, S. J., Jagota, A., Smith, C. A., 1999. Fracture of glass/poly(vinyl butyral) (Butacite®) laminates in biaxial flexure. Journal of the American Ceramic Society 82, 1761–1770.

CEN/TC129, C. T. C., 2008. Glass in buildings - determination of the strength of glass panes. Part 3: General method of calculation and determination of strength of glass by testing. prEN 13474-3. British Standards Institute, London.

Charles, R. J., 1958. Static fatigue of glass. Journal of Applied Physics 29, 1554 –1560.

Cormie, D., Mays, G., Smith, P. (Eds.), 2009. Blast effects on buildings, Second Edition. Thomas Telford.

Dobratz, B. M., Crawford, P. C., 1985. LLNL explosives handbook: properties of chemical explosives and explosives and explosive simulants. UCRL-52997, Lawrence Livermore National Laboratory, CA.

Home Office Scientific Development Branch, 2008. Guidance note: Glazing enhancement to improve blast resistance.

Hooper, J. A., 1973. On the bending of architectural laminated glass. International Journal of Mechanical Sciences 15 (4), 309–323.

Hooper, P. A., Blackman, B. R. K., Dear, J. P., 2011. The mechanical behaviour of poly(vinyl butyral) at different strain magnitudes and strain rates. Journal of Materials Science Accepted.

Johnson, G. R., Cook, W. H., 1985. Fracture characteristics of three metals subjected to various strains, strain rates, temperatures and pressures. Engineering Fracture Mechanics 21 (1), 31–48.

Muralidhar, S., Jagota, A., Bennison, S. J., Saigal, S., 2000. Mechanical behaviour in tension of cracked glass bridged by an elastomeric ligament. Acta Materialia 48, 4577–4588.

Norville, H. S., King, K. W., Swofford, J. L., 1998. Behavior and strength of laminated glass. Journal of Structural Engineering 124 (1), 46–53.

Rose, T. A., 2001. An approach to the evaluation of blast loads on finite and semi-infinite structures. Ph.D. thesis, Cranfield University.

Seshadri, M., Bennison, S. J., Jagota, A., Saigal, S., 2002. Mechanical response of cracked laminated plates. Acta Materialia 50 (18), 4477–4490.

Simulia, 2010. Abaqus theory manual v6.9.

Smith, D. C., 2001. Glazing for injury alleviation under blast loading: United Kingdom practice. In: Glass Processing Days Conference Proceedings. pp. 335–340.

Sutton, M. A., Orteu, J. J., Schreier, H. W., 2009. Image Correlation for Shape, Motion and Deformation Measurements. Springer.

van Duser, A., Jagota, A., Bennison, S. J., 1999. Analysis of glass/polyvinyl butyral laminates subjected to uniform pressure. Journal of Engineering Mechanics 125 (4), 435–442.

Williams, M. L., Landel, R. F., Ferry, J. D., 1955. The temperature dependence of relaxation mechanisms in amorphous polymers and other glass-forming liquids. Journal of the American Chemical Society 77 (14), 3701–3707.

On the blast resistance of laminated glass

P. A. Hooper[a], R. A. M. Sukhram[b], B. R. K. Blackman[a], J. P. Dear[a,*]

[a] *Imperial College London, Department of Mechanical Engineering, Exhibition Road, London, SW7 2AZ*
[b] *Arup, 13 Fitzroy Street, London, W1T 4BQ*

Abstract

Blast resistant glazing systems typically use laminated glass to reduce the risk of flying glass debris in the event of an explosion. Laminated glass has one or more bonded polymer interlayers to retain glass fragments upon fracture. With good design, the flexibility of the interlayer and the adhesion between layers enable laminated glass to continue to resist blast after the glass layers fracture. This gives protection from significantly higher blast loads when compared to a monolithic pane. Full-scale open-air blast tests were performed on laminated glass containing a polyvinyl butyral (PVB) interlayer. Test windows of size 1.5 m × 1.2 m were secured to robust frames using structural silicone sealant. Blast loads were produced using charge masses of 15 kg and 30 kg (TNT equivalent) at distances of 10 m to 16 m. Deflection and shape measurements of deforming laminated glass were obtained using high-speed digital image correlation. Measurements of loading at the joint, between the laminated glass and the frame, were obtained using strain gauges. The main failure mechanisms observed were the cohesive failure of the bonded silicone joint and delamination between the glass and interlayer at the pane edge. A new finite element model of laminated glass is developed and calibrated using laboratory based tests. Predictions from this model are compared against the experimental results.

Keywords: Laminated, glass, blast, digital image correlation, polyvinyl butyral

1. Introduction

Annealed float glass is often used in windows but is a brittle material that offers little resistance to the blast waves produced by explosions. When it fails it breaks into very sharp fragments that can travel at high velocity. Historically, the majority of injuries from bomb blasts have been from flying glass fragments Smith (2001). Laminated glass has been found to be effective at mitigating these risks and is now often used

*Corresponding author
Email address: j.dear@imperial.ac.uk (J. P. Dear)

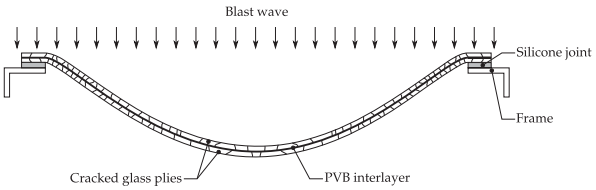

Figure 1: Example of postcrack deformation in laminated glass due to blast loading.

to protect building occupants by retaining glass fragments on a polyvinyl butyral (PVB) interlayer upon fracture (Figure 1). Significant resistance to blast loading is seen in laminated glass even after the glass layers have fractured. It is important to understand the conditions for and types of failure mechanism in laminated glass in order to optimise the design of facade structures.

Whilst there are some analytical and finite-element (FE) based approaches to predicting the response of laminated glass to blast loading, there is little experimental data available for validation of these models. Furthermore current FE models deal only with the uncracked phase of the laminated glass response. This phase only makes up a small portion of the total resistance offered to a blast wave. There is a therefore a need to develop models that predict the laminated glass response after the glass fractures. This paper aims to address these gaps by describing experimental results from four well instrumented full-scale open-air blast tests on lamented glass. The paper also details a FE based approach to modelling the post-fracture laminated glass response and compares it with the experimental data acquired.

2. Background

The behaviour of uncracked laminated glass has been studied by several researchers including Norville et al. (1998), Behr et al. (1993) and Hooper (1973). The flexural stiffness of laminated glass is dependent on the fraction of horizontal shear force transferred between the glass layers by the PVB interlayer. At one extreme the PVB transfers no horizontal shear stress and its only function is to maintain the separation distance between the glass layers. In this case, each glass layer bends independently and the total laminate flexural stiffness is the sum of the flexural stiffness of the individual glass layers. At the other extreme, significant flexural stresses exist within the interlayer in addition to the transfer of all the horizontal shear stress between the glass layers. The limiting case occurs when the stress distribution varies linearly through the thickness and would only be obtained when the elastic modulus of the PVB interlayer equals that of the glass layers.

The analysis by Norville et al. showed that for most laminates the PVB interlayer only needs to transfer

a fraction of horizontal shear stress between the glass layers to give a section modulus exceeding that of the equivalent monolithic pane. The equivalent monolithic pane was defined as a monolithic pane of the same thickness as the total thickness of the glass layers in a laminate. For example, a 6 mm monolithic pane would be equivalent to a 7.52 mm laminated pane consisting of two 3 mm glass layers and 1.52 mm PVB interlayer. Since PVB is a viscoelastic material, the amount of horizontal shear stress transferred between the glass layers is dependent on the rate of applied loading and temperature. It was found that under short duration loads that laminated glass has a higher section modulus than the equivalent monolithic pane. The increase in section modulus also reduces the peak tensile stress on the outer surface of the glass layers for a given load and accounts for an apparent increase in fracture strength for a given load when compared to an equivalent monolithic pane.

Bennison et al. (1999) and van Duser et al. (1999) used a Generalized Maxwell Series model to account for the time dependent modulus of PVB interlayers. Terms in the Maxwell model were determined experimentally using dynamic mechanical analysis. The time dependent PVB material model was used in finite element models of a plate subjected to uniform pressure loading and biaxial flexure. It was found that for most laminates the peak tensile stress on the outer surface of the glass layers was lower than that for an equivalent monolithic pane. The advantage of this approach is that the PVB shear modulus is calculated during the analysis and therefore accounts for time dependent effects. Variation in shear modulus at different temperatures was also taken into account by using the Williams-Landel-Ferry (WLF) equation (Williams et al., 1955) to shift the time dependent shear modulus curve to a different temperature.

The strength of annealed glass has a wide statistical variation. Test data gathered in the development of the glazing standard prEN 13474-3 (CEN/TC129, 2008) includes tensile strength results from over 700 annealed glass samples from different manufacturers using the ring-on-ring test method. As expected, a wide variation in breaking strength was found, from 30 MPa to 120 MPa at a loading rate of 2 $^{\mathrm{MPa}}/_{\mathrm{s}}$. The data can be characterised statistically using a Weibull distribution. For normal design purposes a breaking strength of 45 MPa is given based on 95% of samples not failing below this stress. Smith (Cormie et al., 2009) extrapolated this strength data to the higher strain rates experienced in blast loading using a relationship proposed by Charles (1958) and arrived at a dynamic breaking strength for annealed glass in the region of 80 MPa.

The mechanical behaviour of laminated glass after cracking has been investigated by Muralidhar et al. (2000). In this study, laminated glass with an aligned crack in each glass layer was subjected to constant rate tensile loading (a displacement rate of 1 $^{\mathrm{mm}}/_{\mathrm{s}}$ was used). Under these conditions, PVB delaminates

from the glass at the crack edge and deforms to bridge the crack. It was found that under constantly increasing displacement, the tensile force rises to a steady state value. They also used different hyperelastic material models to calculate the fracture energy associated with the delamination process. However, no viscous energy dissipation was accounted for in the analysis. The calculated fracture energy values include this dissipation energy and therefore overestimate the actual energy involved in the fracture process. The loading rates investigated were also too slow relative to those experienced during blast loading.

Static loading of fractured laminated glass plates was studied theoretically and experimentally by Seshadri et al. (2002). Plates constructed from a single glass and a single PVB layer were loaded centrally by a spherical steel surface at a constant rate of displacement. The glass layer was indented before loading to create a known flaw and a simple regular fracture pattern. Post breakage behaviour of the laminate was modelled using the work on PVB delamination described previously. Good agreement between experimental results and predictions was found. However, only a single glass layer was studied so the restraining effects of a second glass layer were not taken into account. Their approach is also difficult to apply to practical situations where there may be many thousands of cracks and where the crack pattern is not known in advance.

2.1. Glazing materials for blast protection

For increased protection from blast, modern glazing systems use laminated glass bonded to robust framing with structural silicone adhesives. Laminated glass consists of one or more polymer layers sandwiched between layers of glass. Polyvinyl butyral (PVB) is the most common interlayer and is bonded between the glass layers by the application of pressure and heat. It is commercially manufactured in sheets 0.38 mm thick for the architectural glazing market. More than one PVB sheet can be used in an interlayer, increasing the overall interlayer thickness in multiples of 0.38. Current recommendations for blast resistance advise a minimum interlayer thickness of 1.52 mm (Home Office Scientific Development Branch, 2008). Annealed float glass is the most common material used for the glass layers due its low cost. However, tempered glass can also be used where increased initial strength is required, although slight undulations from the tempering process can make laminating difficult. For situations where impact and ballistic strength is a consideration, additional layers of polycarbonate are used in the laminate.

Under blast loading a laminated glass pane initially deflects in a manner similar to a monolithic pane, that is as an elastic plate. This is termed the precrack phase of the laminated glass response. Fracture of the glass layers again occurs when the tensile stress at a flaw anywhere on the glass surface is high enough to cause crack propagation. After the glass layers fracture, the laminate is said to be in the postcrack phase

of the response. In this phase the glass fragments are held bonded to the PVB interlayer, giving continued resistance to the blast wave. The cracked laminate behaves similarly to a membrane and is able to undergo large deflections without further damage (Figure 1). Failure of the laminate occurs by PVB tearing and the conditions for this are not well understood. To be effective the laminated glass needs to be strongly fixed to a supporting structure. If the joint or framing structure is not strong enough, the pane could detach and enter a building at high velocity, injuring occupants.

Structural silicone sealant is commonly used to bond the laminate to a framing structure. In commercial buildings the framing is often constructed from extruded aluminium alloy sections. The laminate is restrained at two or four edges of the pane with a silicone bonded joint on one or both faces of the laminate. Securing all four edges on both sides is the recommended practice for blast resistance. However, single-sided joints are increasingly preferred by architects for aesthetic reasons. Minimum joint dimensions are calculated with reference to the dead-weight of the pane, the wind loading and thermal expansion. Current recommendations for blast resistance advise a double-sided silicone joint of at least 35 mm in depth (Home Office Scientific Development Branch, 2008). Other methods of restraining laminated glass exist such as rubber gaskets, glazing tape and mechanical point fixings. These systems are generally considered to give inferior blast protection to silicone bonded edges.

3. Air blast experimental method

In this paper, laminated glass panes have been tested with different blast loads in four open-air blast experiments. For each test an explosive charge was detonated in front of a test cubicle housing a matching pair of windows. The aim of the experiments was to measure the deflections, strains and edge reaction forces produced in a full-scale blast test for validation of analytical and finite element models. All eight laminated glass panes were of size 1.5 m × 1.2 m and were constructed from two 3 mm thick layers of annealed float glass and a 1.52 mm thick PVB interlayer. Two windows were tested at a time and were secured to the front of a steel cubicle approximately 3 m × 3 m × 3 m as detailed in Figure 2a. Window 1 was fully instrumented and provides the results described in this paper. Window 2 was not fully instrumented and was there to provide a symmetrical setup. The basic cubicle was designed and constructed by the Centre for the Protection of National Infrastructure (CPNI). The laminated glass was bonded on all four edges to a steel subframe with a 6 mm thick single-sided joint and nominal bonded depth of 20 mm. A two-part structural silicone sealant was used for the joint (Dow Corning 993 structural glazing sealant). The subframe was attached to the front of the steel cubicle using bolts.

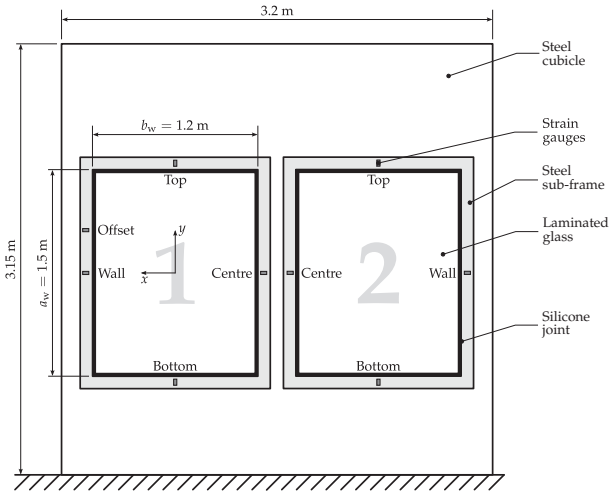

(a) Test cubicle front

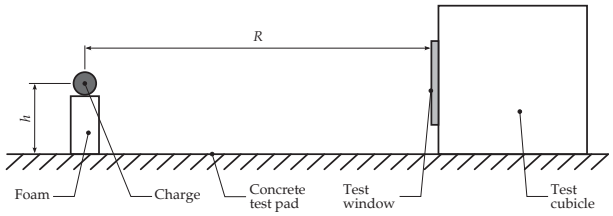

(b) Side elevation

Figure 2: Test view plan and side on with DIC view

In each test the charge was positioned symmetrically in front of the cubicle, raised on foam blocks to height of 1.5 m (corresponding to the window centre height) as shown in Figure 2b. Testing took place on a 100 m × 100 m concrete test pad to minimise energy loss in ground shock and crater formation. Tests 1 and 2 were conducted with 12.8 kg C4 charges (15 kg TNT equivalent) at stand off distances of 10 m and 13 m respectively. Tests 3 and 4 were conducted with 25.6 kg C4 charges (30 kg TNT equivalent) at stand off distances of 16 m and 14 m respectively. The blast pressure-time history for each test was recorded using stand-alone free-field and reflected pressure gauges (type 102-A06 from PCB Piezotronics) at the same stand-off distances as the cubicle. The reflected pressure gauges were mounted in a concrete block of the same dimensions as the test cubicle. Three gauges were located around the centre position of where the window would be located and an average was taken. The test parameters are summarised in Table 1 and were chosen to take the laminated glass up to the point of PVB tearing.

3.1. High-speed digital image correlation

High-speed 3D digital image correlation was used to measure the full-field rear-surface position of a single window during each blast test. Two high-speed cameras were positioned inside the test cubicle at a working

Table 1: Blast test configurations.

Test	Charge weight* W (kg)	Stand-off R (m)	Window size $a_w \times b_w$ (m)	Number of panels	Laminate layup $[d_g, d_{PVB}, d_g]$ (mm)
1	15	10	1.5 × 1.2	2	[3, 1.52, 3]
2	15	13	1.5 × 1.2	2	[3, 1.52, 3]
3	30	16	1.5 × 1.2	2	[3, 1.52, 3]
4	30	14	1.5 × 1.2	2	[3, 1.52, 3]

* TNT equivalent

distance s_w from the test window and centred on the window centre point. The camera setup used is shown in Figure 3a. Only Window 1 in Figure 2a was imaged due to limited availability of matching pairs of high speed cameras.

The included angle between the cameras was set to 25° to provide good sensitivity to out-of-plane motion without sacrificing in-plane sensitivity (Sutton et al., 2009). Two models of high-speed camera were used in this testing; the Phantom V4 and Phantom V5 manufactured by Vision Research. Table 2 details the configuration of each camera type and which camera type was used in each test.

The aperture of each lens was set to the widest opening (smallest f-number) that would allow the object to remain in focus over the anticipated movement range. This ensured that the maximum amount of light reached the camera sensor, enabling smaller exposure times. Exposure time, t_{ex}, for each camera was set to the smallest possible time whilst still obtaining a high-contrast speckle pattern. This approach minimises any motion blur during the exposure. The cameras were synchronised using a TTL pulse, generated when a frame exposure starts, from the first camera into the second camera. If the cameras were not synchronised, movement in between the starting times for the frame exposures for each camera would cause errors in the positions calculated by the DIC algorithm. The cameras were remotely triggered simultaneously, 150 ms before the charge was detonated.

A heavy duty studio-type camera stand was used to hold the cameras in position during the blast. Rubber isolating feet were used on the stand base to isolate it from ground shock. Ballast was also added to the stand base to increase mass and minimise any motion of the stand. The cameras were mounted on a single beam which was then attached to the camera stand. This arrangement minimises any movement of cameras relative to each other.

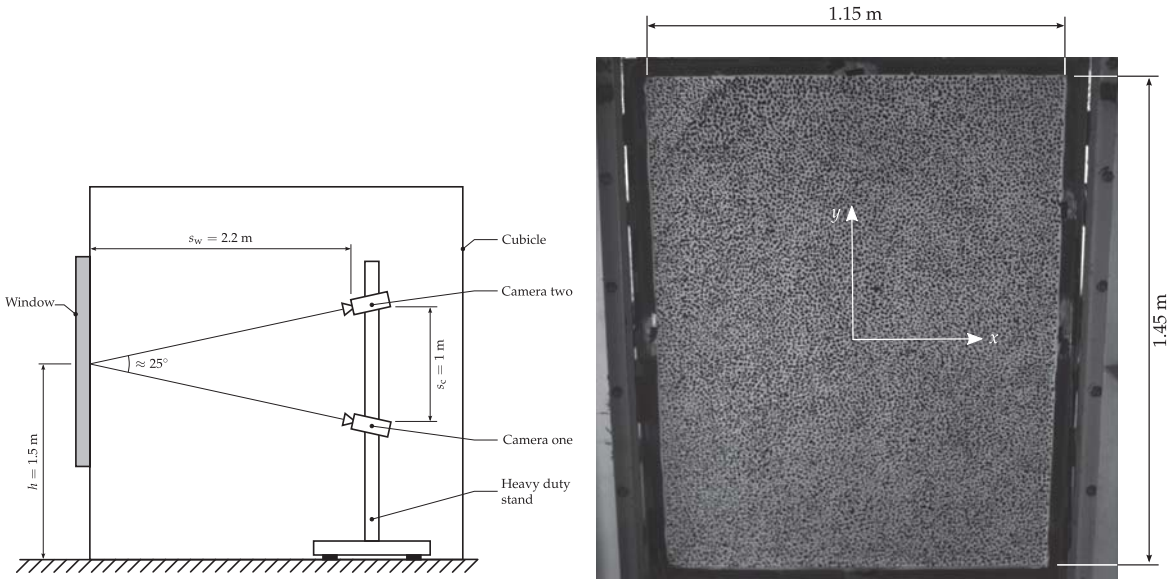

(a) High-speed camera setup.

(b) Speckle pattern viewed from the top camera.

Figure 3: High-speed camera setup.

Table 2: Digital image correlation setup.

Test	Camera Type	Resolution (pixels)	Frame rate (Hz)	Focal length (mm)	Pixel size (μm)	t_{ex} (μs)	s_w (m)	s_c (m)	d_s (mm)	d_p (mm)	n_p
1	Phantom V4	512 × 512	1000	8	16	40	2.2	1	9	28	2100
2	Phantom V4	512 × 512	1000	8	16	40	2.2	1	9	31	1600
3	Phantom V5	1024 × 1024	1000	24	16	76	2.2	1	5	21	3300
4	Phantom V5	1024 × 1024	1000	24	16	76	2.2	1	5	19	4400

3.1.1. Speckle pattern and lighting

To enable the image correlation algorithm to track the window surface a stochastic speckle pattern was applied to the rear surface of the window as shown in Figure 3b. Acrylic paint was used as it provides good flexibility and good adhesion to the glass surface. The image correlation technique is more robust with high-contrast speckle patterns. A high-contrast pattern was achieved by applying a white base coat and allowing it to dry before painting black speckles over the top. The black speckles were either painted by hand using an artists brush or with a foam block (containing multiple speckles carved into the base), with care taken to ensure a random pattern was achieved

The minimum speckle diameter, d_s, was determined from the size of the test panel and the camera resolution. For accurate pattern matching, each speckle should be sampled by at least a 3 by 3 pixel array (Sutton et al., 2009). Each speckle should therefore be over 3 pixels in diameter. Dividing the panel size by the camera resolution and multiplying by 3 then gives the minimum speckle diameter. The approximate speckle size used for each panel is given in Table 2.

Light from the explosion can cause over-exposure of the cameras inside the cubicle. To mitigate this problem black acrylic paint was applied to the front of the window (facing the charge) to reduce the light transmitted through the window. Two 1.25 kW halogen flood lights were used to illuminate the window from inside the cubicle, providing even and constant lighting conditions during the test.

3.1.2. Computation of 3D position and strain

In each window the position and strain of the entire rear surface was calculated using the ARAMIS image correlation software produced by GOM mbH. For full details of the image correlation method refer to Sutton et al. (2009). Each camera setup was calibrated before the blast by taking between 14-25 image pairs of a known calibration grid. These image pairs were imported into the software to determine the calibration parameters for each of the eight particular test setups. Accuracy of the calibration was verified by placing a speckled object 300 mm away from the window surface and capturing an image. This image was then analysed in ARAMIS to check the calculated distance between the object and window surface, as well as the overall window dimensions. Central displacement calculated by this system during a blast test has been verified using a linear displacement laser gauge (Arora et al., 2011). The sequences of image pairs captured during the blast were then imported for analysis. The flash from the detonation was used synchronise the image sequences with the pressure and strain data. An image of the undeformed window was set as the reference image and all correlation calculations were made relative to this image. After calculation the coordinates and corresponding strain values of each point were then exported for further analysis. The

calculated data for each image pair will be referred to as stage data. The number of points computed, n_{p}, and the approximate point spacing, d_{p}, are given in Table 2 for each test.

An estimate of the uncertainty introduced by noise in the images was made by comparing images of the laminated pane before detonation of the charge. The maximum error in the computed out-of-plane displacement was of the order of ± 0.1 mm. The maximum error in the computed in-plane strain components was of the order of $\pm 0.05\%$.

The coordinate system origin was defined as the centre point of each window as viewed in Figure 3b. The x-axis was defined as positive in the horizontal direction towards the right-hand edge of the cubicle and the y-axis was defined as positive in the vertical direction towards the top of the cubicle. In an undeformed state the rear surface of a window lies on the xy-plane. The z-axis, normal to the xy-plane, was defined as positive for inward deflection (towards the cameras).

3.1.3. Post-processing of image correlation data

Analysis of the image correlation data was conducted using the numerical computation software MATLAB. The computed displacements and strains at each stage were imported into the software and interpolated onto to a regular spaced grid to enable easy analysis. Central displacement time histories were generated by compiling values at the regular grid centre. Cross-sections were generated by taking values across the centre of the regular grid in the horizontal and vertical direction for each stage.

Out-of-plane velocity fields were found by computing the numerical derivative of the displacement field with respect to time, using the central differencing method. The acceleration fields were then found by computing the numerical derivative of the velocity field with respect to time. Central velocity and acceleration time-histories were then compiled from the values at the grid centre. The strain rate fields were found using the same method, computing the numerical derivative of the strain field with respect to time. The slope at each point on the deformed window surface was found by computing the numerical gradient of the displacement field in the x and y directions. The numerical gradient was again calculated using the central differencing method. The slope at the centre of each edge was then used to calculate the angle formed between the displaced window and the frame.

3.2. Edge reaction force measurement

Strain gauges were used to measure the edge reaction forces for all eight test windows. Pairs of foil strain gauges were bonded to the steel subframe at the midpoint of each edge. Strain gauges of type CAE-06-062UW-120 were used with AE-10 adhesive, both from Vishay Measurements Group. The position of the gauges on the subframe cross-section is shown in Figure 4a. Four strain gauge pairs were bonded to the

midpoint on each frame edge. An additional pair was attached to the frame of window one in tests three and four offset by 350 mm above the midpoint on the wall edge to record variation in reaction force along the edge. Each gauge was connected in quarter bridge configuration to a Vishay 2120A strain gauge amplifier housed in a smaller cubicle behind the main test cubicle. The output from each strain gauge amplifier was recorded at 500 kHz.

3.2.1. Postfracture edge reaction analysis

The strain readings from each gauge were used to calculate the tension in the cracked laminate, F, by considering the subframe as a built-in cantilever beam. The geometry of the joint used in this analysis is shown in Figure 4b where θ is the angle of pull, l_g is the distance between the centre of the strain gauges and the end of the steel angle, d_e is the distance between the middle of the steel angle thickness and the middle of the laminate thickness, and d_a is the thickness of the steel angle.

The strain variation across the beam at point P is a combination of the direct axial strain, ε_A, and the bending strain, ε_B, as shown in Figure 4c. The strain, ε, varies across the thickness as a function of the distance from the centre, y_a,

$$\varepsilon = \varepsilon_\mathrm{B}\frac{2y_\mathrm{a}}{d_\mathrm{a}} + \varepsilon_\mathrm{A} \tag{1}$$

and ε is positive in tension. At the outer surface of the beam (facing the blast wave) $y_\mathrm{a} = {}^{d_\mathrm{a}}/_2$ and the strain $\varepsilon_\mathrm{o} = \varepsilon_\mathrm{B} + \varepsilon_\mathrm{A}$. At the inner surface $y_\mathrm{a} = -{}^{d_\mathrm{a}}/_2$ and the strain $\varepsilon_\mathrm{i} = \varepsilon_\mathrm{A} - \varepsilon_\mathrm{B}$. The axial and bending strain can be calculated directly from the gauge readings ε_o and ε_i ,

$$\varepsilon_\mathrm{A} = \frac{\varepsilon_\mathrm{o} + \varepsilon_\mathrm{i}}{2} \tag{2}$$

$$\varepsilon_\mathrm{B} = \frac{\varepsilon_\mathrm{o} - \varepsilon_\mathrm{i}}{2} \tag{3}$$

The axial strain is produced by the horizontal component of F and can be found by assuming the beam is linear elastic and that F and θ are constant along the edge length,

$$\varepsilon_\mathrm{A} = \frac{F\cos\theta}{bEd_\mathrm{a}} \tag{4}$$

where ${}^F/_b$ is the force per unit edge length (perpendicular to the page in Figure 4b) and E is the Young's modulus of the beam. Rearranging in terms of force per unit length of edge bond gives,

$$\frac{F}{b} = \frac{E d_{\mathrm{a}}}{\cos\theta}\varepsilon_{\mathrm{A}} \tag{5}$$

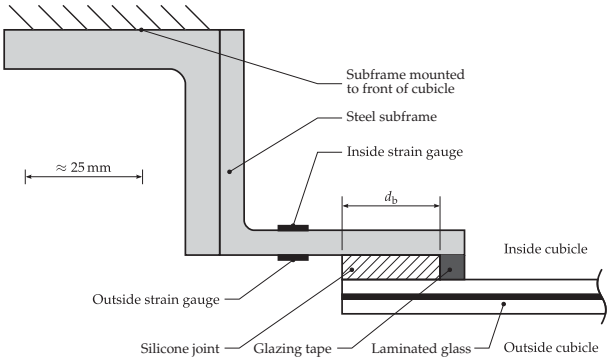

(a) Subframe cross section.

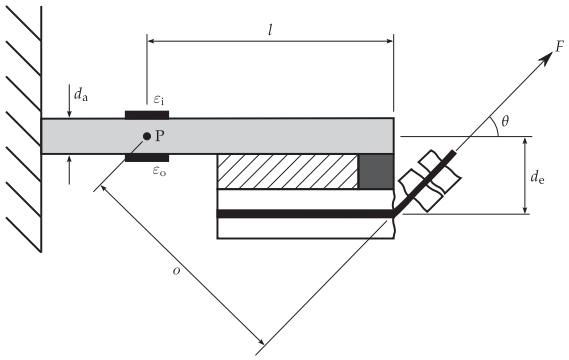

(b) Simplified geometry.

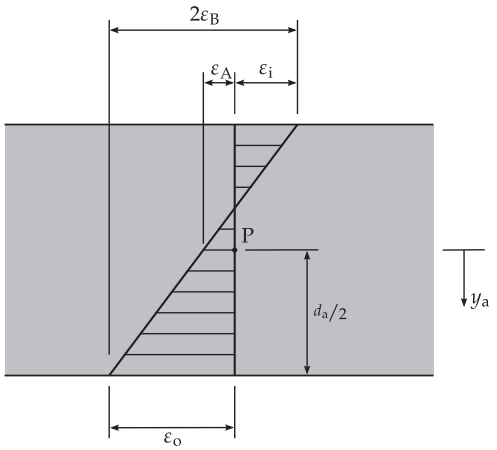

(c) Strain variation across the steel angle at the strain gauge location.

Figure 4: Cross section of edge fixing and strain gauge arrangement.

The bending strain is produced by a moment about point P created by a couple Fd_{o},

$$M_{\mathrm{P}} = Fd_{\mathrm{o}} \tag{6}$$

where distance d_{o} can be calculated from,

$$d_{\mathrm{o}} = l_{\mathrm{g}} \sin\theta + d_{\mathrm{e}} \cos\theta \tag{7}$$

assuming the steel angle only experiences small deflections. This moment causes the internal strains at P. The incremental force due to the strain at a point on the beam cross-section is $\mathrm{d}F_{\varepsilon} = E\varepsilon b\,\mathrm{d}y_{\mathrm{a}}$. The moment of $\mathrm{d}F_{\varepsilon}$ about P is $\mathrm{d}M_{\mathrm{P}} = y_{\mathrm{a}}\,\mathrm{d}F_{\varepsilon}$. The total moment over the entire cross section is therefore,

$$M_{\mathrm{P}} = Eb \int_{-d_{\mathrm{a}}/2}^{d_{\mathrm{a}}/2} y_{\mathrm{a}}\varepsilon\,\mathrm{d}y_{\mathrm{a}} \tag{8}$$

Substituting Equation 1 into 8 and integrating across the thickness gives,

$$M_{\mathrm{P}} = Ebd_{\mathrm{a}}^2 \frac{\varepsilon_{\mathrm{B}}}{6} \tag{9}$$

Equation 9 is simply the bending equation for a rectangular beam. The axial strain present in the beam does not contribute to M_{P} since its net moment is zero.

Setting Equation 6 equal to 9 and rearranging gives the force per unit of edge length in terms of bending strain,

$$\frac{F}{b} = \frac{Ed_{\mathrm{a}}^2}{6(l_{\mathrm{g}} \sin\theta + d_{\mathrm{e}} \cos\theta)} \varepsilon_{\mathrm{B}} \tag{10}$$

Equations 5 and 10 can be solved simultaneously to give,

$$\tan\theta = \frac{d_{\mathrm{a}}}{6l_{\mathrm{g}}} \frac{\varepsilon_{\mathrm{B}}}{\varepsilon_{\mathrm{A}}} - \frac{d_{\mathrm{e}}}{l_{\mathrm{g}}} \tag{11}$$

$$\frac{F}{b} = Ed_{\mathrm{a}} \sqrt{\varepsilon_{\mathrm{A}+}^2 \left(\varepsilon_{\mathrm{B}} \frac{d_{\mathrm{a}}}{6l_{\mathrm{g}}} - \varepsilon_{\mathrm{A}} \frac{d_{\mathrm{e}}}{l_{\mathrm{g}}} \right)^2} \tag{12}$$

These equations can be used to find both the force and angle of pull at the frame edge after the glass layers have fractured. However, both equations rely on the ability to separate out the axial strain from the bending strain using the gauge readings ε_{o} and ε_{i}. The axial strain is particularly difficult to extract reliably and is sensitive to a number of variables. It was found that the measured axial strain, ε_{A}, was not accurate

enough to reliably calculate the angle and force using Equations 11 and 12. Therefore, measurements for the angle of pull were made directly from analysis of the DIC displacement results. This was done using the two deflection points closest to the specimen edge at each strain gauge location. Then, using the measured angle in Equation 10 removes the need to find the axial strain component. For these reasons Equation 10, combined with the angle measured by DIC, was used to calculate all the edge forces after fracture of the glass plies.

4. Laminated glass finite element model

A finite element (FE) model of a 1.5 m × 1.2 m laminated glass pane with layup [3, 1.52, 3] mm was constructed in the Abaqus finite element software package. To simplify the modelling procedure the response of the laminated glass was split into two separate models, one to describe the precrack response and one to describe the postcrack response. A maximum stress criterion was used to determine the time of fracture of the glass layers. When a maximum principal stress greater than 80 MPa was observed (Cormie et al., 2009), the glass was assumed to have fractured and precrack model was stopped, with the current strain, position, and velocity of each element in the model then written to an output file. These were then imported into the postcrack model as initial conditions, along with any remaining load if the precrack model failed before the blast pressure pulse was over. The time-varying blast pressure was applied as a uniform pressure field across the window surface. This simplification allows symmetry conditions to be used, reducing computation time.

4.1. Precrack model

Two models were developed to describe the initial precrack response of the laminated glass, one simplified model using shell elements and one using solid continuum elements to capture the viscoelastic response of the PVB interlayer. The more complex solid continuum element model was developed to show that the simplified shell element model adequately captures the precrack response.

4.1.1. Shell element model

Shell elements describe the bending and in-plane (membrane) deformation of structures in which one dimension is significantly smaller than the others (plate-like structures). The S4R shell element in Abaqus is a 3D quadrilateral finite-membrane-strain shell element and was chosen to capture the laminated glass behaviour in this model.

A typical mesh generated by discretising the laminated glass pane into shell elements is shown in Figure 5. The coordinate system origin was defined at the centre of the laminated pane (shown by **O** in Figure 5) with the x-axis in the horizontal direction, the y-axis in the vertical direction and the z-axis positive in the

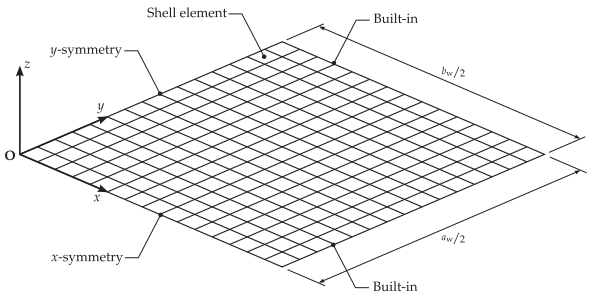

Figure 5: Simplified one-quarter model of laminate glass pane with shell elements.

direction of the applied pressure. This is the same coordinate system used in the DIC measurements. Only one quarter of the laminated glass pane was modelled as the assumption of a uniform pressure field across the window surface allows symmetry conditions to be imposed along the x-axis and y-axis. Displacements and rotations at the remaining two edges were assumed to be zero, giving a built-in type boundary condition similar to that provided by a deep joint. This is a simplification as the elasticity of a silicone joint will allow for some movement at the laminated glass edges. However, results of the simulation will be conservative since preventing this movement will increase stress levels in the pane, causing failure to occur earlier than in reality.

The cross-sectional behaviour of the shell elements was calculated from the material properties and thickness of each layer in the laminated glass. The glass layers were modelled with a linear elastic material model and their material properties are given in Table 3. Two material models for the PVB interlayer were analysed, a simple linear elastic material model and a viscoelastic material model to capture stress relaxation in the interlayer.

The solution of the model was found using the explicit solver in Abaqus (version 6.9). The time step used in the analysis was automatically controlled by the program to ensure numerical stability throughout the analysis. The number of elements in the finite element mesh was increased until the deflection profile at time of fracture converged on a solution. The converged shell element model had 1008 elements, each 20 mm × 20.4 mm. Typical computation time using a 2 GHz dual-core desktop processor was between 20 and 60 seconds for a refined mesh.

4.1.2. Small strain viscoelastic properties of PVB

The viscoelastic properties of PVB at small strains was measured using a TA Instruments Q800 dynamic mechanical analysis (DMA) machine. In DMA a sinusoidal strain is applied to a sample and the resulting stress is measured in order to calculate the storage modulus (the ratio between in-phase stress component

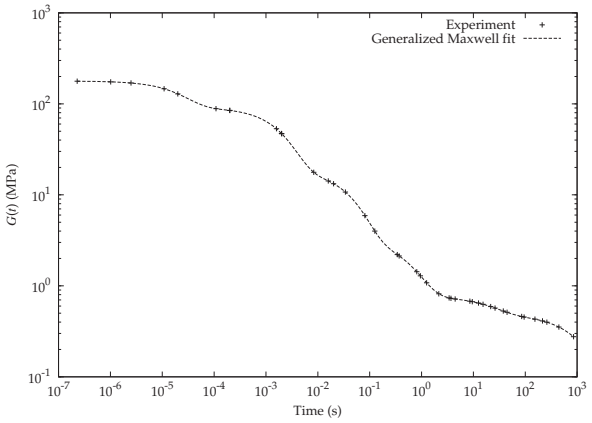

Figure 6: Shear relaxation curve for PVB measured using DMA.

Table 3: Section properties for laminated glass.

Layer	Material	Thickness (mm)	Density (kg/m^3)	Young's modulus (GPa)	Poisson's ratio
1	Glass	3	2530	72	0.22
2	PVB	1.52	1100	0.53*	0.485
3	Glass	3	2530	72	0.22

* Instantaneous elastic modulus for linear-elastic behaviour.

and strain) and loss modulus (the ratio between out-of-phase stress component and strain). This method was performed over a range of frequencies and temperatures to characterise the material at different time scales. The results of the DMA testing were used to construct a shear relaxtion curve using the procedure outlined in Bennison et al. (1999).

The experimentally determined shear relaxation curve is shown in Figure 6 along with a Generalized Maxwell model fit. In the linear elastic model a Young's modulus value of 530 MPa was used. This value corresponds to the instantaneous shear modulus value measured using dynamic mechanical analysis (DMA) and describes the behaviour at short time scales. The viscoelastic material model was defined in Abaqus using the Generalized Maxwell model fitted to DMA results. The terms used in the Generalized Maxwell model are given in Table 4.

4.1.3. Limitations of shell elements

The S4R shell element formulation in Abaqus accounts for nonlinear material behaviour and changes in layer thickness due to in-plane stress by recalculating section properties during the analysis (Simulia, 2010). However, shell elements assume that there is a linear variation of in-plane strain across the thickness of the

Table 4: Terms for viscoelastic material model of PVB.

i	G_i/G_0	τ_i (s)
1	0.49016	2.45×10^{-5}
2	0.40844	2.21×10^{-3}
3	0.08522	4.98×10^{-2}
4	0.01389	6.24×10^{-1}
5	0.00159	2.49×10^{1}

* Instantaneous shear modulus $G_0 = 178\,\text{MPa}$, long-term shear modulus $G_\infty = 0.125\,\text{MPa}$

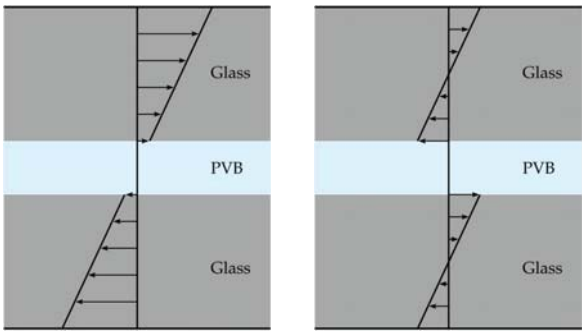

(a) Linear (b) Nonlinear

Figure 7: In-plane stress distribution through laminated glass thickness.

shell section when placed under bending. This is similar to the assumption in classical beam theory that plane sections in the undeformed beam remain plane when the beam is loaded.

In laminated glass this assumption may not be valid if there is a significant difference in the modulus values between the glass and PVB layers. Figure 7a shows the flexural stress distribution in the laminated glass if the in-plane strain varies linearly. The flexural stress distribution in each glass layer is collinear, that is they lie on a single straight line. The stress in the PVB layer is not visible because it is orders of magnitude less than that in the glass due to the difference in moduli. If the modulus in the PVB is drastically lower than that of the glass, the in-plane strain across the thickness of the shell section may depart significantly from the assumed linear variation. The extreme case is when the PVB's only function is to maintain the separation distance between the glass layers. The stress distribution in this case is shown in Figure 7b.

Norville et al. (1998) developed an analytical model of laminated glass beams where the in-plane strain across the thickness was allowed to depart from the linear assumption. The effective section moduli that they

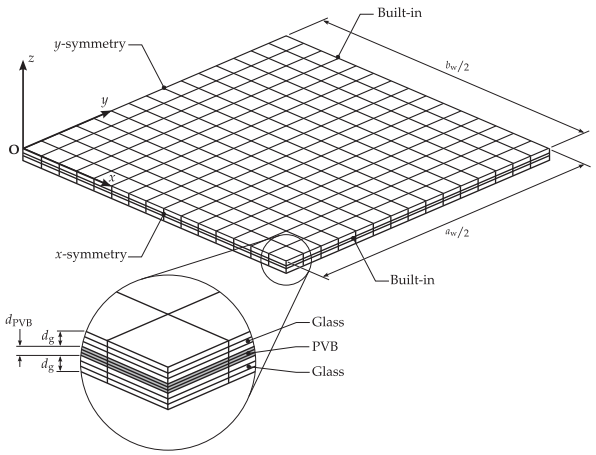

Figure 8: Solid element one-quarter model of laminate glass pane.

calculated for laminated glass beams approached those of monolithic beams of the same overall thickness when the loading duration was short or the temperature was low. This indicates that the assumption of a linear variation of in-plane strain across the thickness of the shell section is likely to be valid. To validate this further a full 3D solid element model of the laminated glass pane was also developed.

4.1.4. Solid element model

To fully capture cross-sectional behaviour of the laminated glass and the effects of viscoelasticity in the PVB interlayer a model using 3D solid continuum elements was constructed. By using a number of solid continuum elements over the thickness of the laminated glass the nonlinear variation of in-plane strain across the laminate thickness can be accounted for. The C3D8I solid continuum element in Abaqus was chosen for this model as it provides a good description of bending behaviour whilst remaining relatively computationally efficient (Simulia, 2010).

A typical structured regular mesh generated by discretising the laminated glass pane into solid elements is shown in Figure 8. The model is very similar to the shell element model except that each layer has three elements across its thickness, giving a total of nine elements across the thickness of the laminated pane. The material properties used were the same as those for the shell element model, as given in Tables 3 and 4. Simulation were conducted with both a linear elastic and viscoelastic material model of the PVB interlayer. This was to verify the results of the shell element model and to investigate the effect of the viscoelasticity on the laminated pane response. In both cases geometric nonlinearity was accounted for in the simulation.

The explicit solver in Abaqus was used again to find the solution and the number of elements in the finite element mesh was increased until the deflection profile at time of fracture converged on a solution. The

converged solid element model had 3 elements through each ply, giving a total of 9 through the thickness of the laminate. The laminated pane was divided into 5 mm × 5 mm blocks, giving a total of 162,000 elements. Typical computation time for the solid element model using a 2 GHz dual-core desktop processor was between 10 and 20 hours for a refined mesh, a significant increase over the shell element model.

4.1.5. Effect of viscoelasticity in the PVB

To determine the effect of viscoelasticity in the PVB interlayer on the blast response of the laminate glass, the two precrack models were solved with and without viscoelasticity in the interlayer. A blast load with a peak reflected pressure of 130 kPa and a positive phase duration of 6.5 ms, giving a total reflected impulse of 423 kPa · ms, was applied to the laminated glass pane. This blast loading would be equivalent to that generated by a 30 kg TNT charge at a stand off distance of 14 m, the same loading as in test 4. The analysis was run until the maximum principal tensile stress in the glass layers exceeded 80 MPa (Cormie et al., 2009).

Figure 9 shows a comparison of the profiles predicted by the two models with and without viscoelasticity in the interlayer at a time of 1.2 ms, the approximate time of fracture in the glass. The solid element model without viscoelasticity and both shell element models give near identical deflection profiles. Viscoelasticity in the shell element model has little effect because a nonlinear variation of in-plane strain across the pane thickness is not possible with these elements. The flexural stresses in the interlayer are too small compared to those in the glass layers to make a significant difference to the response. The agreement between the elastic solid element and elastic shell element models suggests that the difference in modulus between the glass and PVB layers is not large enough to cause a significant departure from the assumption of a linear variation of in-plane strain across the pane thickness.

The deflection profile predicted by the viscoelastic solid element model departs slightly from those generated by the other three simulations. This is because a small amount of relaxation occurs in the interlayer, increasing the difference in modulus between the glass and PVB layers and reducing the flexural stiffness of the laminated glass section. Figure 10 shows the in-pane stress distribution across the thickness, y_l, of the laminate at $x = 360$ mm and $y = 0$ mm, the location of maximum stress on the horizontal cross-section, for the different models. As expected the shell elements show a collinear stress distribution in each glass layer and small stresses in the PVB interlayer. The stress distribution does not intersect through zero since there is also a tensile membrane stress; the shell is not in pure bending.

In the solid element model, the in-plane stress distributions in each glass layer remain parallel but are now offset. The linear in-plane strain distribution across the laminate thickness is no longer enforced and

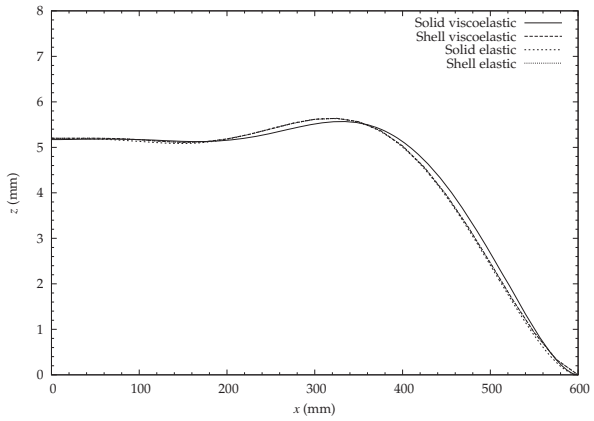

Figure 9: Comparison of deflection profiles at the pane centre ($y = 0\,\text{mm}$) and a time of 1.2 ms produced by different models.

each glass layer is allowed to bend somewhat independently. The offset in the stress distributions in each glass layer is determined by how much horizontal shear force the PVB interlayer transfers from one glass layer to the other. In the extreme case shown in Figure 7b no horizontal shear force was transferred between the glass layers. In Figure 10 only a small reduction in the horizontal shear force transfer is seen. The reduction in the horizontal shear force transfer is dependent on the PVB modulus. The solid viscoelastic model shows a greater offset in the stress distributions in each glass layer than the solid elastic model due to stress relaxation in the interlayer.

The effect of this stress relaxation in the interlayer on the overall deflection profile is small (Figure 9). The maximum principal stress in the glass layers is also reduced by stress relaxation in the interlayer,

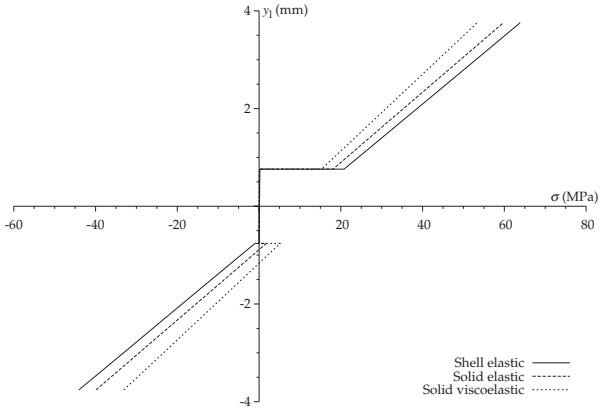

Figure 10: Comparison of maximum principal in-plane stress predicted at $x = 360\,\text{mm}$ and $y = 0\,\text{mm}$ by different models.

meaning the glass is likely to fracture at a later time. The effects of stress relaxation may become more pronounced in long duration loading cases, in which the peak pressure to cause failure is lower and in which the glass takes tens of milliseconds to fracture. In these cases the flexural stiffness of the laminate would decrease over time, reducing the stress in the glass layers and delaying fracture.

4.2. Postcrack model

A shell element model was constructed to model the postcrack phase of the laminated glass response. The postcrack model was identical to the precrack shell element model except for modified material properties to describe the stress-strain response of cracked laminated glass. Cracks in the glass layers were assumed to have developed instantaneously and densely across the whole window pane at the end of the precrack model. The elastic modulus of the glass layers was therefore reduced to approximately zero to account for this[1]. The glass layers were not removed completely from the model since their mass still contributed to the response of the laminate.

The material properties of the interlayer were changed to describe the overall tensile stress-strain response of the cracked laminated glass, investigated experimentally using a high-speed servo-hydraulic test machine. Figure 11 shows the experimental setup for measuring the stress-strain response of cracked laminated glass at different strain rates. A Johnson-Cook (JC) plasticity model was chosen to describe the rate dependent stress-strain response of cracked laminated glass. The JC model is empirically based and was originally developed to describe the effects of strain rate and temperature on the plastic deformation of metals (Johnson and Cook, 1985). When the effects of temperature are ignored, the stress required for plastic flow is defined as

$$\sigma = \left(A + B\varepsilon_{\mathrm{p}}^{n}\right)\left(1 + C\ln\frac{\dot{\varepsilon}}{\dot{\varepsilon}_0}\right) \tag{13}$$

where ε_{p} is the plastic strain, $\dot{\varepsilon}$ is the strain rate, $\dot{\varepsilon}_0$ is a reference strain rate and A, B, C and n are material constants. The terms in the first bracket describe the yield stress of the material as the plastic strain increases at the reference strain rate. The second bracket accounts for the increase in yield stress with increasing strain rates.

The JC plasticity model does not completely capture the behaviour of cracked laminated glass. Use of the JC plasticity model in Abaqus requires that the initial elastic modulus is independent of strain rate. The modulus of cracked laminated glass was observed to show a dependence on strain rate. For randomly cracked

[1] A value of 1 Pa was used as Abaqus will not accept zero stiffness.

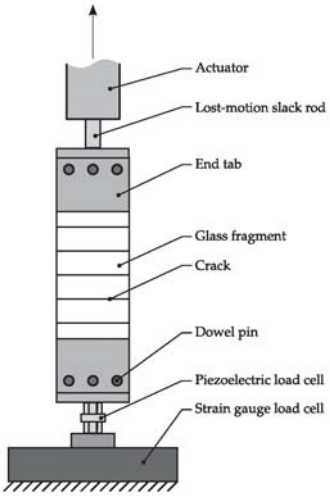

(a) Test setup

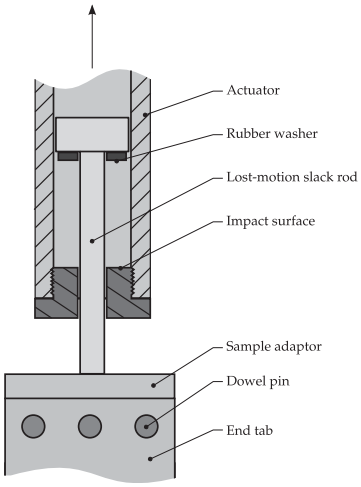

(b) Lost motion device

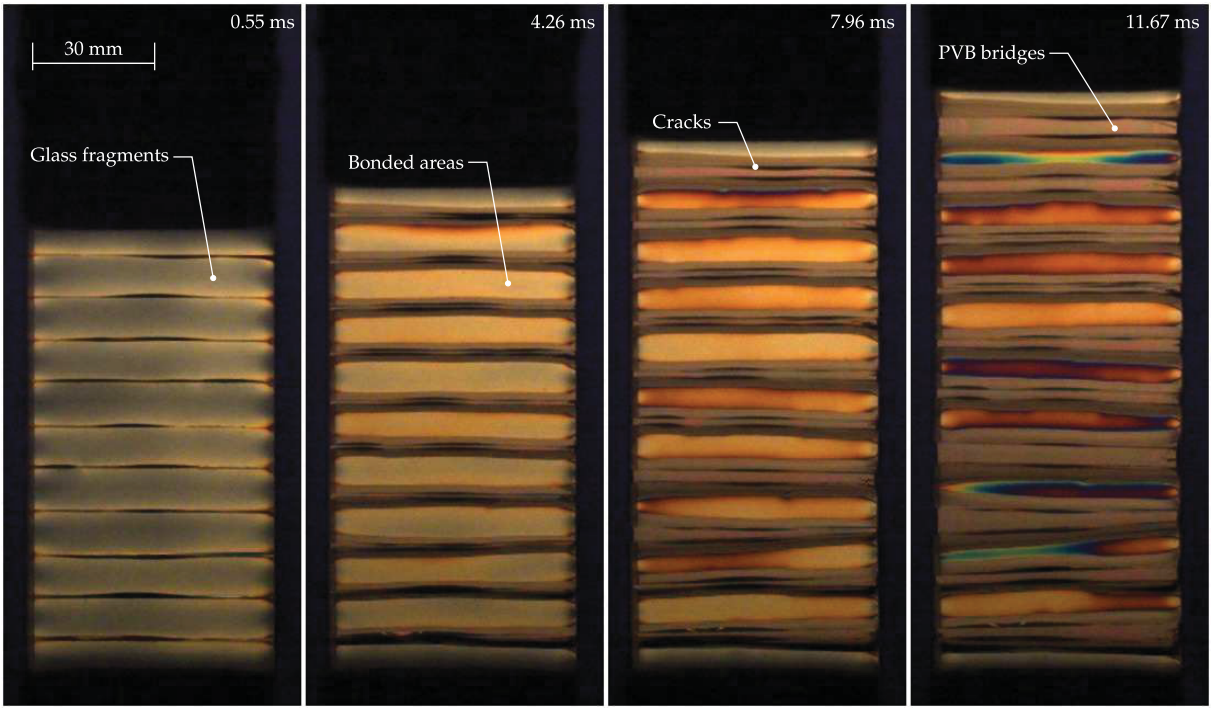

(c) Cracked laminated glass test viewed through polarizing filters

Figure 11: Cracked laminated setup with images of delamination process.

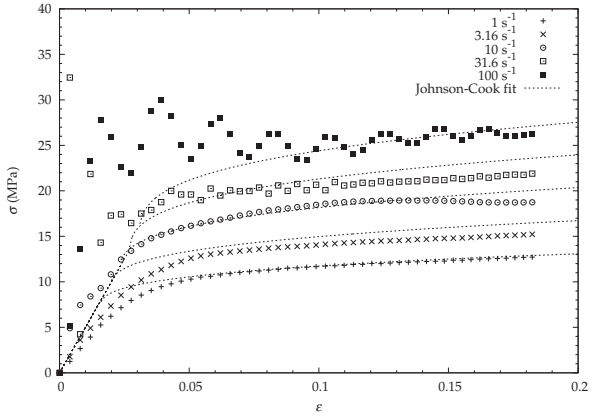

Figure 12: Johnson-Cook model of 7.52 mm cracked laminated glass.

laminated glass with an interlayer thickness of 1.52 mm the observed modulus varied between 0.3 GPa and 14 GPa for strain rates between $1\,s^{-1}$ and $100\,s^{-1}$. However, strain rates observed in blast testing were in the order of $1\,s^{-1}$ to $10\,s^{-1}$. These equate to moduli values of 0.3 GPa to 0.8 GPa. An assumed initial modulus of 0.55 GPa was therefore chosen to represent the modulus at the expected strain rates.

The JC model was designed for plasticity. Any deformation above the yield stress is permanent and only the elastic deformation is recovered on the removal of the applied stress. The cracked laminated glass is not fully plastic and if given enough time will exhibit some recovery to almost its initial length. If it is assumed that the time scale for complete recovery is orders of magnitude greater than the duration of the blast response, then the deformation of cracked laminated glass is essentially plastic over the time scales of interest. If the postcrack model is only used up to the point of maximum deflection, it is assumed that recovery effects can be ignored.

Equation 13 was fitted to the experimental data obtained for randomly cracked laminated glass with an interlayer thickness of 1.52 mm using nonlinear regression. Material constants A, B and n were determined first by fitting the model to the data obtained at a reference strain rate $\dot{\varepsilon}_0$ of $1\,s^{-1}$. The constant C was then determined by fitting the model to the data obtained at increased strain rates. Figure 12 shows a comparison between the stress-strain curves calculated by the JC model and the experimental results. The determined material constants are given in Table 5. The oscillation of stress at the high strain rates ($100\,s^{-1}$) are dynamic inertial effects due to the test method and are not part of the material response.

4.3. Blast load prediction

The blast load applied to the window in the laminated glass finite element model was predicted using the Air3D software packages (Rose, 2001). The Air3D simulations were conducted using the ftt_air3d

Table 5: Constants for Johnson-Cook model of cracked 7.52 mm laminated glass.

A (MPa)	B (MPa)	C	n
6.72	10.6	0.248	0.303

(version 1) variant of the Air3D code with adaptive mesh refinement and detonation modelling using the Jones-Wilkins-Lee (JWL) equation-of-state (Dobratz and Crawford, 1985). Each simulation was conducted with an initial 1D solution of the detonation and blast wave between the charge centre and the ground (the charge was assumed to be spherical). Once the wavefront reached the ground the 1D solution was remapped to a 2D analysis of the blast wave. This was so that ground reflections were included in addition to the wave directly from the charge (the ground was assumed to be a perfect reflector). This analysis was carried out until the wavefront reached the test cubicle. After this a full 3D analysis of the interaction between the blast wave and the cubicle was performed. This was to account for the reduced impulse on the window due to clearing effects. The cubicle was modelled as a rigid target and a plane of symmetry was defined in the vertical direction between the charge centre and the centre of the test cubicle. A pressure monitoring point was defined at the centre of the window to record reflected pressure. The cell size used in the simulations was refined until the calculated reflected impulse converged on a solution.

5. Results and discussion

The experimental results from the full scale blast tests are presented and compared with the predictions of the laminated glass finite element model to give a clear account of the behaviour of laminated glass under blast loading and to demonstrate the applicability of the model to different blast loads. The FE predictions were made using the pressure output from the Air3d simulations. Figure 13 shows measured central displacement-time histories for each test and these data are compared with predictions from the FE model. Measured reflected pressure time histories are also shown along with those predicted by Air3d as detailed in Section 4.3. These data are synchronised so that $t = 0$ ms corresponds to the arrival of the blast wave.

The measured central displacement data shows good agreement with predictions in the early phase of the laminated glass response. The effect of restraint at the edges on the central displacement is minimal at this stage and the central displacement is largely determined by the applied pressure and the area mass density of the laminate. A summary of the blast pressures and the response of the laminated glass pane in

Table 6: Summary of DIC measurements for each test.

Test	W (kg)	R (m)	$z_{\max}$ (mm)	$v_{\max}$ (m/s)	$a_{\max}$ (km/s^2)	$\varepsilon_{\max}$	$\dot{\varepsilon}_{\max}$ (s^{-1})	$\theta_{a,\max}$ (deg)	$\theta_{b,\max}$ (deg)	Failure description
1*	15	10	179	27.3	6.1	0.15	20	34	37	Joint failed at all edges. Pane came to rest soon after joint failed and fell outside the cubicle.
2	15	13	173	17.4	3.4	0.04	10	24	23	Pane rebounded. Joint failed at inner edge on rebound.
3*	30	16	205	20.5	3.6	0.06	10	26	27	Joint failed at inner edge leading to top edge.
4*	30	14	140	29.0	6.0	0.06	15	30	34	Joint failed at all edges. Significant inward velocity after failure and pane impacted screen protecting cameras.

* Values taken up to the point of failure.

each test is given in Table 6 and Table 7.

In Test 1 (15 kg at 10 m) the single sided joint failed around the perimeter. The joint failure was first observed at 9 ms (180 mm displacement). The pane reaches a maximum velocity of 26 m/s and came to rest at a displacement of approximately 350 mm.

In Test 2 (15 kg at 13 m) the pane reached a maximum deflection of approximately 170 mm at 14 ms before rebounding. The single sided joint began to fail on the rebound phase. No tearing of the PVB interlayer was observed. The peak velocity was approximately 18 m/s.

In Test 3 (30 kg at 16 m) a displacement of approximately 200 mm was reached before the joint began to fail down the left hand edge at a time of 12 ms. The DIC technique was unable to compute results beyond this time due saturation of the images from light entering around the failed joint. No tearing of the PVB interlayer was observed. The peak velocity was approximately 21 m/s.

In Test 4 (30 kg at 14 m) the joint had completely failed around the perimeter by 8 ms at a displacement of approximately 265 mm. The pane was still accelerating at this point and continued travelling into the cubicle until it impacted a screen protecting the cameras. The peak velocity was approximately 34 m/s. No tearing of the PVB interlayer was observed.

The following figures (Figures 14 to 17) show the images captured by the high speed camera alongside the displacement and strain measured using DIC and are compared with the predictions from the laminated glass FE model. In all cases, the magnitude and contour shape of the out-of-plane displacement plots for DIC measurements and FE predictions agree very well. The maximum in-plane principal strain plots show regions of high strain along the edges for both DIC and laminated glass FE model but there are some

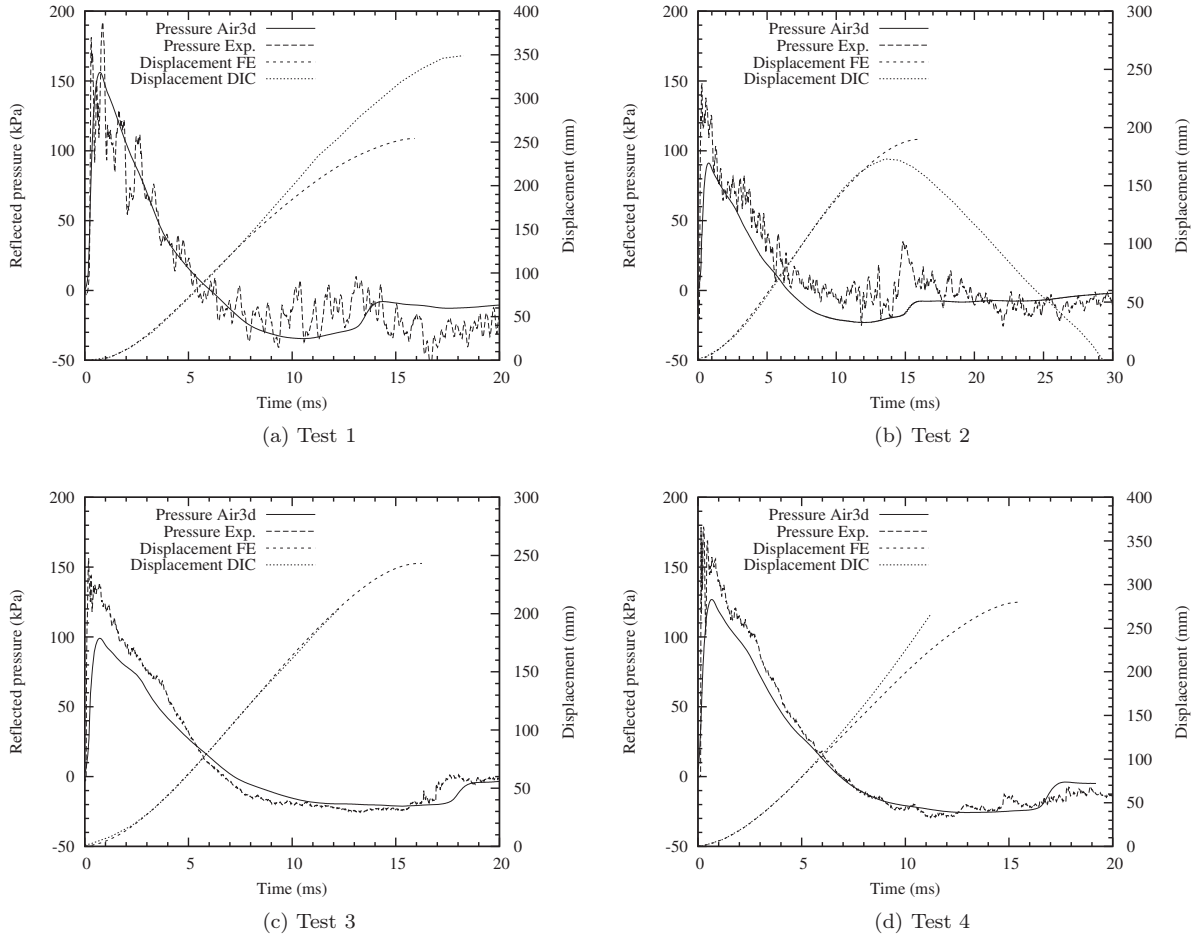

(a) Test 1 (b) Test 2

(c) Test 3 (d) Test 4

Figure 13: Comparison of measured and predicted reflected pressure and central displacement for each test.

differences in strain magnitude.

5.1. Deflected shape and strain

The contour lines in Figures 14 to 17 are approximately rectangular in shape and are spaced more tightly close to the window edges. This indicates that the deformed areas are concentrated around the window edges and that the central region of the window is largely flat and undeformed. In some of the DIC displacement plots the contour lines are not rectangular and surround an area towards the bottom left of the plots, indicating that the window has deflected more in this region. This is because the pressure and impulse on the window are higher near to the bottom of the window due to the blast wave reflecting from the ground. The blast wave arrival time was also sooner here.

Under blast loading the window pane has a peak initial acceleration and quickly acquires an approxim-

Table 7: Peak pressure and positive impulse at pane centre.

			Experiment		Air3d	
Test	W (kg)	R (m)	p_r (kPa)	i_r (kPa · ms)	p_r (kPa)	i_r (kPa · ms)
1	15	10	180	391	155	391
2	15	13	140	284	91.2	284
3	30	16	132	413	99.0	344
4	30	14	152	461	127	413

ately uniform velocity field across its surface. If the blast wave duration is short compared to the natural period of the pane response the subsequent deflection occurs entirely due to the momentum of the pane. At the edges of the window the pane is at rest due to the frame. This restraint causes a transverse deceleration wave to propagate inwards from each edge towards the centre. In the early stages of the response, the centre region of the window is ahead of the deceleration wavefront and continues to travel inwards, unaffected by the restraint at the edge. Behind the deceleration wavefront the pane loses the momentum it initially acquired and effectively comes to rest. The result is a deflected shape that consists of a relatively flat central region with deformed curved regions close to the edges. The maximum deflection occurs when the transverse waves reach the window centre and the whole profile is curved (when taken across the shortest dimension).

Figures 14 to 17 also show how the strain is not uniform and concentrates close to the window edge, leaving the central region relatively unstrained. Lines of strain can be seen passing through the central region in the later frames of the DIC measurements and are indicators for the fracture paths in the glass plies. The white areas in the last frames of Test 1 are where the image correlation has been unable to calculate strain data due to missing facets.

Figure 18 shows displacement cross-sections taken horizontally through the window at $y = 0\,\text{mm}$ for each test. The axes have both been scaled equally so that the profile is not exaggerated. Each line is plotted at 2 ms intervals and clearly show the relatively flat central region deflecting into the cubicle and deformed curved regions close to the edges. As the pane deflects further the flat central region becomes smaller until the whole profile is curved. This is due to the restraint at the edges causing transverse waves to propagate inwards towards the centre from each edge.

The ends of the profiles measured using DIC deflect approximately into the cubicle despite the window being restrained at this point. There are two reasons for this behaviour. The frame to which the window was attached exhibited a small degree of compliance and deflected in response to the blast load. Also, the

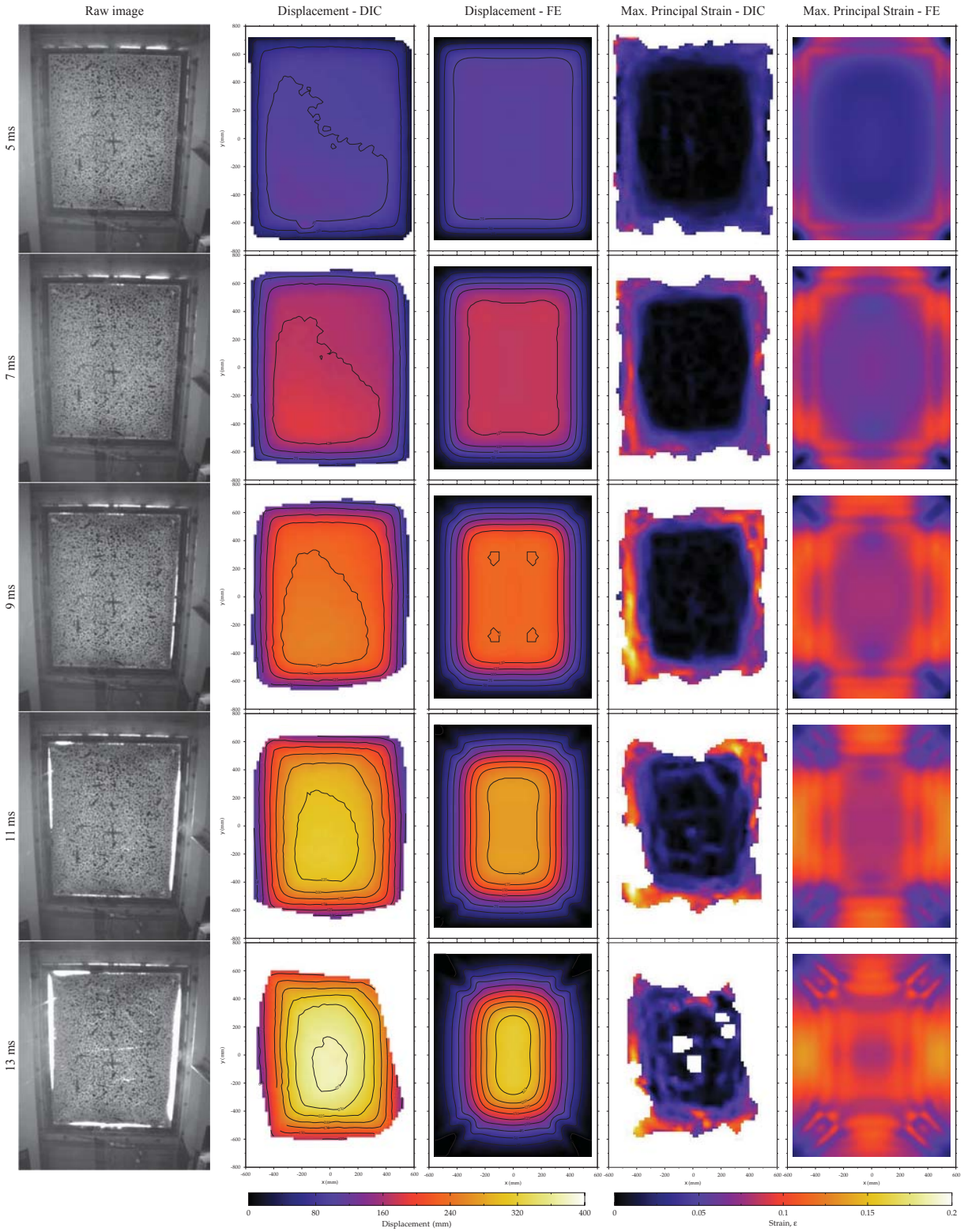

Figure 14: Sequence of images from high speed camera alongside out-of-plane displacement and maximum in-plane principal strain measured using DIC and predictions from the laminated glass FE model for Test 1 (15 kg at 10 m).

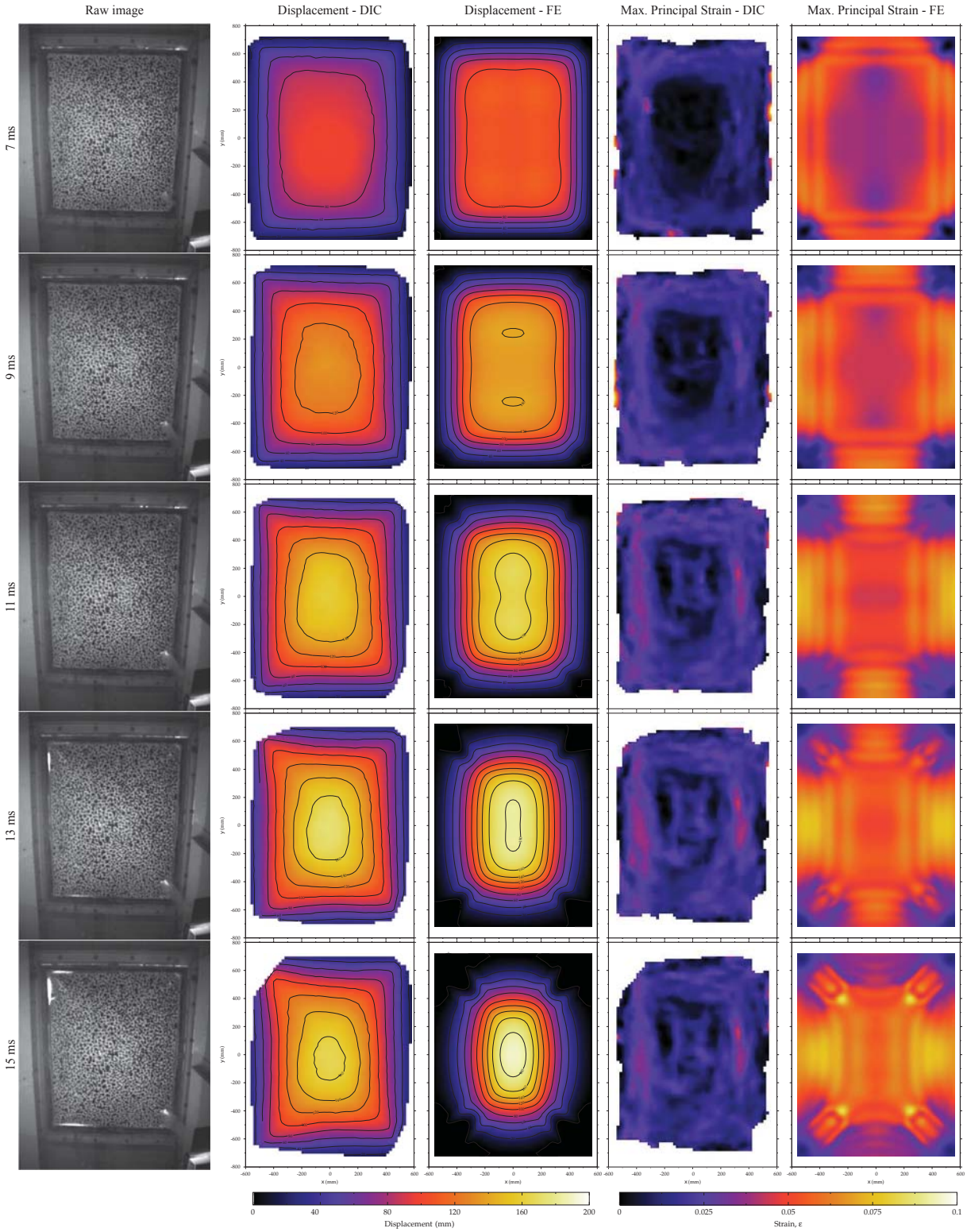

Figure 15: Sequence of images from high speed camera alongside out-of-plane displacement and maximum in-plane principal strain measured using DIC and predictions from the laminated glass FE model for Test 2 (15 kg at 13 m).

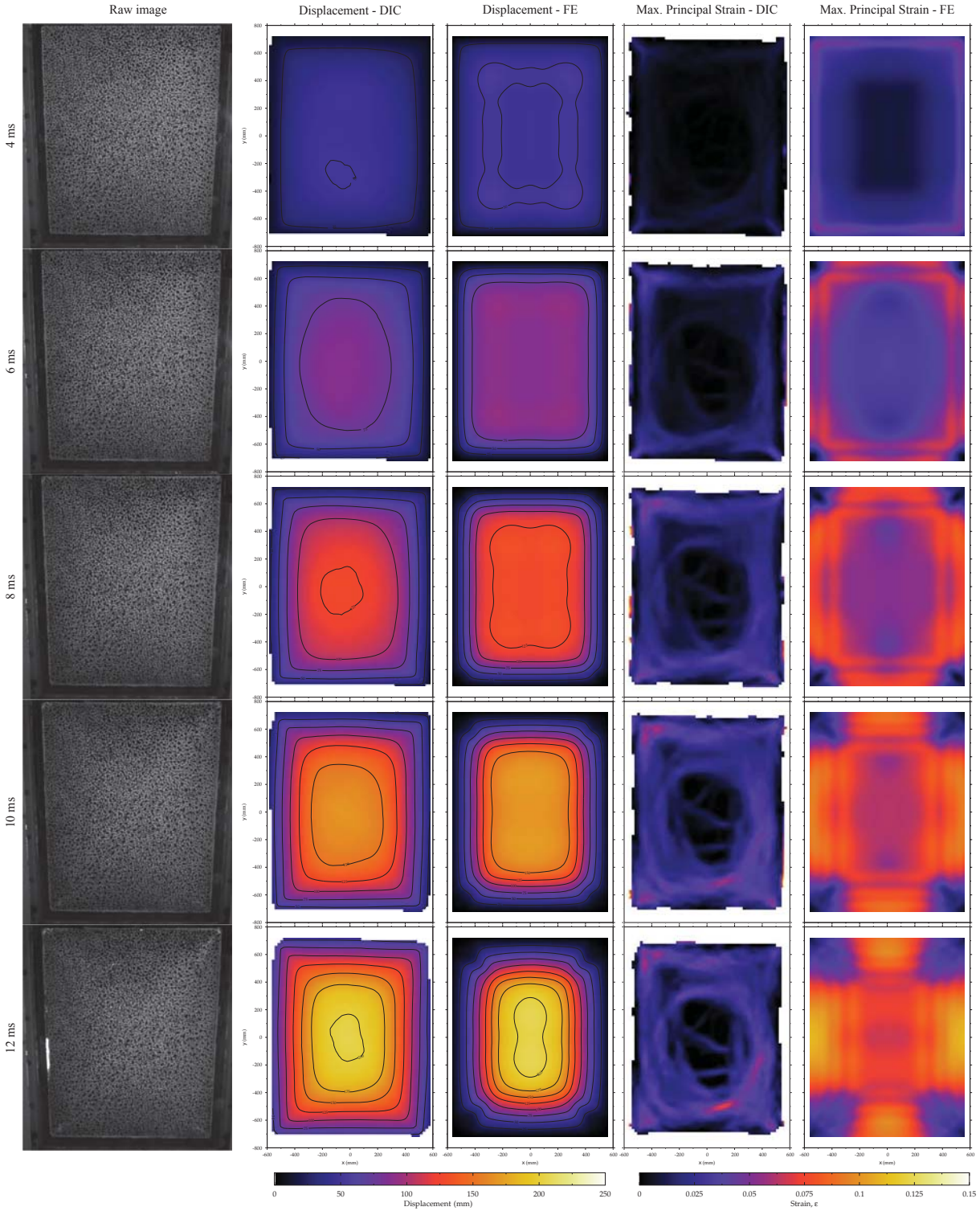

Figure 16: Sequence of images from high speed camera alongside out-of-plane displacement and maximum in-plane principal strain measured using DIC and predictions from the laminated glass FE model for Test 3 (30 kg at 16 m).

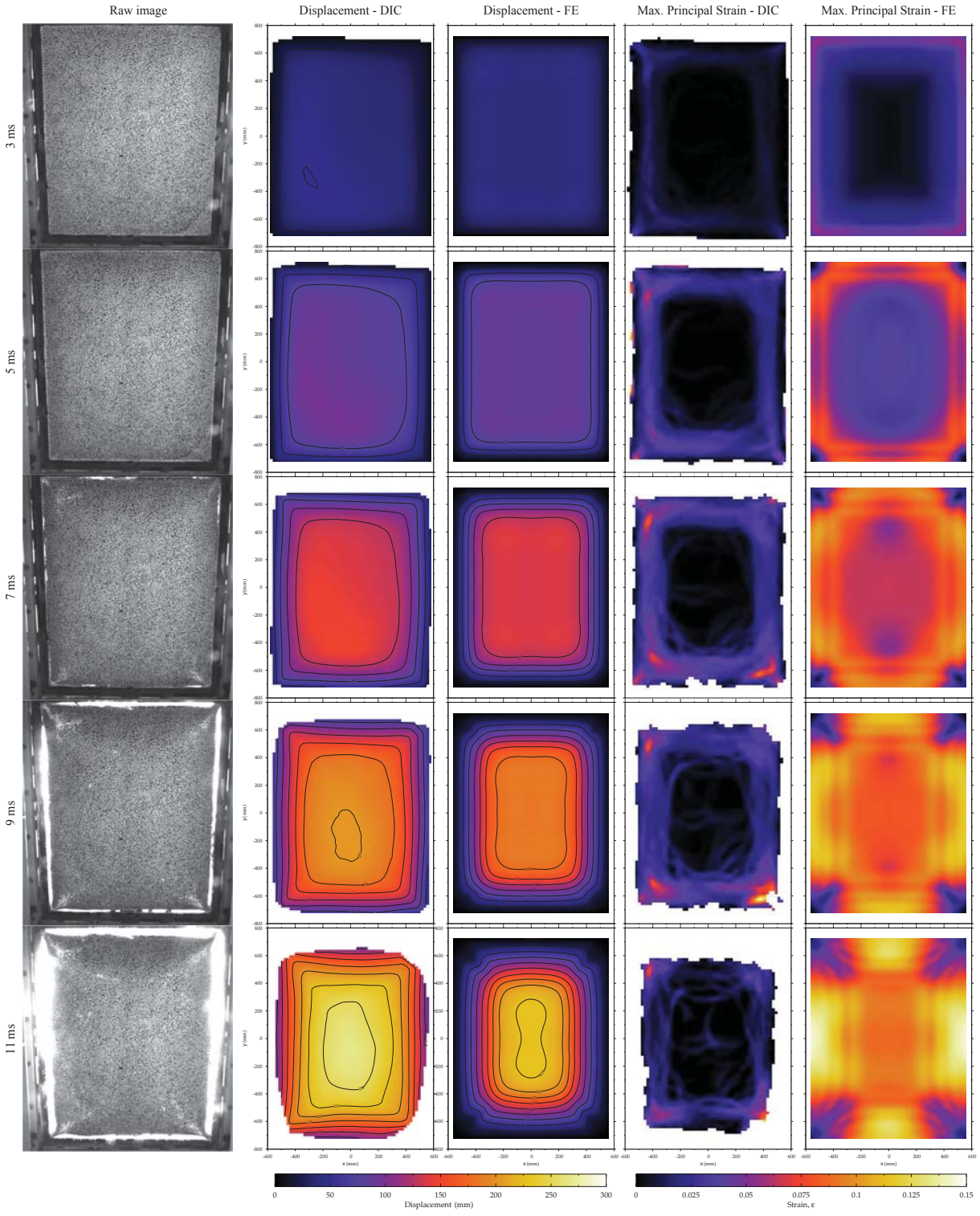

Figure 17: Sequence of images from high speed camera alongside out-of-plane displacement and maximum in-plane principal strain measured using DIC and predictions from the laminated glass FE model for Test 4 (30 kg at 14 m).

DIC method can not track right into the window edges. As a result there will always be an offset between the window edge and the last point tracked.

Figure 18 also shows a comparison of the experimentally obtained deflection profiles against the laminated glass finite element model. In early phases the profiles show good agreement with the experimental profile, except for a small deviations close to the edge. These differences result from the assumption that the window edges are fixed to a rigid structure in the finite element model when in the experiments this boundary condition is impossible to obtain. In the later stages of Tests 1 and 4, the predicted profiles begin to depart more significantly from the measured profiles. In these tests the joint fails completely, allowing large displacements at the edges. In later stages of Tests 2 and 3, the measured and predicted profiles also depart but less significantly. At the edge of the profile, the laminated pane begins to rebound, giving the pane a negative velocity in this region. The region that has rebounded increases in size until it reaches the centre of the pane, at which point the maximum central deflection is reached. This behaviour was not observed in the experimental profiles. Possible reasons for this deviation are discussed in more detail in Section 5.4.

5.2. Reaction force and edge angles

Figure 19 compares the predicted and measured edge reactions forces and angle of pull at the midpoint of the vertical edge ($x = 570\,\text{mm}$, $y = 0\,\text{mm}$) for each test. A definition of the angle of pull and reaction force can be found in Section 3.2.1. The reaction forces measured in blast testing have a shape that is similar to the FE predictions if the high frequency oscillations in the experimental data are ignored. These high frequency oscillations are due to vibrations in the supporting window frame and cubicle which were not included in the finite element simulation. The magnitude of the force predicted by the FE model is consistently larger than that measured in blast testing. This is possibly due to the flexibility of the test cubicle. Also shown in Figure 19 is the time-history of the angle of pull (θ in Figure 4b) formed at the same location for each test. The angle at each edge increases steadily after the blast wave arrives reaching values of the order of 30° to 40°. The angles measured in the experiments increase slower than those predicted by the FE model. This is due to the movement of cubicle at the window edge reducing the effective angle formed. Peak measured edge reaction forces and angles of pull are summarised in Table 8.

5.3. Pressure impulse analysis

A pressure-impulse analysis was conducted using the finite element model to determine the level of predicted damage over a wide range of charge sizes and stand-off distances. The model was run with peak reflected pressures in the range of 1 kPa to 1 MPa and positive impulses in the range of $10\,\text{kPa}\cdot\text{ms}$ to $10\,\text{MPa}\cdot\text{ms}$. For simplicity the blast load applied to the pane was idealised as a triangular pressure pulse

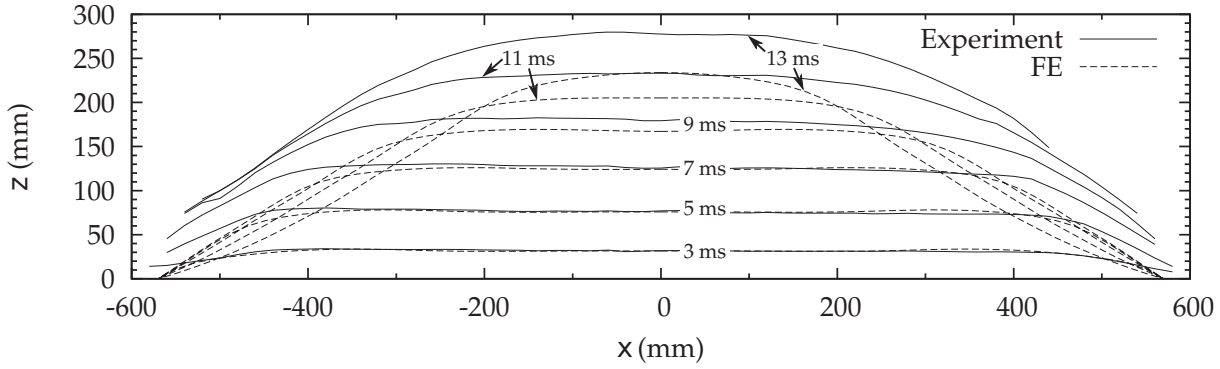

(a) Test 1

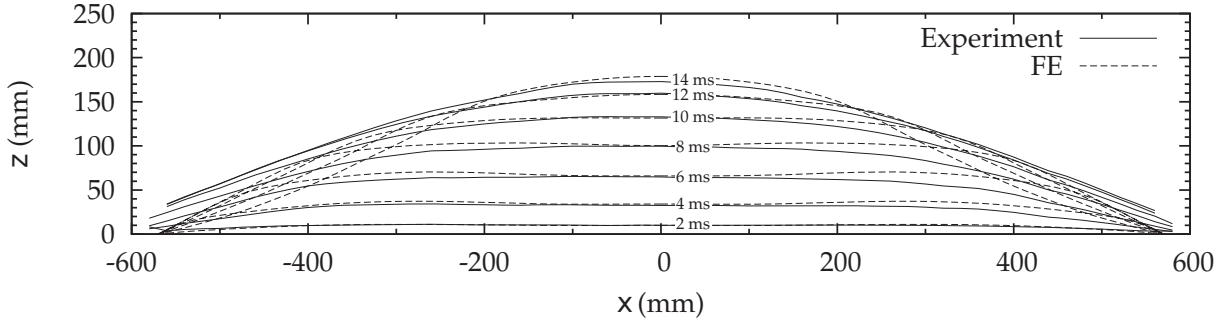

(b) Test 2

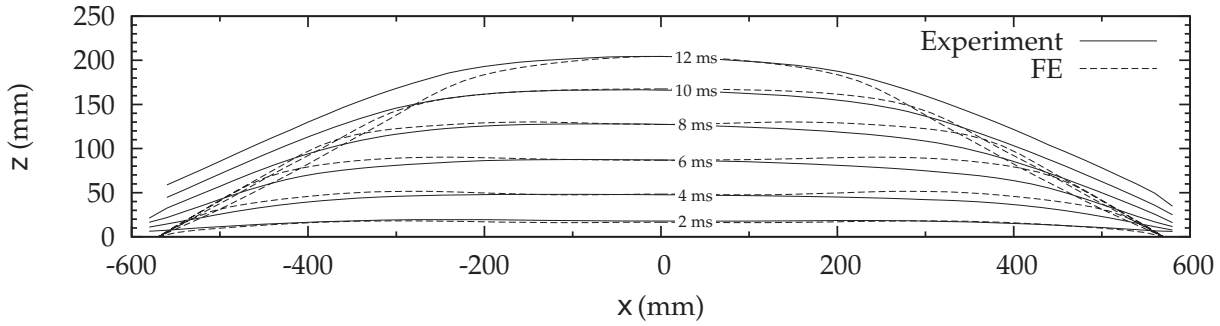

(c) Test 3

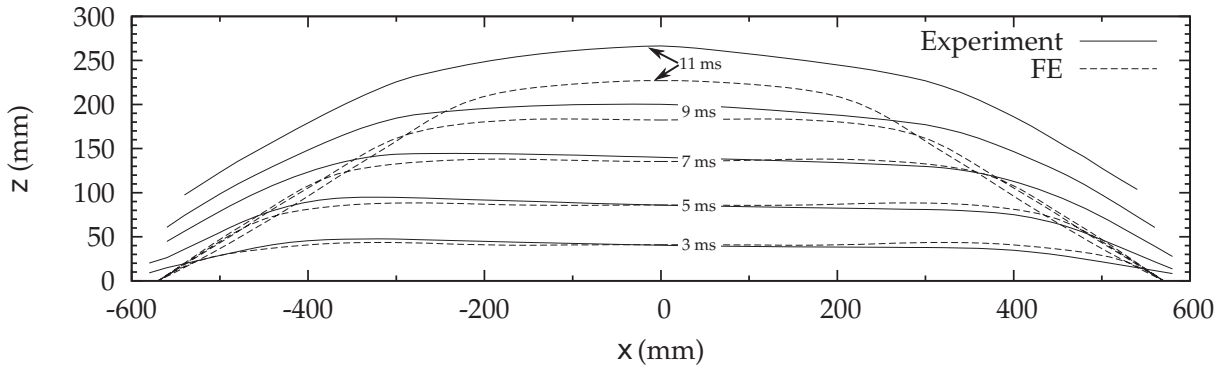

(d) Test 4

Figure 18: Comparison of the measured DIC and predicted laminated glass FE model profiles taken horizontally at the window centre for each test.

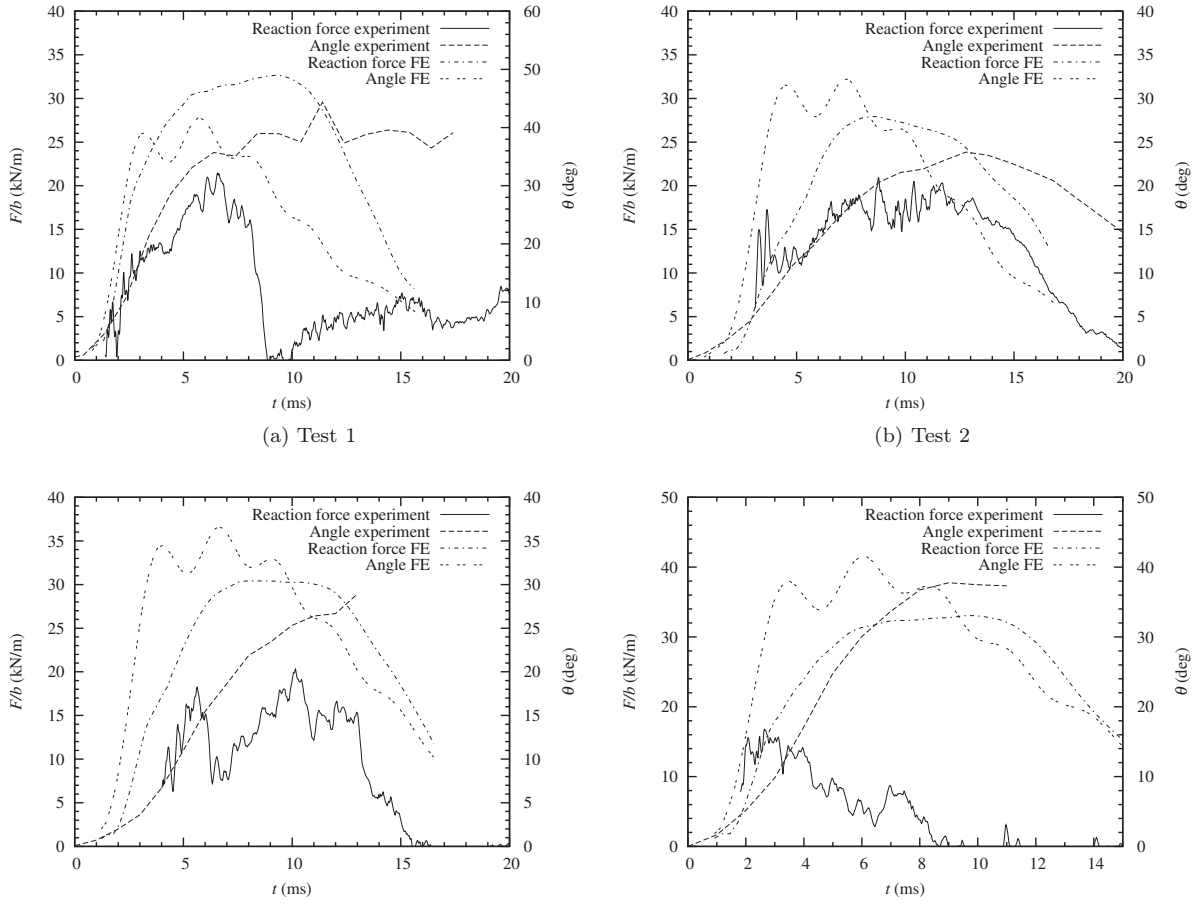

(a) Test 1 (b) Test 2

(c) Test 3 (d) Test 4

Figure 19: Comparison of reaction forces and angle formed at window edge.

Table 8: Edge reaction failure forces (see Figure 2a for strain gauge locations).

			F_f/b (kN/m)					θ_f (deg)				
Test	W (kg)	R (m)	Top	Bottom	Centre	Wall	Offset	Top	Bottom	Centre	Wall	Offset
1	15	10	22	-	-	21	-	34	26	27	35	-
2*	15	13	-	16	24	30	-	20	24	23	23	-
3	30	16	15	10	20	19	11	26	26	27	26	23
4	30	14	19	23	18	15	14	30	30	34	18	31

* Maximum values on inward stroke.

with zero rise-time and no negative phase. A bracketing procedure was used to find the pressures and impulses required to produce constant levels of damage. The levels of constant damage investigated were

defined by the point of first cracking in the glass plies and when the peak in-plane principal strain in the cracked laminated glass reached levels of 5%, 10%, 15% and 20% before maximum deflection.

Figure 20 shows the iso-damage curves produced by the model at these damage levels. Lines of constant charge weight and stand-off distance have been overlaid on the figure to allow easy determination of the reflected pressure and impulse for a particular threat (assuming infinite facade dimensions). If the applied pressure and impulse for a particular blast load lies toward the lower left of an iso-damage line then the laminate will not reach that level of damage. If the applied pressure and impulse lie toward the upper right of an iso-damage line then the laminate will have exceeded that level of damage.

The curves show asymptotic behaviour in both pressure and impulse. The pressure asymptote (horizontal) is formed at the minimum pressure required to cause a certain level of damage. At this pressure the level of damage experienced will not increase with an increasing impulse. This asymptote is also known as the quasi-static asymptote as it represents loads which vary slowly with respect to the response of the pane. Similarly the impulsive asymptote (vertical) is formed at the minimum impulse required to cause a certain level of damage. At this asymptote, any increase in the applied pressure has no effect on the damage level obtained. A maximum strain of 20% is suggested as being the maximum strain that the laminate can safely experience. This iso-damage level can be used to assess whether the laminate is safe for a particular blast load.

Smith (Smith, 2001; Cormie et al., 2009) has developed a single-degree-of-freedom (SDOF) model, consisting of an equivalent load, mass and nonlinear resistance function, to describe the behaviour of laminated glass under blast loading. Figure 20 compares the predicted iso-damage curve of the SDOF model against the laminated glass FE model developed in this paper for a 7.52 mm thick 1.5 m $\times$ 1.2 m laminated pane.

The predicted iso-damage curves for fracture of the glass plies show good agreement on the pressure asymptote (long duration pulses) but differ on the impulsive asymptote (short duration pulses). In the impulsive case, the SDOF model predicts that a greater impulse is required for cracking at any given pressure. The pressures and impulses required to produce this behaviour are only reproducible from small charges at small stand-off distances. Under these conditions the pressure distribution across the window will not be uniform. Both models assume a uniform pressure distribution and as a result will overestimate the resistance at these loads. The laminated glass FE model could be extended to include the nonuniform pressure distribution to yield more accurate estimates of cracking in this regime.

The predictions of safe strain levels in the cracked laminate produced by the finite element and SDOF models are also shown in Figure 20. The safe limit used by the SDOF model for this pane size was determined

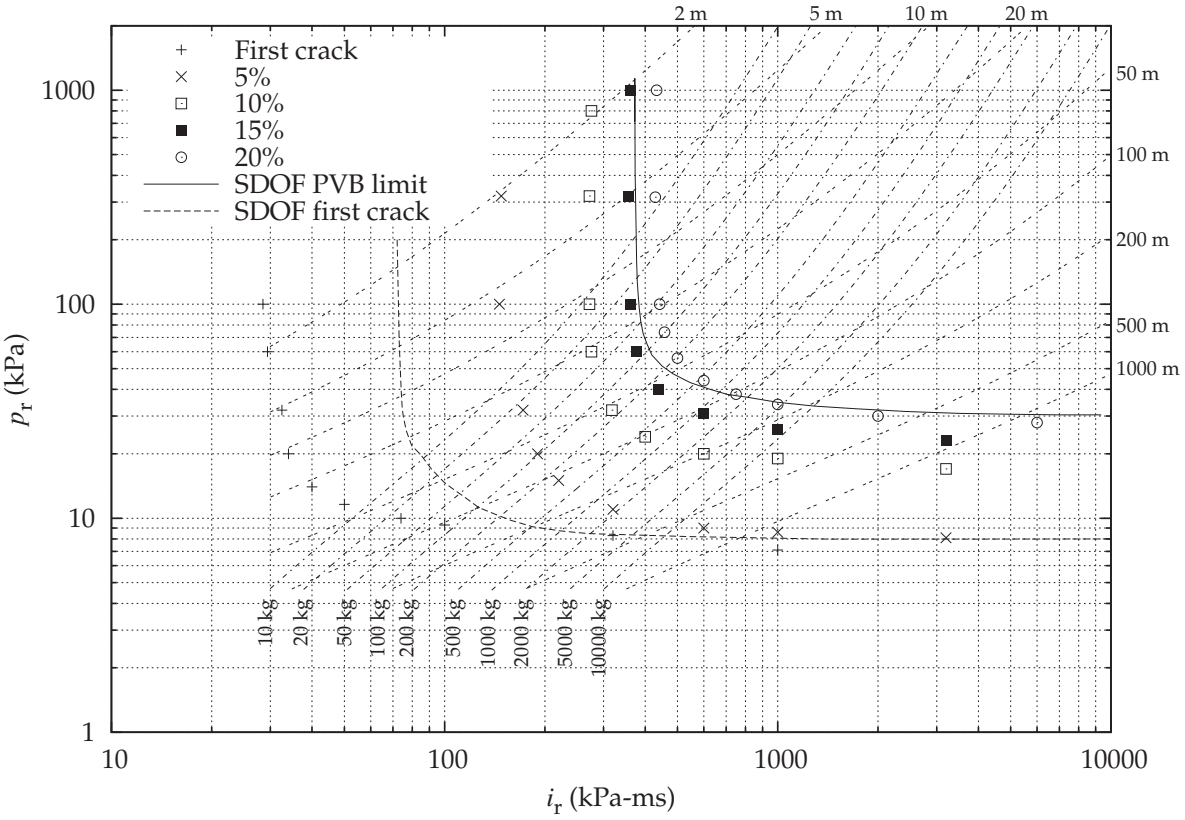

Figure 20: Iso-damage curve predictions compared with SDOF model (Cormie et al., 2009).

from the pressures and impulses required to produce a peak central deflection of 200 mm. This equates to a maximum in-plane strain of approximately 9%. This limiting deflection was set from observations made in numerous blast tests. Good agreement is seen between the SDOF iso-damage curve and the 20% strain level iso-damage curve produced by the finite element model. A slight increase in the position of the impulsive asymptote is seen with the 20% strain finite element iso-damage curve when compared to the SDOF prediction. The finite element iso-damage curves are shown at different strain levels to show the sensitivity to the maximum acceptable strain criteria. The use of an iso-damage curve at a reduced strain may be more appropriate in certain applications, for example, where the window is expected to operate at low temperatures.

5.4. Limitations of the finite element model

5.4.1. Material model of cracked laminated glass

In the development of the finite element model it was assumed that the behaviour of cracked laminated glass could be adequately modelled by reducing the stiffness in the glass layers to zero and using a Johnson-

Cook plasticity law to describe the overall response of the cracked laminate. The reduction in stiffness in the glass layers gives the cracked laminate very little flexural stiffness. It was assumed that the cracked laminate only acts as a membrane. However, the cracked laminate will only act as a pure membrane if all the cracks in the glass plies are aligned and there is enough tensile strain in the membrane to ensure that adjacent fragments do not make contact as it curves. It is more likely that cracks in each ply do not line up exactly, resulting in some residual flexural stiffness after the glass fractures. Omitting this residual flexural stiffness from the model is likely to be a contributing factor to the differing deflection profiles in Figure 18.

An initial rate-independent modulus was combined with a rate-dependent plasticity law to describe the behaviour of the cracked laminate. The initial modulus was based on results from tensile tests on cracked laminated glass at the strain rates observed in blast testing. Strain rates of the same order were predicted by the finite element model for the blast test discussed and give confidence in this assumption.

The model assumes that fracture of the glass plies occurs instantaneously and with an even density across the laminate. The fracture pattern is known to vary across the laminate (Hooper et al., 2011), with the crack density largely being a function of the stress distribution at the time of fracture. In the cracked laminated glass tests it was observed that the initial modulus increased and nominal failure strain decreased with increased crack spacing, whereas the plateau stress was unaffected. The finite element model used here ignores these effects and could as a result overestimate the safety limit of the pane.

5.4.2. Boundary conditions

The boundary conditions used in the finite element model correspond to an infinitely stiff supporting structure. Comparisons with the experimental deflection profiles show that there is flexibility at the boundary. If the period of oscillation of the boundary coincides with that of the laminated pane then it will act to reduce the stresses in the laminate and joint. If the boundary rebounds before the laminate pane reaches maximum deflection then the stress in the laminate and joint could increase. This effect has been neglected in this analysis and could be a factor in determining the safe limit of a laminated pane under blast loading.

5.4.3. Fluid structure interaction

In this analysis the pressure distribution across the window face was assumed to be uniform. Furthermore, the blast pressure in the model acts as a time varying static pressure, always resulting in a force normal to the face of each shell element. This is not an accurate representation of the way in which the blast wave interacts with the structure and is likely to be another contributing factor to the differing deflection profiles in Figure 18. The load acting on the pane arises from both the static and dynamic pressure in the blast wave. The pressures calculated here assume that the blast wave is reflecting normal to an infinitely rigid

surface. However, the pane quickly accelerates when hit by the blast wave, reducing the effective dynamic pressure of the wave and the total impulse acting on the pane. Air behind the pane has also been neglected and is likely to offer some damping effect. It is therefore possible that the calculated pressures overestimate the load on the pane, giving conservative estimates for the pressures and impulses required to cause failure. More accurate modelling of the interaction between the blast wave and moving pane is possible with coupled fluid dynamics simulations, but at the expense of a significant increase in computational time.

6. Conclusions

In this paper, a series of four open-air blast experiments on laminated glass windows to measure deflection and edge reaction forces are described. Four laminated glass samples of layup $[3, 1.52, 3]$ mm were loaded with peak reflected pressures and positive reflected impulses ranging from 91.2 kPa to 155 kPa and 284 kPa · ms to 413 kPa · ms respectively.

The high-speed image correlation results have allowed a detailed analysis of the response of laminated glass under blast loading. The deflected shape of the windows showed a flat central region deflecting into the cubicle with curved and strained regions concentrated close to the edges. The fracture pattern in the glass plies was largely determined by the stress created by the curvature at the time of fracture. As the panes deflected further the flat central region became smaller until the whole profile was curved. The restraint at the edges caused transverse deceleration waves to propagate inwards towards the centre from each edge. Displacements before failure of over 200 mm were observed. Peak observed velocities and accelerations at the centre of the pane ranged from 17 $^{\mathrm{m}}/_{\mathrm{s}}$ to 31 $^{\mathrm{m}}/_{\mathrm{s}}$ and 3 $^{\mathrm{km}}/_{\mathrm{s}^2}$ to 6 $^{\mathrm{km}}/_{\mathrm{s}^2}$ respectively. Strain in the cracked laminated glass was observed to reach values of 15% without tearing for a 1.52 mm interlayer. Strain rates between $10\,\mathrm{s}^{-1}$ and $40\,\mathrm{s}^{-1}$ were also observed.

For three of the tests, the samples failed at the silicone joint but for one test the joint did not fail and the window rebounded, coming to rest without significant joint damage. The image correlation results showed that the angle of pull was approximately constant along the edges. The mean tension in the cracked laminate and angle of pull at failure were found to be 20 ± 5 $^{\mathrm{kN}}/_{\mathrm{m}}$ and $30° \pm 5°$ respectively. Failure in the joint region is the most undesirable mode of failure because the majority of the laminated pane becomes detached from the frame and can contain sufficient kinetic energy to cause serious injury to building occupants. This highlights the need for proper specification of joint sizes and framing relative to the tearing strength of the cracked laminated glass.

A finite element model has been developed to predict the response of the laminated glass to blast loading

in the precrack and postcrack phases. The model was constructed using shell elements and was split into two distinct phases to describe the precrack and postcrack response. In the precrack phase it was determined that the effects of viscoelasticity in the PVB interlayer were negligible at short time scales by comparing the results of the shell element model against a full solid continuum element model.

The postcrack phase of the laminate response was modelled by reducing the stiffness of the glass layers to zero and using a rate-dependent plasticity law to describe the membrane response of the cracked laminate. A pressure-impulse analysis was conducted using the model to determine iso-damage levels for varying charge weights and stand off distances. The iso-damage curves agreed well with those generated using a single-degree-of-freedom analysis, with a 20% maximum strain damage curve being approximately equivalent to a maximum 200 mm deflection damage curve produced using the single-degree-of-freedom model.

Comparisons between the predictions generated using the model and experimental data from blast testing showed that the finite element model agrees very well initially. Differences in the predicted response could be due to the omission of any residual flexural stiffness in the cracked laminate after the glass plies fracture and flexibility in the supporting structure. Overall, the response of the laminated glass FE model captures the deformation behaviour up to maximum deflection for full-scale blast evaluation of laminated glass panes subject to different charge and stand-off conditions. As such it is a useful design tool for optimising blast mitigation of glass facade structures. The model is also applicable to laminated glass under impact and blast conditions such as those experienced in transport applications.

Acknowledgements

The authors acknowledge the Engineering and Physical Sciences Research Council (EPSRC) and Arup for financially supporting Dr Paul Hooper during his PhD. We acknowledge the many constructive discussions with David C. Smith and David Hadden of Arup. The authors also thank the Centre for the Protection of National Infrastructure (CPNI) for providing access to the GL group test facilities at RAF Spadeadam and Amit Puri and Hari Arora for their assistance during the full scale blast tests.

References

References

Arora, H., Hooper, P. A., Dear, J. P., 2011. Dynamic response of full-scale sandwich composite structures subject to air-blast loading. Composites Part A: Applied Science and Manufacturing 42 (11), 1651 – 1662.
URL http://www.sciencedirect.com/science/article/pii/S1359835X11002247

Behr, R. A., Minor, J. E., Norville, H. S., 1993. Structural behavior of architectural laminated glass. Journal of Structural Engineering 119 (1), 202–222.

Bennison, S. J., Jagota, A., Smith, C. A., 1999. Fracture of glass/poly(vinyl butyral) (Butacite®) laminates in biaxial flexure. Journal of the American Ceramic Society 82, 1761–1770.

CEN/TC129, C. T. C., 2008. Glass in buildings - determination of the strength of glass panes. Part 3: General method of calculation and determination of strength of glass by testing. prEN 13474-3. British Standards Institute, London.

Charles, R. J., 1958. Static fatigue of glass. Journal of Applied Physics 29, 1554 –1560.

Cormie, D., Mays, G., Smith, P. (Eds.), 2009. Blast effects on buildings, Second Edition. Thomas Telford.

Dobratz, B. M., Crawford, P. C., 1985. LLNL explosives handbook: properties of chemical explosives and explosives and explosive simulants. UCRL-52997, Lawrence Livermore National Laboratory, CA.

Home Office Scientific Development Branch, 2008. Guidance note: Glazing enhancement to improve blast resistance.

Hooper, J. A., 1973. On the bending of architectural laminated glass. International Journal of Mechanical Sciences 15 (4), 309–323.

Hooper, P. A., Blackman, B. R. K., Dear, J. P., 2011. The mechanical behaviour of poly(vinyl butyral) at different strain magnitudes and strain rates. Journal of Materials Science Accepted.

Johnson, G. R., Cook, W. H., 1985. Fracture characteristics of three metals subjected to various strains, strain rates, temperatures and pressures. Engineering Fracture Mechanics 21 (1), 31–48.

Muralidhar, S., Jagota, A., Bennison, S. J., Saigal, S., 2000. Mechanical behaviour in tension of cracked glass bridged by an elastomeric ligament. Acta Materialia 48, 4577–4588.

Norville, H. S., King, K. W., Swofford, J. L., 1998. Behavior and strength of laminated glass. Journal of Structural Engineering 124 (1), 46–53.

Rose, T. A., 2001. An approach to the evaluation of blast loads on finite and semi-infinite structures. Ph.D. thesis, Cranfield University.

Seshadri, M., Bennison, S. J., Jagota, A., Saigal, S., 2002. Mechanical response of cracked laminated plates. Acta Materialia 50 (18), 4477–4490.

Simulia, 2010. Abaqus theory manual v6.9.

Smith, D. C., 2001. Glazing for injury alleviation under blast loading: United Kingdom practice. In: Glass Processing Days Conference Proceedings. pp. 335–340.

Sutton, M. A., Orteu, J. J., Schreier, H. W., 2009. Image Correlation for Shape, Motion and Deformation Measurements. Springer.

van Duser, A., Jagota, A., Bennison, S. J., 1999. Analysis of glass/polyvinyl butyral laminates subjected to uniform pressure. Journal of Engineering Mechanics 125 (4), 435–442.

Williams, M. L., Landel, R. F., Ferry, J. D., 1955. The temperature dependence of relaxation mechanisms in amorphous polymers and other glass-forming liquids. Journal of the American Chemical Society 77 (14), 3701–3707.